POLISH ACADEMY OF SCIENCES

THERMODYNAMICS AND COMBUSTION COMMITTEE

archives of thermodynamics

Wydawnictwo IMP
Gdańsk

QUARTERLY
Vol. 38
2017
No. 2

Editorial Office

Archives of Thermodynamics
The Szewalski Institute of Fluid Flow Machinery, Fiszera 14, 80-231 Gdańsk, Poland,
Tel.: (+48) 58-341-12-71 int. 141, E-mail: redakcja@imp.gda.pl
http://www.imp.gda.pl/archives-of-thermodynamics/
http://at.czasopisma.pan.pl/

Publication funding of this journal is provided by resources of the Polish Academy of Sciences and the Szewalski Institute of Fluid-Flow Machinery PASci

Terms of subscription outside Poland
Annual subscription rate outside Poland (2017) is 120 EUR. Price of single issue is 30 EUR. Back of previously published volumes are available on request. Subscription orders should be sent directly to **IMP PAN Publishers, The Szewalski Institute of Fluid-Flow Machinery PASci, ul. Fiszera 14, 80-231 Gdansk, Poland**; fax: (+48) 58-341-61-44; e-mail: now@imp.gda.pl. Payments should be transferred to the bank account of IMP PAN: IBAN 28 1130 1121 0006 5498 9520 0011 at Bank Gospodarstwa Krajowego; Code SWIFT: GOSKPLPW

Warunki prenumeraty w Polsce
Roczna prenumerata (2017 r.) wynosi 168 PLN. Cena pojedynczego numeru wynosi 42 PLN. Osiągalne są również wydania archiwalne. Zamówienia z określeniem okresu prenumeraty, nazwiskiem i adresem odbiorcy należy kierować bezpośrednio do Wydawcy (Instytut Maszyn Przepływowych im. R. Szewalskiego PAN, ul. Fiszera 14, 80-231 Gdańsk, Aleksandra Nowaczewska, e-mail: now@imp.gda.pl). Wpłaty prosimy kierować na konto Instytutu Maszyn Przepływowych PAN nr 28 1130 1121 0006 5498 9520 0011 w Banku Gospodarstwa Krajowego

Articles in *Archives of Thermodynamics* are abstracted and indexed within:

Applied Mechanics Reviews • BazTech • Arianta • Baidu Scholar • Cabell's Directory • Celdes • Chemical Abstracts Service (CAS) - CAplus • CNKI Scholar (China National Knowledge Infrastucture) • CNPIEC • DOAJ • EBSCO (relevant databases) • EBSCO Discovery Service • Elsevier - SCOPUS • Genamics JournalSeek • Google Scholar • Inspec • Index Copernicus • J-Gate • Journal TOCs • Naviga (Softweco) • Paperbase • Pirabase • POL-index • Polymer Library • Primo Central (ExLibris) • ProQuest (relevant databases) • ReadCube • Referativnyi Zhurnal (VINITI) • SCImago (SJR) • Summon (Serials Solutions/ProQuest) • TDOne (TDNet) • TEMA Technik und Management • Ulrich's Periodicals Directory/ulrichsweb • WorldCat (OCLC)

Online ISSN 2083-6023
DE GRUYTER – http://www.degruyter.com/view/j/aoter

Typeset in LaTeX
Printed and bound by
Centrum Poligrafii Sp. z o.o., Łopuszańska 53, 02-232 Warszawa

archives
of thermodynamics
Vol. **38**(2017), No. 2, 3–20
DOI: 10.1515/aoter-2017-0008

Unconfined laminar nanofluid flow and heat transfer around a rotating circular cylinder in the steady regime

RAFIK BOUAKKAZ[a*]
FOUZI SALHI[b]
YACINE KHELILI[c]
MOHAMED QUAZZAZI[d]
KAMEL TALBI[e]

[a] Military Academy of Cherchell, Tipaza, Algérie

[b] Université Mouloud Mammeri Tizi ouzou, Département de Génie Mécanique, Algérie

[c] University Saad Dahlab, Department of Mechanical Engineering, Blida 1, Algeria

[d] Université Kasdi Merbah Ouargla, Département de Génie Mécanique, Algérie

[e] Université Constantine 1, Département de Génie Mécanique, Constantine, Algérie

Abstract In this work, steady flow-field and heat transfer through a copper-water nanofluid around a rotating circular cylinder with a constant nondimensional rotation rate α varying from 0 to 5 was investigated for Reynolds numbers of 5–40. Furthermore, the range of nanoparticle volume fractions considered is 0–5%. The effect of volume fraction of nanoparticles on the fluid flow and heat transfer characteristics are carried out by using a finite-volume method based commercial computational fluid dynamics solver. The variation of the local and the average Nusselt numbers with Reynolds number, volume fractions, and rotation rate are presented for the range of conditions. The average Nusselt number is found to decrease with increasing value of the rotation rate for the fixed value of the Reynolds num-

*Corresponding Author. Email rafik.bouakkaz@gmail.com

ber and volume fraction of nanoparticles. In addition, rotation can be used as a drag reduction technique.

Keywords: Nanofluid; Rotating circular cylinder; Forced convection; Steady regime

Nomenclature

C_D	–	drag coefficient
C_L	–	lift coefficient
C_p	–	pressure coefficient
D	–	drag force, N
D_t	–	diameter of the cylinder, m
H	–	the location of the outer boundary of the domain
h_{Dt}	–	the radial step size of the first layer of cells
k	–	thermal conductivity
L	–	lift force, N
Nu	–	average Nusselt number
Nu_0	–	average Nusselt number for the stationary cylinder
Nu_L	–	local Nusselt number
N_t	–	number of points
p	–	local pressure, Nm^{-2}
Pr	–	Prandl number
Re	–	Reynolds number, $(= U_\infty D_t/\nu)$
T_∞	–	free-surface temperature, K
u	–	streamwise velocity, $\mathrm{m\,s}^{-1}$
U_∞	–	free-stream velocity, $\mathrm{m\,s}^{-1}$
U	–	non-dimensional streamwise velocity $(= u/U_\infty)$
V	–	non-dimensional cross-stream velocity $(= v/U_\infty)$
x	–	streamwise dimension of coordinates, m
X	–	non-dimensional streamwise dimension of coordinates $(= x/D)$
y	–	cross-stream dimension of cordinates, m
Y	–	non-dimensional cross-stream dimension of cordinates $(= y/D_t)$

Greek symbols

α	–	non-dimensional rotation rate $(\Omega D_t/2U_\infty)$
β	–	fluid thermal expansion coefficient
θ	–	non-dimensional temperature
μ	–	dynamic viscocity, $\mathrm{N\,s/m}^2$
ν	–	kinematic viscosity, $\mathrm{m}^2\mathrm{s}^{-1}$
ρ	–	density, $\mathrm{kg/m}^3$
φ	–	angular displacement from the front stagnation point
ϕ	–	nanoparticle volume fractions
τ	–	non-dimensional time
ω	–	vorticity on the surface of the cylinder, s^{-1}
ϖ	–	dimensionless vorticity on the surface of the cylinder $(= 2\omega D_t/U_\infty)$
Ω	–	constant angular velocity of the cylinder rotation, $\mathrm{rad\,s}^{-1}$

Subscripts

nf	–	nanofluid

bf – base fluid
s – solid nanoparticles

1 Introduction

The fluid flow and heat transfer around a rotating circular cylinder are considered to be fundamental fluid mechanics problems with a huge number of practical applications such as cooling devices in plastics and glass industries, chemical processing industries and food processing. In these flows, the results depend not only on the Reynolds number, Re, but also on rotation rate, α, defined as the ratio of rotational velocity of the cylinder wall to the incoming free stream flow velocity, expressed as: $\mathrm{Re} = U_\infty D_t/\upsilon$ and $\alpha = \Omega D_t/2U_\infty$.

In recent years, many researches have been performed to study the effects of rotation rate on the flow and convective heat transfer. The authors of the paper [1] investigated numerically the effect of rotation rate on the flow and heat transfer across a rotating cylinder in the range $0 \leq \alpha \leq 6$ with Re number varying in the range 20–160. They concluded that the rotation can be used as a drag reduction and heat transfer suppression technique. Subsequently, [2] studied numerically the free stream flow and forced convection heat transfer across a rotating cylinder, dissipating heat flux for Reynolds numbers of 20–160 and a Prandtl number of 0.7. Their results show that, at higher rotational velocity, the Nusselt number is almost independent of Reynolds number and thermal boundary conditions. The suppression of von Karman Street was also reported numerically in [3] for Reynolds numbers of 80–160 and rotation rate was examined up to a maximum value of 5.3 in the range of 0–6 at Pr equal 7. For steady regime, a well-organized numerical study was published in [4]. In that paper, the numerical calculations were solved via the finite volume method in order to examine the characteristics of flow and heat transfer for varying rotation rate (α = 0–5) in the Reynolds number range 1–35 and Prandtl numbers range 0.7–100. They found that the average Nusselt number increases with increasing Prandtl number for the fixed value of the Reynolds number for the particular value of rotation rate.

In past studies, the fluids used have a low value of thermal conductivity, which limits the heat transfer. For this reason, there are several methods to improve the heat transfer characteristics, which consist in adding high conducting solid particles to the base fluid. The resulting fluid is called the 'nanofluid' [5–8].

The steady flow-field and heat transfer through a copper-water nanofluid around circular cylinder was numerically simulated by Valipour and Ghadi [9]. The values of vorticity, pressure coefficient, recirculation length are increased by the addition of nanoparticles into the base fluid. Subsequently, El-Bashbeshy *et al.* examined the effect of heat treatment process with a new cooling medium (nanofluid), which contains water with Cu, Ag, or Al_2O_3 particles, on heat transfer characteristics and mechanical properties of an unsteady continuous moving cylinder in the action of thermal forces [10]. They reported that the Al_2O_3 nanofluid is the best type of nanofluid for improving the mechanical properties of the surface (increase the heat flux). This nanofluid is also the best type for decreasing the surface shear stress.

Recently, numerical study has been focused on heat transfer phenomena over an isothermal cylinder, for low Reynolds number flow of nanofluid [11]. Heat transfer characteristic and flow over the stationary cylinder has been studied for water based copper nanofluid with different solid fraction values. It has been shown that the presence of nanoparticle has no effect on the point of flow separation for a fixed Reynolds number, howener, the effect of buoyancy force has not been taken into consideration. On the other hand, the momentum and forced convection heat transfer for a laminar and steady free stream flow of nanofluids past a square cylinder have been studied [12]. Different nanofluids consisting of Al_2O_3 and CuO with base fluids of water and a 60:40 (by mass) ethylene glycol and water mixture were selected to evaluate their superiority over conventional fluids. It has been showed that for any given particle diameter there is an optimum value of particle concentration that results in the highest heat transfer coefficient. The fluid flow and heat transfer around a square cylinder utilizing $Al_2O_3-H_2O$ nanofluid over low Reynolds numbers varied within the range from 1 to 40 and the volume fraction of nanoparticles is varied within the range of $0 < \phi < 0.05$ was investigated [13]. They found that increase of the nanoparticles volume fractions augments the drag coefficient. Moreover, pressure coefficient increases by increasing the solid volume fraction for sides where pressure gradient is inverse but for sides where the pressure gradient is favourable the pressure coefficient decreases.

The present investigation had been motivated by increased interest and research in potential improvements in heat transfer characteristics using nanofluids. Effort has been made to investigate numerically the steady flow of nanofluid and heat transfer characteristics of a rotating circular cylinder

for a range of Reynolds numbers ($5 \leq \mathrm{Re} \leq 40$) and particle volumetric concentrations ranging from 0% to 5% for rotation parameters ($0 \leq \alpha \leq 5$) in the two-dimensional laminar flow regime.

2 Problem statement, governing equations, and boundary conditions

The system here consists of a 2D infinitely long circular cylinder having a diameter D_t which is maintained at a constant temperature T_w and is rotating in a counter clockwise direction with a constant angular velocity of Ω. It is exposed to a constant free stream velocity of U_∞ at a uniform temperature of T_∞ at the inlet. The nanoparticles are assumed to be of the uniform shape and size. In addition, we have assumed that nanoparticles are in thermal equilibrium state and flowing at the same velocity. Flow configuration is shown in Fig. 1.

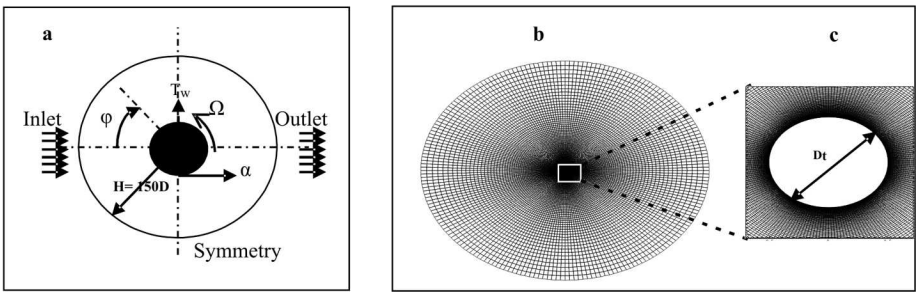

Figure 1: Schematic of the unconfined flow and heat transfer around a rotating circular cylinder (a), grid structure (b), close up view in the vicinity of the cylinder (c).

2.1 Governing equations and boundary conditions

The governing partial differential equations here are the Navier-Stokes and energy equations in two dimensions and steady state nanofluid flow around a rotating circular cylinder in dimensionless form are given form:

$$\frac{\partial U}{\partial X} + \frac{\partial V}{\partial Y} = 0 \,, \tag{1}$$

$$U\frac{\partial U}{\partial X} + V\frac{\partial U}{\partial Y} = \frac{1}{\rho_{nf}}\left[-\frac{\partial P}{\partial X} + \mu_{nf}\left(\frac{\partial^2 U}{\partial X^2} + \frac{\partial^2 U}{\partial Y^2}\right)\right] \,, \tag{2}$$

$$U\frac{\partial V}{\partial X}+V\frac{\partial V}{\partial Y}=\frac{1}{\rho_{nf}}\left[-\frac{\partial P}{\partial Y}+\mu_{nf}\left(\frac{\partial^2 V}{\partial X^2}+\frac{\partial^2 V}{\partial Y^2}\right)\right] , \tag{3}$$

$$U\frac{\partial T}{\partial x}+V\frac{\partial T}{\partial y}=\alpha_{nf}\left(\frac{\partial^2 T}{\partial x^2}+\frac{\partial^2 T}{\partial y^2}\right) , \tag{4}$$

where: $U=\frac{u}{U_\infty}, V=\frac{v}{U_\infty}, \tau=\frac{tU_\infty}{D_t}, X=\frac{x}{D_t}, Y=\frac{y}{D_t}, P=\frac{p}{\rho U_\infty^2}, \theta=\frac{T-T_\infty}{T_W-T_\infty}$. Here U and V are the velocity components along X and Y axes, T denotes the temperature, P is the pressure, ρ is the density, μ – the dynamic viscosity. The subscript nf stands for the nanofluid.

The thermophysical properties taken from [9], for the base fluid and copper oxide (at 300 K) are shown in Tab. 1.

Table 1: Thermophysical properties of the base fluid and cooper nanoparticles.

Property	Unit	Water	Copper
C_p	$(\mathrm{J\,kg^{-1}K^{-1}})$	4179	385
ρ	$(\mathrm{kg\ m^{-3}})$	997.1	8.933
k	$\mathrm{Wm^{-1}K^{-1}})$	0.613	401
$\alpha\times10^7$	$(\mathrm{m^2s^{-1}})$	1.47	1.163

The effective density, thermal diffusivity, heat capacitance, and thermal expansion coefficient of the nanofluid are calculated using the following expressions:

$$\rho_{nf}=(1-\phi)\,\rho_{bf}+\phi\rho_s \tag{5}$$

$$(\rho C_p)_{nf}=(1-\phi)\,(\rho C_p)_{bf}+\phi\,(\rho C_p)_s , \tag{6}$$

$$\alpha_{nf}=\frac{k_{nf}}{(\rho C_p)_{nf}} , \tag{7}$$

$$\beta_{nf}=(1-\phi)\,(\rho\beta)_{bf}+\phi(\rho\beta)_s , \tag{8}$$

where ϕ is the solid volume fraction, α is the non-dimensional rotation rate, β is the fluid thermal expansion coefficient, and C_p is the pressure coefficient. Subscript bf stands for base fluid and the subscript s stands for solid nanoparticles. The effective dynamic viscosity of the nanofluid is calculated using the formula suggested in [6]

$$\mu_{nf}=\frac{\mu_{bf}}{(1-\phi)^{2.5}} . \tag{9}$$

The effective thermal conductivity of the nanofluid is approximated by the Maxwell-Garnett model, for a suspension of spherical nanoparticles in the base fluid, the formula suggested by [14] is applied:

$$k_{nf} = k_{bf}\left[\frac{(k_s + 2k_{bf}) - 2\phi\,(k_{bf} - k_s)}{(k_s + 2k_{bf}) + \phi\,(k_{bf} - k_s)}\right] . \tag{10}$$

2.2 Boundary conditions

The dimensionless boundary conditions for the flow across a rotating circular cylinder can be written as (Fig. 1). The left-hand arc (Fig. 1a) is the inflow section or upstream section, where there is a Dirichlet-type boundary condition for the Cartesian velocity components

$$V = 0 \quad \text{and} \quad \theta = 0 , \tag{11}$$

where θ is the non-dimensional temperature. The right-hand arc represents the outflow boundary, where it is considered that the diffusion flux in the direction normal to the exit surface is zero for all variables

$$\frac{\partial U}{\partial X} = \frac{\partial V}{\partial X} = \frac{\partial \theta}{\partial X} = 0 . \tag{12}$$

Finally, the dimensionless peripheral or tangential velocity is prescribed on the surface of the rotating cylinder, along with a no-slip boundary condition

$$U = -\alpha \sin(\varphi); \qquad V = -\alpha \cos(\varphi), \qquad \theta = 1 , \tag{13}$$

where φ is the angular displacement from the front stagnation point.

2.3 Force coefficients

Two relevant parameters computed from the velocity and pressure fields are the drag and lift coefficients, which represent dimensionless expressions of the forces that the fluid produces on the circular cylinder. These are defined, respectively, as follows:

$$C_D = \frac{D}{\rho U_\infty^2 D_t} , \qquad C_L = \frac{L}{\rho U_\infty^2 D_t} , \tag{14}$$

where D is the drag force and L is the lift force with respect to the centre of the cylinder.

3 Numerical details

The computational grid for the problem under consideration was generated by using a commercial grid generator Gambit [19] and the numerical calculations were performed in the full computational domain using Fluent [20] for varying conditions of Re number and rotation rate. This computer program applies a control-volume method to integrate the equations of motion, constructing a set of discrete algebraic equations with conservative properties. In particular, the O-type grid structure similar to that adopted in [15] was created here. The steady, laminar, segregated solver was employed here to solve the incompressible flow on the collocated grid arrangement. Semi implicit method for the pressure linked equations (SIMPLE) [4] was used to solve Navier-Stokes and energy equations for above noted boundary conditions. Second order upwind scheme is used to discretize the convective terms of momentum equations, whereas the diffusive terms are discretized by the central difference method. A convergence criterion of 10^{-8} is used for continuity, and Cartesian components components of momentum equations, while for energy equation the criterion of convergence was 10^{-10}.

3.1 Domain independence study

The mesh used for all the two-dimensional computations consisted of 40 000 quadrilateral cells and 40 200 nodes. The cylinder (of diameter D_t) resides in a computational domain whose outer edges located at a distance of H from the centre of the cylinder (see Fig. 1). There are N_t points in the circumferential direction on the cylinder surface and the radial thickness of the first layer of cells (i.e., cells attached to the wall) is h_{Dt}. A close-up view of a typical mesh is shown in Fig. 1c. It can be observed that the mesh is very fine close to the cylinder and the cells become larger with increasing distance from the cylinder. The location of the outer boundary of the domain is expected to become more crucial for larger values of α [16,17]. In this study, following [4], the computational domain covers 150 times the diameter of the cylinder in all directions. The grid sensitivity analysis was performed for Re = 40 and $\phi = 0.05$. Table 2 lists the details for the meshes that were employed. Bearing in mind the influence of the number of grid points on the average Nusselt number on the cylinder wall, it was decided to carry out computations with mesh M2.

Table 2: Effect of grid number on averaged Nusselt number (Nu) at Re = 40, Pr = 6.264 ($\phi = 0.05$) for $\alpha = 0$ and $\alpha = 5$.

Mesh	Cells	Nt	h_{Dt}	Nu	
				$\alpha = 0$	$\alpha = 5$
M1	32000	160	0.0015	7.5880	4.6222
M2	40000	200	0.0010	7.6139	4.6464
M3	50000	250	0.0010	7.6.76	4.6495

4 Results and discussion

4.1 Comparison with other results

The first step was to validate the problem set-up, the choice of numerical methods and mesh attributes by comparing results from our numerical simulations with results obtained from the literature. The outcomes included in the comparison were the mean Nusselt number, as well as lift and drag coefficients.

The average Nusselt number for stationary cylinder at Re = 40 (base fluid) and $\phi = 0.05$ (Pr = 6.26), is found to be in good agreement with the correlation [18].

$$\mathrm{Nu} = 0.593\mathrm{Re}^{1/2}\mathrm{Pr}^{1/3} \ . \tag{15}$$

Using this relation for same parameters, the value of the average Nusselt number Nu = 7.66 is obtained, which is in excellent agreement with present calculations, Nu = 7.61.

It is interesting to remind that the Reynolds and Prandtl number of nanofluids can be expressed as

$$\mathrm{Re}_{nf} = \frac{\rho_{nf}}{\rho_{bf}}\frac{\mu_{bf}}{\mu_{nf}}\mathrm{Re}_{bf} \ , \qquad \mathrm{Pr}_{nf} = \frac{\mu_{nf}}{\mu_{bf}}\frac{C_{P,nf}}{C_{P,bf}}\frac{k_{bf}}{k_{nf}}\mathrm{Pr}_{bf} \ . \tag{16}$$

Comparison of the average Nusselt number results for a rotating circular cylinder under different Reynolds numbers with data from [1] is given in Tab. 3. The present results of the average Nu number are in excellent agreement with the literature ones.

Table 4 compares the lift and drag coefficients computed here with results cited in scientific publications. We have noted that the lift coefficient

values are in superb agreement with numerical data reported by other researchers, but discrepancies in the values of the drag coefficient are larger; the drag coefficients are so small that the relative errors are magnified.

Table 3: Comparison of Nusselt number computed in the present study with literature data (Pr = 0.7).

Re	α	Nu		Relative error (%)
		Present study	Paper[1]	
20	0	2.4092	2.4189	0.40
20	2	2.2785	2.2861	0.33
20	4	2.2511	2.2554	0.19
40	0	3.2496	3.2465	0.10
40	2	3.0402	3.0115	0.95
40	4	3.0614	3.0422	0.63

Table 4: Comparison between the lift and drag coefficients computed in the present study with values given by literature data.

Re		C_D			C_L		
Re	α	Present study	Paper [1]	Relative error (%)	Present study	Paper [1]	Relative error (%)
40	0	1.503	1.504	0.066	0	0	0
40	1	1.3132	1.315	0.15	-2.5817	-2.6013	0.75
40	4	-0.038	-0.052	26.92	-16.083	-16.033	0.31

4.2 Mean lift and drag coefficients

Figure 2 shows that the negative/downward lift coefficient, C_L, increases monotonically with increasing α and with increasing Re. However, the increase is marginal with increasing Re. Thus, the lift coefficient is strongly dependent on the rotation rate and weakly dependent on Re. Very high lift coefficients are observed for high rotation rates of the cylinder.

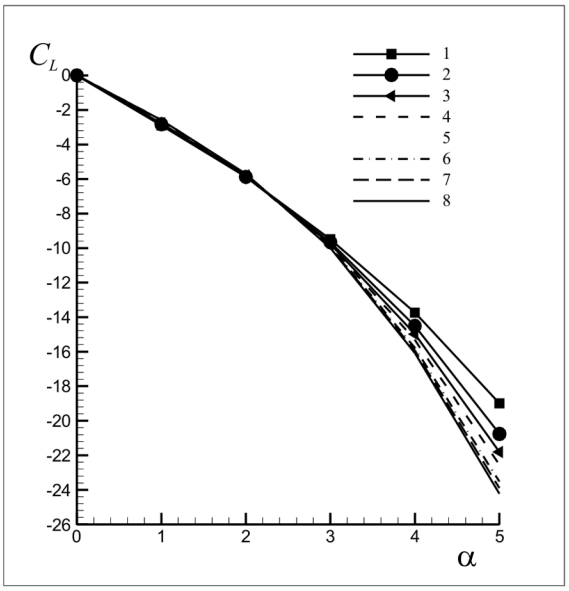

Figure 2: Variation of mean lift coefficient, C_L, with rotation rate, α, for various Reynolds number; Re= 5 (1), 10 (2), 15 (3), 20 (4), 25 (5), 30(6), 35 (7), 40 (8).

Figure 3 shows the variation of the drag coefficient, C_D, with rotation rate $0 \leq \alpha \leq 5$ for Re = 5, 10, 15, 20, 25, 30, 35, and 40. It can be noted that with the increase in rotation rate, drag coefficient values for all the Reynolds number converge at approximately the same value for α of 5 with the exception of Re equal to 5 and 10.

4.3 Isotherm patterns

The isotherms profiles around the rotating cylinder for Reynolds number of 20 and 40 for α of 0 and 5 are compared between the base fluid and nanofluid ($\phi = 0.05$) in Fig. 4a. Clearly, the temperature distribution contours for base fluid are overlaid with that for nanofluid. This can be explained by the fact that the addition of solid particles to the base-fluid increases the Reynolds number of nanofluid. Hence results the higher capacity of transferring the heat from the cylinder. For a stationary cylinder, it is obvious from Fig. 4a that the isotherms have maximum density close to the front surface of the cylinder; this indicates high values of the local Nusselt number near the front stagnation point on the front surface as compared to other points on the cylinder surface. On other hand, as the

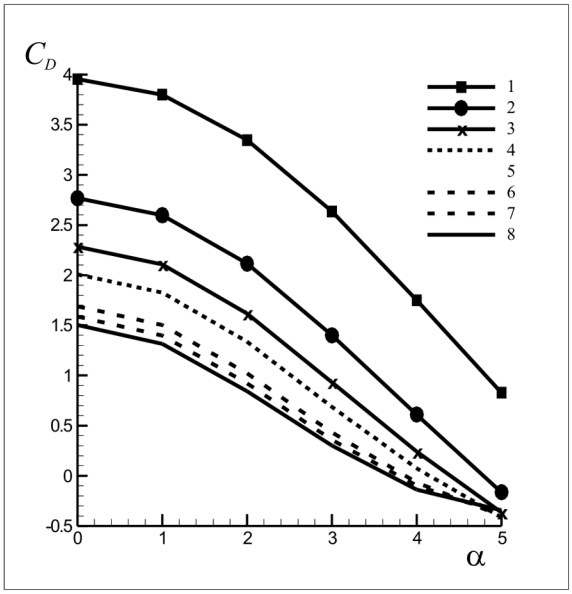

Figure 3: Variation of mean drag coefficient, C_D, with rotation rate, α, for various Reynolds number. For legend see page 13.

Re increase, the recirculation region behind the cylinder grows yields to increase in the density of isotherms close to the rear surface as shown in Fig. 4b. On increasing the value of the rotation rate, the maximum density of the isotherm shifts from the front surface towards the bottom surface of the rotating cylinder (rotating counter clockwise), Fig. 4c. In addition, as the solid concentration, ϕ, increases, the thermal boundary layer becomes thinner which leads to the increase in the Nusselt number, Fig. 4d.

4.4 Local Nusselt number

Figure 5 shows the variation of local Nusselt number, Nu_L, on the surface of the cylinder with increase in Reynolds number, Re, for various rotation rates, α, and volume fraction, ϕ. When the solid concentration increases the thermal conductivity improves and consequently the local Nusselt number increase. Additionally, the thermal boundary layer is decreased by any increase in the solid volume fraction (Fig. 4). Therefore, the local Nusselt number is enhanced by any increase in solid volume fraction. On the other hand, for a stationary cylinder and for all Re, the variation of Nu_L is found to be symmetrical at $\varphi = 180°$. The value of the local Nu number is

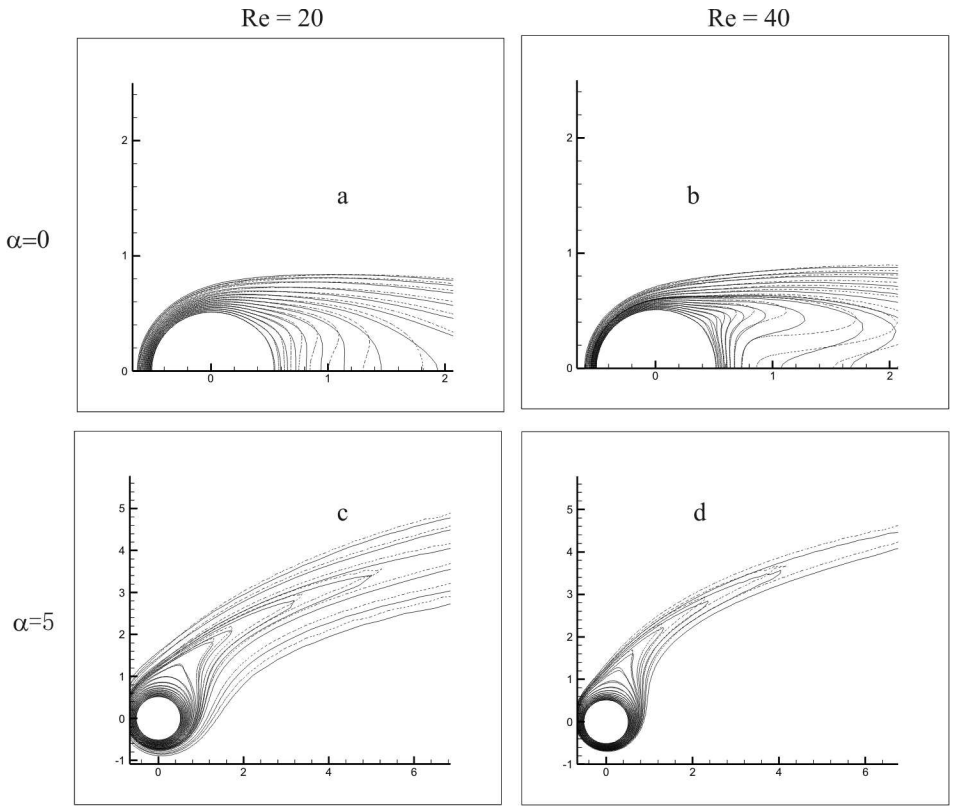

Figure 4: Temperature contours for the flow around the cylinder (solid line refers to base fluid and dashed line refers to nanofluid with solid volume fraction 0.05) at: (a) Re = 20, $\alpha = 0$, $\phi = 0$; (b) Re = 20 $\alpha = 0$, $\phi = 0.05$; (c) Re = 20, $\alpha = 5$, $\phi = 0$; (d) Re = 40, $\alpha = 5$, $\phi = 0.05$.

maximum on the front ($\varphi = 0$) and minimum on the rear ($\varphi = 180°$) side of the cylinder. Also, at this former angle, a kink is observed in the values of local Nusselt number and the size of this kink increases as the value of the Re number increases for the fixed value of ϕ. It can be explained on the basis that higher Reynolds number results in larger recirculation region. Also, the symmetrical variation of Nu_L seen in the figures for $\alpha = 0$ is lost under the effect of rotation. On increasing the value of the rotation rate, the local Nu number curve becomes smooth and the kink disappears. Finally, the rotation causes overall reduction in heat transfer across the cylinder, thus lowering the local Nusselt number at higher rotations.

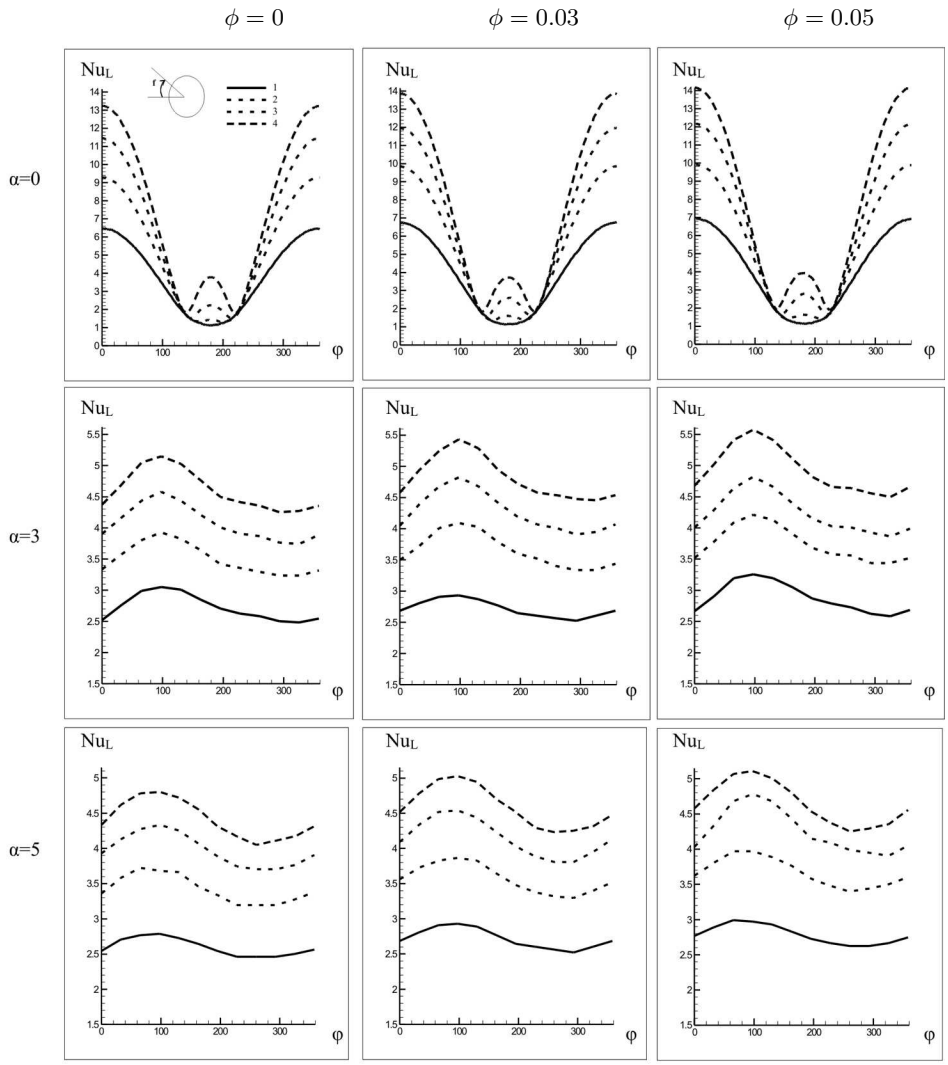

Figure 5: Local Nusselt number variation at various solid volume fractions for varying values of Reynolds number and rotation rate: Re = 10 (1), 20 (2), 30 (3), 40 (4).

4.5 Averaged Nusselt number

Figure 6 indicates that the averaged Nusselt number increases monotonically with increasing Re at constant α for a fixed volume fraction of nanoparticles, ϕ. This can be explained as when Reynolds number in-

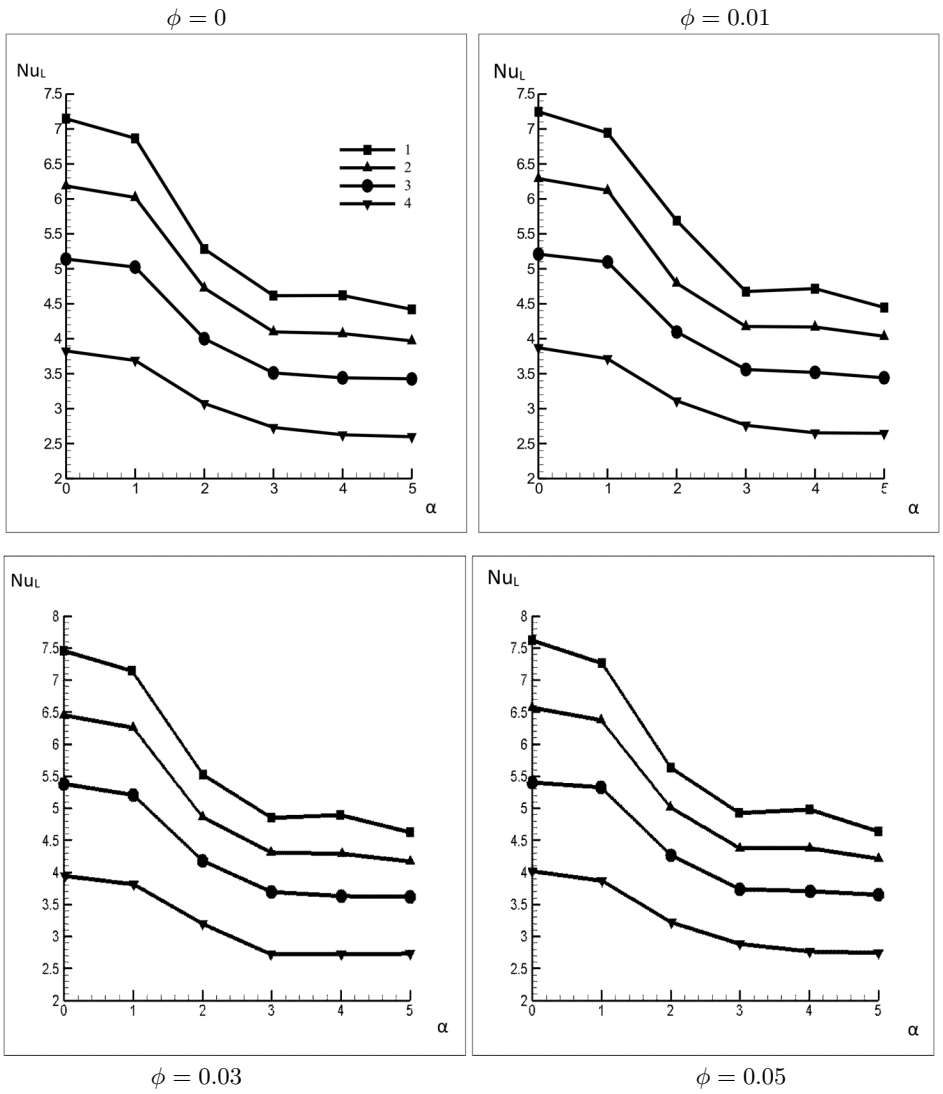

Figure 6: Variation of local Nusselt number with increasing Reynolds number for various rotation rates at various solid volume fractions: Re = 40 (1), 30 (2), 20 (3), 10 (4).

creases the inertia of flow increases thus increasing the heat transfer. The effect of Reynolds number also increases with increase in volume fraction number. Considering the case of the static cylinder, the change in average Nusselt number at volume fraction of 0 when Reynolds number increases

from 5 to 40 is 4.409. While the corresponding change in average Nusselt number due to increase in Reynolds number for volume fraction of 0.05 is 4.220. Further increase in rotation rate, for the fixed value of volume fraction, the value of the average Nusselt number decreases for all Reynolds numbers. The decrease in the Nusselt number with increasing rotational velocity can be explained on the basis that the fluid entrapped inside the enveloping vortex acts as a buffer zone for heat transfer between the cylinder and free stream and restrict the heat transfer to conduction only as detailed in [1].

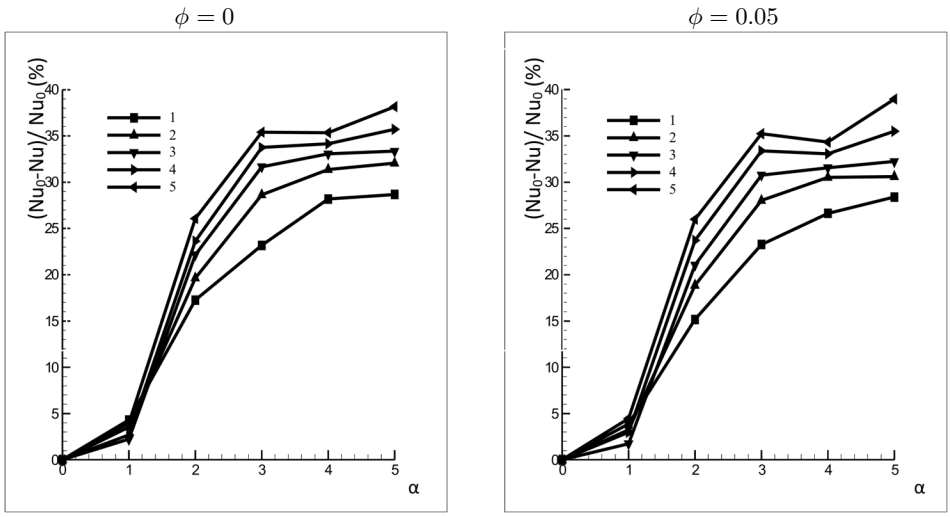

Figure 7: Percentage heat transfer suppression with increasing Reynolds number for various rotation rates. Nu_0 is the Nusselt number of the stationary cylinder: Re = 5 (1), 10 (2), 20 (3), 30 (4), 40 (5).

Figure 7 shows the normalized Nusselt number obtained as the ratio of average Nusselt number of the rotating cylinder, Nu, to that of the stationary cylinder, Nu_0, for base fluid and nanofluid ($\phi = 0.05$) at various rotation rates, α, to understand the suppression of heat transfer. For ϕ of 0, it can be seen from this figure that the suppression increases with increasing Re and increasing α, with a minimum value of 4.30% for Re =5 and a maximum value of 38.17% for Re = 40 at $\alpha = 5$. Thus, cylinder rotation can be used not only for controlling flow, but also as an efficient heat transfer suppression technique. Moreover, for the case $\phi = 0.05$, the

suppression curves remain practically similar. This can be explained that the Prandlt number is nearly the same: the change in the value of the Prandtl for the case $\phi = 0$ is in the range from 7.066 to 6.264 for the case $\phi = 0.05$. Hence, the suppression of heat transfer is not enhanced due to adding nanoparticles into the base fluid.

5 Conclusions

The present study focuses on the unconfined laminar flow of nanofluid and heat transfer characteristics around a rotating circular cylinder subjected to constant wall temperature. Heat transfer suppression due to rotation increases with increasing Reynolds number and increasing rotation rate. Moreover, the heat transfer suppression is not enhanced due to adding nanoparticles into the base fluid. Also, a downward drag coefficient is found due to rotation, which decreases monotonically with increasing rotation rate. Thus, rotation can be used as a drag reduction technique.

Further, the average Nusselt number is found to decrease with increasing rotation rate and increase with increasing Reynolds number . Suppression due to rotation increases with increasing Reynolds number and increasing rotation rate for all Reynolds number .

Received 12 October 2016

References

[1] Paramane S.B., Sharma A.: *Numerical investigation of heat and fluid flow across a rotating circular cylinder maintained at constant temperature in 2D laminar flow regime*. Int. J. Heat Mass Tran. **52**(2009), 13-14, 3205–3216.

[2] Paramane S.B., Sharma A.: *Heat and fluid flow across a rotating cylinder dissipating uniform heat flux in 2D laminar flow regime*. Int. J. Heat Mass Tran. **53**(2010), 21-22, 4672–4683.

[3] Sufyan M., Manzoor S., Sheikh N.A.: *Heat transfer suppression in flow around a rotating circular cylinder at high Prandtl number*. Arab. J. Sci. Eng. **39**(2014), 11, 8051–8063.

[4] Sharma V., Dhiman A.K.: *Heat transfer from a rotating circular cylinder in the steady regime: Effects of Prandtl number*. Thermal Sci. **16**(2012), 1, 79–91.

[5] Sarit K. Das, Stephen U. Choi, Wenhua Yu, T. Pradeep: *Nanofluids: Science and Technology*. Wiley, New York 2007.

[6] Brinkman H.C.: *The viscosity of concentrated suspensions and solutions*. J. Chem. Phys. **20**(1952), 4, 571–581.

[7] Chang H., Jwo C.S., Lo C.H., Tsung T.T., Kao M.J., Lin H.M.: *Rheology of CuO nanoparticle suspension prepared by ASNSS*. Rev. Adv. Mater. Sci. **10**(2005), 2, 128–132.

[8] Cieśliński J.T., Ronewicz K., Smoleń S.: *Measurement of temperature-dependent viscosity and thermal conductivity of alumina and titania thermal oil nanofluids*. Arch. Thermodyn. **36**(2015), 4, 35–47.

[9] Valipour M.S., Ghadi A.Z.: *Numerical investigation of fluid flow and heat transfer around a solid circular cylinder utilizing nanofluid*. Int. Commun. Heat Mass **38**(2011), 9, 1296–1304

[10] El-Bashbeshy E.S.M.A , Emam T.G., Abdel-Wahed M.S.: *The effect of thermal radiation, heat generation and suction/injection on the mechanical pro properties prieties of unsteady continuous moving cylinder in a a nanofluid*. Therm. Sci. **19**(2015), 5, 1591–1601.

[11] Vegad M., Satadia S., Pradip P., Chirag P., Bhargav P.: *Heat transfer characteristics of low Reynolds number flow of nanofluid around a heated circular cylinder*. Proc. 2nd Int. Conf. Innovations in Automation and Mechatronics Engineering, ICIAME 2014, Procedia Technology **14**(2014), 348–356.

[12] Farooji V.E., Bajestan E.E.,Niazmand H.,Wongwises S.: *Unconfined laminar nanofluid flow and heat transfer around a square cylinder*. Int. J. Heat Mass Tran. **55**(2012), 5-6, 1475–1485.

[13] Valipour M.S.,Masoodi R., Rashidi S., Bovand M., Mirhosseini M.: *A numerical study on convection around a square cylinder using AL2O3-H2O nanofluid*. Therm. Sci. **18**(2014), 4, 1305–1314.

[14] Yu W., Choi S.U.S.: *The role of interfacial layers in the enhanced thermal conductivity of nanofluids: A renovated Maxwell model*. J. Nanopart. Res. **5**(2003), 1, 167–71.

[15] Kang S., Choi H., and Lee S.: *Laminar flow past a rotating circular cylinder*. Phys. Fluids **11**(1999), 11, 3312–3321; DOI: http://dx.doi.org/10.1063/1.870190.

[16] Mittal S., Kumar B.: *Flow past a rotating cylinder*. J. Fluid Mech. **476**(2003), 303–334.

[17] Padrino J.C., Joseph D.D.: *Numerical study of the steady-state uniform flow past a rotating cylinder*. J. Fluid Mech. **557**(2006), 191–223.

[18] Stojkovic D., Breuer M., Durst F.: *Effect of high rotation rates on the laminar flow around a circular cylinder*. Phys. Fluids **14**(2002), 9, 3160–3178.

[19] *GAMBIT. Gambit User's guide V2.2*, 2001.

[20] *Fluent 6.3. User's guide*. Fluent Inc. 2006.

[21] Bouakkaz R., Talbi K., Khelil Y., Salhi F., Belghar N., Ouazizi M.: *Numerical investigation of incompressible fluid flow and heat transfer around a rotating circular cylinder*. Thermophys. Aeromech. **21**(2014), 1, 87–97.

archives
of thermodynamics
Vol. **38**(2017), No. 2, 21–60
DOI: 10.1515/aoter-2017-0009

On wave propagation in a random micropolar generalized thermoelastic medium

MANINDRA MITRA[a]
RABINDRA KUMAR BHATTACHARYYA[b*]

[a] Department of Mathematics, Presidency College, Kolkata 700073, India

[b] Department of Applied Mathematics, Calcutta University Kolkata 700009, India

Abstract This paper endeavours to study aspects of wave propagation in a random generalized-thermal micropolar elastic medium. The smooth perturbation technique conformable to stochastic differential equations has been employed. Six different types of waves propagate in the random medium. The dispersion equations have been derived. The effects due to random variations of micropolar elastic and generalized thermal parameters have been computed. Randomness causes change of phase speed and attenuation of waves. Attenuation coefficients for high frequency waves have been computed. Second moment properties have been briefly discussed with application to wave propagation in the random micropolar elastic medium. Integrals involving correlation functions have been transformed to radial forms. A special type of generalized thermo-mechanical auto-correlation functions has been used to approximately compute effects of random variations of parameters. Uncoupled problem has been briefly outlined.

Keywords: Waves; Random; Micropolar; Thermoelastic; Propagation

1 Introduction

A large number of research papers covering various branches of theoretical and computational micropolar elasticity are being reported in the literature

*Corresponding Author. Email rabindrakb@yahoo.com

every year in recent time. Eringen has published many pioneering papers and treatises on various aspects of micropolar elasticity. The coupled stress theory developed by Eringen comprises granular materials as also composite fibrous materials [1]. For this reason authors from different research fields have been taking interest in micropolar elasticity. The associated microrotational motions, spin, couple stress inertia, couple stress and distributed body couples were defined. Micropolar thermoelasticity also has become an important field of research these days. Eringen derived equations of motion, constitutive equations and boundary conditions for a class of micromorphic elastic solids whose microelements can undergo expansions or contractions defined as stretch [2]. He also defined and proposed a theory of thermomicrostretch fluids and bubbly liquids [3]. Microstretch and micropolar continua and all other aspects of micropolar studies can be found in Eringen's foundational treatise entitled *Microcontinuum Field Theories* [4]. Micropolar thermoelastcity and stretch have attracted the attention of many authors. Marin formulated some theorems on elastostatics of micropolar material with voids [5]. He investigated the behaviour of porous solids in which the matrix material is elastic and the interstices are voids of materials. In a more recent paper Marin [6] considered the concept of domain of influence in the context of displacement and microrotation fields along with the microstretch function. Marin and Lupu [7] on the other hand discussed the problem of harmonic vibrations of micropolar elastic materials under thermoelasticity. Marin and Marinescu [8] studied thermoelasticity of initially stressed bodies. Kumar [9] examined the problem of wave propagation in a micropolar viscoelastic medium under generalized thermoelasticity. Singh [10] studied plane wave propagation in a homogeneous transversely isotropic thermally conducting elastic solid with two relaxation times. Singh and Kumar [11] investigated the problem of reflection and refraction of plane waves at an interface between micropolar elastic solid and viscoelastic solid. Kumar and Deswal [12] discussed the problem of surface wave propagation in a micropolar thermoelastic medium. Kumar and Singh [13] studied effects of stretch in wave propagation in a micropolar material again under generalized thermoelasticity. Kumar and Tomar [14] studied aspects of reflected and refracted micropolar waves. Aouadi [15] considered a medium with a microstructure and derived general equations of motion and constitutive equations. On the other hand, Suiker, Borst and Chang [16] derived a second-gradient micro-polar constitutive theory on micro-mechanical modelling of granular medium. Majewski [17] dealt

with seismic rotation waves in a micropolar elastic earth. In fact varieties of papers on wave propagation in micropolar elastic, micropolar thermoelastic and coupled micropolar elastic media are being frequently reported in the literature. It is not found necessary to cite more of these recent publications simply because they fall exclusively to the non-random domain.

The present paper instead proposes to focus on the procedure to evaluate effects of random variation of parameters of the inhomogeneous micropolar medium on propagation of waves and associated phenomena. To date none other than a single paper by Mitra and Bhattacharyya [18] has appeared in the literature dwelling on randomness in relation to waves in micropolar medium.

The present paper therefore aims at investigating wave propagation phenomenon in a random generalized thermal micropolar elastic medium, and associated statistical properties such as second moment and its application. The parameters representing inhomogeneities of the coupled medium are assumed to vary slightly from their mean values. The originality of the paper lies in attempting to measure effects of random variations of parameters on wave propagation in the micropolar generalized thermoelastic medium following procedures of the authors' earlier paper [18].

The heat conduction equation and the coupling model have been chosen under the generalized thermoelasticity proposed by Lord and Shulman [19] and Green-Lindsay [20]. The details of L-S and G-L theories of generalized thermoelasticity can be found in Ignaczak and Starzewski [21] and need not to be repeated here. Generalized thermoelasticity attempts at nullifying the physical anomaly of classical thermoelasticity which insists that thermal speed assumes infinite speed at infinity ([21], p. xii). Consequently two relaxation parameters t_0, t_1, appear in the generalized model heat conduction equation.

The methodology adopted is the smooth perturbation technique enunciated by Keller [22]. Karal and Keller [23], Keller and Karal [24], Chow [25], Chen and Tien [26] and many others used it in studying elastic, electromagnetic, thermal and other waves. Bhattacharyya [27,28] and Bera [29] pursued the method in the study of wave propagation phenomena in the coupled media.

In fact the study of problems of wave propagation in random media flourished since the time of Chernov [30]. He first suggested adoption of an exponentially decaying form for a two-point dielectric correlation function. Beran and McCoy [31] proposed the technique of iterative perturbation in

studying mean field variations in the dielectric and other media. Beran, Frankenthal, Deshmukh and Whitman studied propagation of radiation in time-dependent three-dimensional random media [32]. Sobczyk studied elastic wave propagation in a discrete random medium [33]. He developed a general formalism of the analysis of coherent elastic waves in terms of scatters. In fact, Wenzel [34], Sobczyk, Wedrychowicz and Spencer [35], Frankenthal and Beran [36], Uscinski [37] and Frisch [38] have made extensive studies on various aspects of randomness in physical sciences, wave propagation phenomena and random characteristics of media. In particular, Chen and Soong [39] worked on covariance properties of waves propagating in a medium. A detailed discussion on properties and applications of random differential equations can be found, among others, in the treatise of Soong [40]. Akira Ishimaru discussed the development of the theory of wave propagation and scattering in random media in his landmark treatise on the subject [41]. Choudhury, Basu and Bhattacharyya discussed the phenomenon of wave propagation in a rotating random granular medium under generalized thermoelasticity [42]. On the basis of these citations one cannot but admit the importance of the study of randomness in applied mathematics and physical sciences. The present paper however proposes to discuss randomness in respect of waves in a micropolar medium impressed by a generalized thermoelastic field.

2 The problem

Using the smooth perturbation technique [22] the field equations have been put in the form

$$L(\vec{x},t)V(\vec{x},t) = F(\vec{x},t)\ , \tag{1}$$

$$L \ = \ L_0 \ + \ \varepsilon L_1 \ + \ \varepsilon^2 L_2\ , \tag{2}$$

where: L – random linear operator, V – field vector, F – non-random source, L_0 – unperturbed part of L, L_1, L_2 – first and second order perturbation of L respectively, and ε – small parameter measuring the scale of random fluctuation of generalized thermo-micropolar elastic inhomogeneities of the medium.

Then employing iterative operations [23] it can be shown that the mean field $\langle V\rangle$ satisfies the equation

$$[L_0 + \varepsilon\langle L_1\rangle + \varepsilon^2\{\langle L_2\rangle + \langle L_1\rangle L_0^{-1}\langle L_1'\rangle - \langle L_1 L_0^{-1} L_1'\rangle\}]\langle V\rangle = F \tag{3}$$

with

$$L_0 G_{ij}(\vec{x}, \vec{x}', t, t') = \delta(\vec{x}, \vec{x}')\delta(t, t')\delta_{ij} \ . \tag{4}$$

Here$\langle V(\vec{x}, t)\rangle$ is defined as the mean field quantity being the statistical average of the field vectors, an ensemble average. Also G_{ij} is the appropriate Green's matrix (computed in the infinite domain) for L_0, $\delta(\vec{x}, \vec{x'})$ is the Dirac delta function and δ_{ij} is the Kronecker delta. Equation (3) is evidently an integro-differential equation, as in terms of G_0, L_0^{-1} becomes

$$L_0^{-1} f = \int G(\vec{x}, \vec{x'}) f(\vec{x'}) d\vec{x'}.$$

The present analysis aims at investigating the effects of random inhomogeneities on the propagation of waves in an interacting generalized thermo-micropolar elastic medium. The equations of motion, constitutive equations and boundary conditions for the micropolar elastic field have been derived by Eringen [2]. The generalized thermal coupling is assumed to vary randomly only in the perturbed field. It may be recorded here that this assumption was necessitated to facilitate computation of the associated Green's matrix [18,25,42]. Therefore L_0 effectively represents the linear partial differential operator involving parameters of the unperturbed micropolar elastic medium only. Operator L acts on the displacement vector $\vec{u}$, the microrotation vector $\vec{\phi}$ and θ, the temperature. Six different types of body waves, which propagate in the non-random medium, depend upon the random inhomogeneities of the medium. The dispersion equations for these six longitudinal and transverse types of waves have been obtained. They involve terms up to the order of ε^2, since $\langle L_1\rangle \neq 0$ in this case. However, finally the effect of randomness comes to alter the wave number to the order of ε^2 only. Theoretically therefore the effect of randomness comes to be small to the order of ε^2. Deviations in the propagation constants from their unperturbed values have been calculated in terms of $\delta_l, \delta_n, \delta_c, \delta_s$. for different types of waves defined in the text in Sec. 4. These quantities involve auto- and cross-correlation functions between micropolar elastic and generalized thermal field parameters. Assuming simple auto-correlation functions only for density and two thermo-mechanical coupling parameters in the forms [25,29]

$$R_{\rho\rho}(r) = \langle\rho_1^2\rangle e^{-\frac{r}{a}} \ \text{ and } \ R_{mm}(r) = \langle\rho_1^2\rangle e^{-\frac{r}{b}}, R_{mm^*}(r) e^{-\frac{r}{b_1}} \ ,$$

where $\langle\rho_1^2\rangle$ is the mean square value of the perturbation density ρ_1, and a, b, b_1 are correlation lengths of inhomogeneities, and all other parameters

viz., λ, μ, α, etc., to be nonrandom, it has been shown that body waves for which the deviations are measured in terms of δ_c, δ_s, attenuate for high frequencies. It has been proved earlier [18] that second moments of the form $\langle \bar{\bar{v}}^T \bar{v} \rangle - \langle \bar{\bar{v}}^T \rangle \langle \bar{v} \rangle$ is a small quantity of the order of ε only but certainly larger than the order of ε^2, (v being the solution of the equation $Lv(\vec{x}) = 0$ referred to in Sec. 9). The same result applies in this case too. Components of associated Green's matrix which were computed earlier have been quoted in Appendix I as a ready reference. The various integrals *viz.*, a_{11}, b_{63}, etc. involving correlation functions between different micropolar, elastic and generalized thermal parameters have been reduced to radial forms; these are presented in Sec. 6. In all these cases, lengthy and cumbersome computations become unavoidable. Radial transformations ensure symmetrical propagation of radiations in all directions in the infinite medium.

Field equations for a micropolar elastic medium under the influence of a generalized thermal field are written explicitly. The displacement equation of motion in the randomly varying inhomogeneous micropolar elastic medium is written following Eringen [1] and Chow [25] as

$$\begin{aligned}&(\lambda+\mu)\vec{\nabla}(\vec{\nabla}\cdot\vec{u}) + (\mu+\kappa)\nabla^2\vec{u} + \vec{\nabla}\lambda(\vec{\nabla}\cdot\vec{u}) + \vec{\nabla}\mu\times(\vec{\nabla}\times\vec{u})\\ &+ (\vec{\nabla}(2\mu+\kappa)\cdot\vec{\nabla})\vec{u} + \vec{\nabla}\times(\kappa\vec{\phi}) - \vec{\nabla}[m\{\theta + t_1\dot{\theta}\}] + \vec{f} = \rho\ddot{\vec{u}}\,.\end{aligned} \tag{5}$$

The microrotation equation of motion is represented by [1]

$$\begin{aligned}&\kappa(\vec{\nabla}\times\vec{u}) + (\alpha+\beta)\vec{\nabla}(\vec{\nabla}\cdot\vec{\phi}) + (\vec{\nabla}\alpha(\vec{\nabla}\cdot\vec{\phi})) + \gamma\nabla^2\vec{\phi}\\ &+ \vec{\nabla}\beta\times(\vec{\nabla}\times\vec{\phi}) + \{\vec{\nabla}(\beta+\gamma)\cdot\vec{\nabla}\}\vec{\phi} - 2\kappa\vec{\phi} + \vec{l} = \rho j\ddot{\vec{\phi}}\,.\end{aligned} \tag{6}$$

Finally the generalized thermal equation is written following Ignaczak and Ostoja-Starzewski [21], Bera [29], and Singh [10] as

$$\eta[\dot{\theta} + t_0\ddot{\theta}] = \vec{\nabla}\cdot[\nu\vec{\nabla}\theta] - \theta_0 m\vec{\nabla}\cdot[\dot{\vec{u}} + \delta_{lk}t_0\ddot{\vec{u}}] + q\,, \tag{7}$$

where $\dot{\theta} = \frac{\theta(\vec{x},t)}{\partial t}$, $\ddot{\theta} = \frac{\partial^2\theta(\vec{x},t)}{\partial t^2}$, etc. Here

$\vec{u}(\vec{x},t)$	–	displacement vector,
$\vec{\phi}(\vec{x},t)$	–	microrotation vector,
$\theta(\vec{x},t)$	–	temperature,
$m(\vec{x})$	–	thermomechanical coupling parameter,
$=(\lambda+\mu)\bar{\alpha}$, $\bar{\alpha}$	–	thermal expansion coefficient,
$(\alpha,\beta,\gamma,\kappa)(\vec{x})$	–	micropolar elastic moduli,
$(\lambda,\mu)(\vec{x})=Lame'$	–	elastic parameters,
$\rho(\vec{x})$	–	mass density,
j	–	a nonrandom micropolar constant such that $j\geq 0$,
$\vec{f}(\vec{x},t),.\vec{l}(\vec{x},t),q(\vec{x},t)$	–	body force, body couple per unit mass and heat source respectively,
$\eta(\vec{x})=\rho c$, c	–	specific heat,
$\nu(\vec{x})$	–	thermal diffusivity,
$v=$	–	solution of the differential equation $Lv(\vec{x})=0$,
v_0	–	solution of the differential equation $Lv_0(\vec{x})=0$,
θ_0	–	constant reference temperature,
t_0	–	initial thermal relaxation time,
$t_1(\vec{x})$	–	thermal relaxation time, $t_1\geq t_0\geq 0$,
$\delta_{lk}=1,t_1=0,k=1$	–	for Lindsay-Shulman (L-S) model of generalized thermoelasticity,
$\delta_{lk}=0,\ t_1>0,\ k=2$	–	for Green-Lindsay (G-L) model of generalized thermoelasticity.

Let the differential operators $(M,N,R),(P,Q),(K,S)$ act respectively on $\vec{u},\vec{\phi}$, and θ. Then field Eqs. (5)–(7) can be put in matrix form:

$$LV(\vec{x},t)=\begin{bmatrix} M & P & K\\ N & Q & 0\\ R & 0 & S\end{bmatrix}(\vec{x},t)\begin{bmatrix}\vec{u}(\vec{x},t)\\ \vec{\phi}(\vec{x},t)\\ T(\vec{x},t)\end{bmatrix}=F(\vec{x},t)=\begin{bmatrix}\vec{f}(\vec{x},t)\\ \vec{l}(\vec{x},t)\\ q(\vec{x},t)\end{bmatrix}. \quad (8)$$

Differential operators $(M,P,K,N,Q,R,S)(\vec{x},t)$ are explicitly defined as

$$M\vec{u}=\rho\frac{\partial^2\vec{u}}{\partial t^2}-(\lambda+\mu)\vec{\nabla}(\vec{\nabla}\cdot\vec{u})-(\mu+\kappa)\nabla^2\vec{u}-\vec{\nabla}\lambda(\vec{\nabla}\cdot\vec{u})$$
$$-\vec{\nabla}\mu\times(\vec{\nabla}\times\vec{u})-(\vec{\nabla}(2\mu+\kappa)\cdot\vec{\nabla})\vec{u},$$

$$P\vec{\phi}=-\vec{\nabla}\times(\kappa\vec{\phi}),$$

$$K\theta=\vec{\nabla}\left[m(\theta+t_1\frac{\partial\theta}{\partial t})\right]=\vec{\nabla}(m\theta)+\vec{\nabla}(mt_1\frac{\partial\theta}{\partial t})=\left[\vec{\nabla}(m\times)+\vec{\nabla}(mt_1\frac{\partial}{\partial t})\right]\theta,$$

$$N\vec{u}=-\kappa(\vec{\nabla}\times\vec{u}),$$

$$
\begin{aligned}
&Q\vec{\phi} = \rho j\frac{\partial^2\vec{\phi}}{\partial t^2} - (\alpha+\beta)\vec{\nabla}(\vec{\nabla}\cdot\vec{\phi}) - \vec{\nabla}\alpha(\vec{\nabla}\cdot\vec{\phi}) - \gamma\nabla^2\vec{\phi} - \vec{\nabla}\beta\times(\vec{\nabla}\times\vec{\phi}) \\
&\qquad -(\vec{\nabla}(\beta+\gamma)\cdot\vec{\nabla})\vec{\phi} + 2\kappa\vec{\phi}\,, \\
&R\vec{u} = \theta_0 m\vec{\nabla}\cdot\left[\frac{\partial\vec{u}}{\partial t} + \delta_{lk}t_0\frac{\partial^2\vec{u}}{\partial t^2}\right] = \left[\theta_0 m\vec{\nabla}\cdot\left(\frac{\partial}{\partial t} + \delta_{lk}t_0\frac{\partial^2}{\partial t^2}\right)\right]\vec{u}\,, \\
&S\theta = \eta\left(\frac{\partial\theta}{\partial t} + t_0\frac{\partial^2\theta}{\partial t^2}\right) - \vec{\nabla}\cdot(\nu\nabla\theta) = \left[\eta\left(\frac{\partial}{\partial t} + t_0\frac{\partial^2}{\partial t^2}\right) - \vec{\nabla}\cdot(\nu\vec{\nabla})\right]\theta\,.
\end{aligned}
\tag{9}
$$

Next let us assume

$$
V(\vec{x},t) = \begin{bmatrix} \vec{u}(\vec{x}) \\ \vec{\phi}(\vec{x}) \\ \theta(\vec{x}) \end{bmatrix} e^{-i\omega t} = V_0(\vec{x})e^{-i\omega t}, (say) \tag{10}
$$

and

$$
F(\vec{x},t) = \begin{bmatrix} \vec{f_0}(\vec{x}) \\ \vec{l_0}(\vec{x}) \\ q_0(\vec{x}) \end{bmatrix} e^{-i\omega t} = F_0(\vec{x})e^{-i\omega t}\,. \tag{11}
$$

Here ω is the frequency of propagating wave and $i = \sqrt{-1}$. The mean field Eq. (3), involving the Green's matrix, can be put in the form

$$
\begin{aligned}
&\Big[L_0(\vec{x}) + \varepsilon\langle L_1(\vec{x})\rangle + \varepsilon^2\Big\{\langle L_2(\vec{x})\rangle + \langle L_1(\vec{x})\rangle L_0^{-1}(|\vec{x}-\vec{x}'|)\langle L_1(\vec{x}')\rangle \\
&-\langle L_1(\vec{x})L_0^{-1}(|\vec{x}-\vec{x}'|)L_1(\vec{x}')\rangle\Big\}\Big]\langle V_0(\vec{x}')\rangle = F_0\,,
\end{aligned}
\tag{12}
$$

where the associated Green's tensor is the kernel of the nonrandom operator equation represented by

$$
L_0 G_{ij}(\vec{x},\vec{x}') = \delta(\vec{x},\vec{x}')\delta_{ij}\,. \tag{13}
$$

Then Eqs. (10) and (11) redefine operators $(M,P,K,N,Q,R,S)(\vec{x},t)$ as

$$
\begin{aligned}
&M = -\rho\omega^2 - (\lambda+\mu)\vec{\nabla}(\vec{\nabla}\cdot) - (\mu+\kappa)\nabla^2 - \vec{\nabla}\lambda(\vec{\nabla}\cdot) - \vec{\nabla}\mu\times(\vec{\nabla}\times) - \Big(\vec{\nabla}(2\mu+\kappa)\cdot\vec{\nabla}\Big)\,, \\
&P = -\vec{\nabla}\times(\kappa), \\
&K = \vec{\nabla}(m\times) - i\omega\vec{\nabla}(mt_1) = \vec{\nabla}(m\times) - i\omega\vec{\nabla}(m^\bullet), m^\bullet = mt_1(say), \\
&N = -\kappa(\vec{\nabla}\times)
\end{aligned}
$$

$$Q = -\rho j\omega^2 - (\alpha+\beta)\vec{\nabla}(\vec{\nabla}\cdot) - \vec{\nabla}\alpha(\vec{\nabla}\cdot) - \gamma\nabla^2 - \vec{\nabla}\beta\times(\vec{\nabla}\times) - \{\vec{\nabla}(\beta+\gamma)\cdot\vec{\nabla}\} + 2\kappa$$
$$R = -\omega\theta_0 m\vec{\nabla}\cdot\Big[i+\delta_{lk}t_0\omega)\Big] = -i\omega\theta_0\Big[1-i\delta_{lk}t_0\omega)\Big]m(\vec{\nabla}\cdot),$$
$$S = -i\omega(1-it_0\omega)\eta - (\vec{\nabla}\cdot\Big(\nu\nabla)\Big)\,. \tag{14}$$

3 Solution

Let us assume plane wave propagation in the medium and set

$$\begin{bmatrix} \vec{u}(\vec{x}) \\ \vec{\phi}(\vec{x}) \\ \theta(\vec{x}) \end{bmatrix} = \begin{bmatrix} \vec{A} \\ \vec{B} \\ C \end{bmatrix} e^{i\vec{k}\cdot\vec{x}} \tag{15}$$

Here $\vec{k}$ indicates direction of the propagating wave and $\left|\vec{k}\right| = k$ is the wave number. Then the physical parameters $\lambda, \mu, \rho, \alpha, \beta, \gamma, \kappa, \eta, \nu, m,$ and $m^\bullet = t_1 m$, are random functions of $\vec{x}(x, y, z)$, and since random deviations are small, we write, following, Karal and Keller [22] and Chow [25]:

$$(\lambda, \mu, \rho, \alpha, \beta, \gamma, \kappa, \eta, \nu, m, m^\bullet) = (\lambda_0, \mu_0, \rho_0, \alpha_0, \beta_0, \gamma_0, \kappa_0, \eta_0, \nu_0,$$
$$m_0 = 0, m_0^\bullet = 0) + \varepsilon(\lambda_1, \mu_1, \rho_1, \alpha_1, \beta_1, \gamma_1, \kappa_1, \eta_1, \nu_1, m_1, m_1^\bullet)(\vec{x})\,, \tag{16}$$

where $(\lambda_0, ..., \nu_0)$ are constants and $(\lambda_1, ..., \nu_1, m_1, m_1^\bullet)$ are functions of $\vec{x}$ representing random fluctuations of the corresponding quantities such that

$$\langle \lambda_1, ..., \nu_1 \rangle = 0\,. \tag{17}$$

Conditions (16) and (17) ensure that fluctuations from nonrandom values of parameters remain small. It is further assumed that

$$m = \varepsilon m_1(\vec{x}), \text{ such that } \langle m_1(\vec{x})\rangle = m_2, (say), m_2 \neq 0\,,$$
$$\text{and } m^\bullet = \varepsilon m_1^\bullet(\vec{x}), \text{ such that } \langle m_1^\bullet(\vec{x})\rangle = m_3, (say), m_3 \neq 0\,. \tag{18}$$

The last two assumptions confirm that the generalized thermal field is taken to be weakly random. A new parameter $m^\bullet(\vec{x}) = (t_1 m)(\vec{x})$, is introduced characterizing the random thermal coupling with the micropolar elastic medium. By the help of Eqs. (16)–(18) one gets

$$L_0 = \begin{bmatrix} M_0 & P_0 & 0 \\ N_0 & Q_0 & 0 \\ 0 & 0 & S_0 \end{bmatrix}, \tag{19}$$

$$L_1(\vec{x}) = \begin{bmatrix} M_1 & P_1 & K_1 \\ N_1 & Q_1 & 0 \\ R_1 & 0 & S_1 \end{bmatrix} (\vec{x}) \tag{20}$$

and

$$\begin{aligned} M_0 &= -\rho_0\omega^2 - (\lambda_0+\mu_0)\vec{\nabla}(\vec{\nabla}\cdot) - (\mu_0+\kappa_0)\nabla^2 \,, \\ P_0 &= -\kappa_0(\vec{\nabla}\times) = N_0 \,, \\ Q_0 &= (2\kappa_0 - \rho_0 j\omega^2) - (\alpha_0+\beta_0)\vec{\nabla}(\vec{\nabla}\cdot) - \gamma_0\nabla^2 \,, \\ S_0 &= -i\omega(1-it_0\omega)\eta_0 - \nu_0\nabla^2 \,. \end{aligned} \tag{21}$$

The deterministic operators save S_0 are independent of generalized thermal relaxation parameters and the thermo-mechanical parameters. However the perturbed operators K_1, R_1, S_1, are characterized by $m_1, m_1^{\bullet}, t_0, t_1$, such that

$$\begin{aligned} &M_1 = -\rho_1\omega^2 - (\lambda_1+\mu_1)\vec{\nabla}(\vec{\nabla}\cdot) - (\mu_1+\kappa_1)\nabla^2 - \vec{\nabla}\lambda_1(\vec{\nabla}\cdot) - \vec{\nabla}\mu_1\times(\vec{\nabla}\times) - \\ &\{\vec{\nabla}(2\mu_1+\kappa_1)\cdot\vec{\nabla}\} \\ &P_1 = -\vec{\nabla}\times(\kappa_1), \\ &K_1 = \vec{\nabla}(m_1) - i\omega\vec{\nabla}m_1^{\bullet} \,, \\ &N_1 = -\kappa_1(\vec{\nabla}\times) \,, \\ &Q_1 = -\rho_1 j\omega^2 - (\alpha_1+\beta_1)\vec{\nabla}(\vec{\nabla}\cdot) - \vec{\nabla}\alpha_1(\vec{\nabla}\cdot) - \gamma_1\nabla^2 - \vec{\nabla}\beta_1\times(\vec{\nabla}\times) - (\vec{\nabla}(\beta_1+ \\ &\gamma_1)\cdot\vec{\nabla}) + 2\kappa_1 \,, \\ &R_1 = -i\omega\theta_0(1-i\delta_{lk}t_0\omega)m_1(\vec{\nabla}\cdot) \,, \\ &S_1 = -i\omega(1-it_0\omega)\eta_1 - \{\vec{\nabla}\cdot(\nu_1\nabla)\} \,. \end{aligned} \tag{22}$$

A computational note is given below:

$$\begin{aligned} S &= -i\omega(1-it_0\omega)\eta - (\vec{\nabla}\cdot(\nu\nabla) \\ &= -i\omega(1-it_0\omega)(\eta_0+\varepsilon\eta_1) - \vec{\nabla}\cdot[(\nu_0+\varepsilon\nu_1)\vec{\nabla}] \\ &= -i\omega(1-it_0\omega)\eta_0 - \vec{\nabla}\cdot(\nu_0\vec{\nabla}) - \varepsilon i\omega(1-it_0\omega)\eta_1 - \varepsilon\vec{\nabla}\cdot(\nu_1\vec{\nabla}) \\ &= \{-i\omega(1-it_0\omega)\eta_0 - \nu_0\nabla^2] + \{-\varepsilon i\omega(1-it_0\omega)\eta_1\varepsilon\vec{\nabla}\cdot(\nu_1\vec{\nabla})\} \\ &= S_0 + \varepsilon S_1] \,. \end{aligned}$$

By virtue of Eqs. (17)–(18) one obtains

$$\langle L_1\rangle = \begin{bmatrix} 0 & 0 & (m_2 - i\omega m_3)\vec{\nabla} \\ 0 & 0 & 0 \\ -i\omega\theta_0(1-i\delta_{lk}t_0\omega)m_2(\vec{\nabla}\cdot) & 0 & 0 \end{bmatrix} \neq 0, \tag{23}$$

where

$$m_2 = \langle m_1(\vec{x})\rangle = \text{const.} \neq 0, m_3 = \langle m_1^{\bullet}(\vec{x})\rangle = \text{const.} \neq 0 \text{ and } \langle L_2\rangle = 0\,. \tag{24}$$

Thus Eq. (3) involves first and second perturbation terms; with vanishing body force, body couple and the heat source, Eq. (12) reduces to

$$\begin{aligned}&\Big[L_0(\vec{x}) + \varepsilon\langle L_1(\vec{x})\rangle + \varepsilon^2\Big\{\langle L_1(\vec{x})\rangle L_0^{-1}(|\vec{x}-\vec{x}'|)\langle L_1(\vec{x}')\rangle\\ &-\langle L_1(\vec{x})L_0^{-1}(|\vec{x}-\vec{x}'|)L_1(\vec{x}')\rangle\Big\}\Big]\langle V_0(\vec{x}')\rangle = 0\,.\end{aligned} \tag{25}$$

The components of Green's tensor corresponding to L_0^{-1} are given by (say),

$$G_{ij} = \begin{bmatrix} G_0 & G_1 & 0\\ G_2 & G_3 & 0\\ 0 & 0 & G_4\end{bmatrix}. \tag{26}$$

The components $G_0(r), G_1(r), G_2(r)$, and $G_3(r)$ have already been evaluated [18] and have been given in the Appendix I. The component $G_4(r)$ is defined by

$$\nabla^2 G_4(r) + \frac{i\omega(1-i\omega t_0)\eta_0}{\nu_0}G_4(r) = \delta(\vec{x}-\vec{x}')\delta_{ij}\,.$$

Hence

$$G_4(r) = -\frac{e^{i\beta r}}{4\pi r}I_3\,, \tag{27}$$

where

$$\beta = \left[\frac{i\omega(1-i\omega t_0)\eta_0}{\nu_0}\right]^{\frac{1}{2}},$$

and I_3 is the identity matrix.
Hence

$$\begin{aligned}\beta &= \sqrt{\tfrac{\omega\eta_0}{2\nu_0}}\left\{\left[\sqrt{\omega^2 t_0^2 - 1} + \omega t_0\right]^{\frac{1}{2}} + i\left[\sqrt{\omega^2 t_0^2 - 1} - \omega t_0\right]^{\frac{1}{2}}\right\}\\ &= \beta_1 + i\beta_2(say).\end{aligned} \tag{28}$$

It is observed that $G_i(r), i = 0, 1, 2, 3$ are independent of thermo-mechanical coupling parameter $m(\vec{x})$ and generalized thermoelastic relaxation times t_0, t_1, and $m^{\bullet}(\vec{x})$. On the other hand $G_4(r)$ is independent of $m(\vec{x})$ but depends upon the generalized thermoelastic relaxation time t_0. Substituting (15) in the mean field Eq. (25) one gets the following three vector equations:

$$[\rho_0\omega^2\vec{A}-(\lambda_0+\mu_0)(\vec{k}\cdot\vec{A})\vec{k}-(\mu_0+\kappa_0)k^2\vec{A}]+i\kappa_0(\vec{k}\times\vec{B})-\varepsilon(im_2+\omega m_3)C\vec{k}$$
$$+\varepsilon^2\left[\omega\theta_0(1-\omega t_0\delta_{lk})m_2(m_2-i\omega m_3)(\vec{k}\cdot\vec{A})\right]\int\left[(\vec{\nabla}G_4)\right]e^{-i\vec{k}\cdot\vec{r}}d\vec{r}$$
$$-\varepsilon^2\int\left[\begin{array}{l}\langle[M_1\{G_0(M_1'\vec{A}+P_1'\vec{B}+K_1'C)+G_1(N_1'\vec{A}+Q_1'\vec{B})\}\\+P_1\{G_2(M_1'\vec{A}+P_1'\vec{B}+K_1'C)+G_3(N_1'\vec{A}+Q_1'\vec{B})\}\\+K_1G_4(R_1'\vec{A}+S_1'C)]\rangle\end{array}\right]e^{-i\vec{k}\cdot\vec{r}}d\vec{r}=0, \tag{29}$$

$$i\kappa_0(\vec{k}\times\vec{A})-[(2\kappa_0-\rho_0 j\omega^2+\gamma_0k^2)\vec{B}+(\alpha_0+\beta_0)(\vec{k}\cdot\vec{B})\vec{k}]$$
$$-\varepsilon^2\int\left[\begin{array}{l}\langle[N_1\{G_0(M_1'\vec{A}+P_1'\vec{B}+K_1'C)+G_1(N_1'\vec{A}+Q_1'\vec{B})\}\\+Q_1\{G_2(M_1'\vec{A}+P_1'\vec{B}+K_1'C)+G_3(N_1'\vec{A}+Q_1'\vec{B})\}]\rangle\end{array}\right]e^{-i\vec{k}\cdot\vec{r}}d\vec{r}=0, \tag{30}$$

and

$$[i\omega(1-it_0\omega)\eta_0-\nu_0k^2]C-\varepsilon\omega\theta_0(1-i\omega t_0\delta_{lk})m_2(\vec{k}\cdot\vec{A})$$
$$+\varepsilon^2[\omega\theta_0(1-i\omega t_0\delta_{lk})m_2(m_2-i\omega m_3)]C\int[(\vec{\nabla}\cdot G_0\vec{k})]e^{-i\vec{k}\cdot\vec{r}}d\vec{r}$$
$$-\varepsilon^2\int\left[\begin{array}{l}\langle[R_1\{G_0(M_1'\vec{A}+P_1'\vec{B}+K_1'C)+G_1(N_1'\vec{A}+Q_1'\vec{B})\}\\+S_1G_4(R_1'\vec{A}+S_1'C)]\rangle\end{array}\right]e^{-i\vec{k}\cdot\vec{r}}d\vec{r}=0. \tag{31}$$

Eliminating C from (29) and (30) with the help of (31) one gets the following two equations:

$$[\rho_0\omega^2\vec{A}-(\lambda_0+\mu_0)(\vec{k}\cdot\vec{A})\vec{k}-(\mu_0+\kappa_0)k^2\vec{A}]+i\kappa_0(\vec{k}\times\vec{B})$$
$$-\varepsilon^2\frac{\omega\theta_0(1-i\omega t_0\delta_{lk})m_2(im_2+\omega m_3)(\vec{k}\cdot\vec{A})}{i\omega(1-it_0\omega)\eta_0-\nu_0k^2}\vec{k}$$
$$+\varepsilon^2\left[\omega\theta_0(1-\omega t_0\delta_{lk})m_2(m_2-i\omega m_3)(\vec{k}\cdot\vec{A})\right]\int\left[(\vec{\nabla}G_4)\right]e^{-i\vec{k}\cdot\vec{r}}d\vec{r}$$
$$-\varepsilon^2\int\left[\begin{array}{l}[\langle M_1G_0M_1'\rangle\vec{A}+\langle M_1G_0P_1'\rangle\vec{B}+\langle M_1G_1N_1'\rangle\vec{A}\\+\langle M_1G_1Q_1'\rangle\vec{B}+\langle P_1G_2M_1'\rangle\vec{A}+\langle P_1G_2P_1'\rangle\vec{B}\\+\langle P_1G_3N_1'\rangle\vec{A}+\langle P_1G_3Q_1'\rangle\vec{B}+\langle K_1G_4R_1'\rangle\vec{A}]\end{array}\right]e^{-i\vec{k}\cdot\vec{r}}d\vec{r}=0, \tag{32}$$

and

$$i\kappa_0(\vec{k}\times\vec{A})-[(2\kappa_0-\rho_0 j\omega^2+\gamma_0 k^2)\vec{B}+(\alpha_0+\beta_0)(\vec{k}\cdot\vec{B})\vec{k}]$$
$$-\varepsilon^2\int\begin{bmatrix}\langle N_1G_0M_1'\rangle\vec{A}+\langle N_1G_0P_1'\rangle\vec{B}+\langle N_1G_1N_1'\rangle\vec{A}\\+\langle N_1G_1Q_1'\rangle\vec{B}+\langle Q_1G_2M_1'\rangle\vec{A}+\langle Q_1G_2P_1'\rangle\vec{B}\\+\langle Q_1G_3N_1'\rangle\vec{A}+\langle Q_1G_3Q_1'\rangle\vec{B}\end{bmatrix}e^{-i\vec{k}\cdot\vec{r}}d\vec{r}=0\,. \tag{33}$$

Some computations of the form

$$\langle M_1G_oM_1'\rangle\vec{A}=e^{-i\vec{k}\cdot\vec{x}'}\langle M_1G_oM_1'\rangle(\vec{A}e^{i\vec{k}\cdot\vec{x}'})\,,$$

are shown in the Appendix II. The integral in the third term of (32)

$$=\int[\vec{\nabla}(G_4(r)]e^{-i\vec{k}\cdot\vec{r}}d\vec{r}$$

$$=-i\hat{k}\int_0^\infty e^{i\beta r}\sin krdr,\beta=\beta_1+i\beta_2,\beta_1=Re\beta,\beta_2=\mathrm{Im}\beta. \tag{34}$$

$$=\frac{-i\hat{k}}{2}\left[\frac{\beta_1+k}{\beta_2^2+(\beta_1+k)^2}-\frac{\beta_1-k}{\beta_2^2+(\beta_1-k)^2}\right.$$
$$\left.+i\beta_2\left(\frac{1}{\beta_2^2+(\beta_1-k)^2}-\frac{1}{\beta_2^2+(\beta_1+k)^2}\right)\right]. \tag{35}$$

Hence (32) can be rewritten as

$$[\rho_0\omega^2\vec{A}-(\lambda_0+\mu_0)(\vec{k}\cdot\vec{A})\vec{k}-(\mu_0+\kappa_0)k^2\vec{A}]+i\kappa_0(\vec{k}\times\vec{B})$$
$$-\varepsilon^2\frac{\omega\theta_0(1-i\omega t_0\delta_{lk})m_2(im_2+\omega m_3)(\vec{k}\cdot\vec{A})}{i\omega(1-it_0\omega)\eta_0-\nu_0k^2}\vec{k}$$

$$-\varepsilon^2\left[\omega\theta_0(1-\omega t_0\delta_{lk})m_2(im_2+\omega m_3)(\vec{k}\cdot\vec{A})\ \widehat{k}\right]\int_0^\infty e^{i\beta r}\sin krdr$$

$$-\varepsilon^2\int\begin{bmatrix}[\langle M_1G_0M_1'\rangle\vec{A}+\langle M_1G_0P_1'\rangle\vec{B}+\langle M_1G_1N_1'\rangle\vec{A}\\+\langle M_1G_1Q_1'\rangle\vec{B}+\langle P_1G_2M_1'\rangle\vec{A}+\langle P_1G_2P_1'\rangle\vec{B}\\+\langle P_1G_3N_1'\rangle\vec{A}+\langle P_1G_3Q_1'\rangle\vec{B}+\langle K_1G_4R_1'\rangle\vec{A}]\end{bmatrix}e^{-i\vec{k}\cdot\vec{r}}d\vec{r}=0. \tag{36}$$

Thus we are left with two vector Eqs. (36) and (33), determining the propagation of waves in the interacting random medium. It is to be noted that none of these equations include any term of the order of ε even though $\langle L_1\rangle\langle V_0(\vec{x})\rangle\neq 0$. Effects of randomness therefore is small to the order of ε^2.

4 Analysis of first perturbation dispersion equations

We get back to considering Eqs. (29)–(31) to ε-order terms only, assuming without loss of generality:

$$\vec{k} = (k, 0, 0), \quad \vec{A} = (A_1, A_2, 0), \quad \vec{B} = (B_1, B_2, B_3)\,. \tag{37}$$

Hence (29)–(31) reduce to

$$[\rho_0\omega^2\vec{A} - (\lambda_0+\mu_0)(\vec{k}\cdot\vec{A})\vec{k} - (\mu_0+\kappa_0)k^2\vec{A}] + i\kappa_0(\vec{k}\times\vec{B}) - \varepsilon(im_2+\omega m_3)C\vec{k} = 0, \tag{38}$$

$$i\kappa_0(\vec{k}\times\vec{A}) - [(2\kappa_0 - \rho_0 j\omega^2 + \gamma_0 k^2)\vec{B} + (\alpha_0+\beta_0)(\vec{k}\cdot\vec{B})\vec{k}] = 0, \tag{39}$$

and

$$[i\omega(1 - it_0\omega)\eta_0 - \nu_0 k^2]C - \varepsilon\omega\theta_0(1 - i\omega t_0\delta_{lk})m_2(\vec{k}\,\vec{A}) = 0. \tag{40}$$

Eliminating C as before from Eq. (38) one gets

$$\begin{aligned}&[\rho_0\omega^2\vec{A} - (\lambda_0+\mu_0)(\vec{k}\cdot\vec{A})\vec{k} - (\mu_0+\kappa_0)k^2\vec{A}] + i\kappa_0(\vec{k}\times\vec{B})\\ &-\varepsilon^2(im_2+\omega m_3)\frac{\omega\theta_0(1 - i\omega t_0\delta_{lk})m_2(\vec{k}\cdot\vec{A})}{i\omega(1 - it_0\omega)\eta_0 - \nu_0 k^2}\vec{k} = 0\,.\end{aligned} \tag{41}$$

Thus (39) and (41) represent two dispersion equations. Terms to the order ε however disappears from these equations. The equations almost reduce to two deterministic equations except for the presence of a second perturbation term in (41) inducing a weak thermoelastic influence on propagation of waves. These equations lead to the following six equations:

$$[\rho_0\omega^2 - (\lambda_0+2\mu_0+\kappa_0)k^2]A_1 - \varepsilon^2(im_2+\omega m_3)\frac{\omega\theta_0(1 - i\omega t_0\delta_{lk})m_2k^2}{i\omega(1 - it_0\omega)\eta_0 - \nu_0 k^2}A_1 = 0\,, \tag{42}$$

$$[\rho_0\omega^2 - (\mu_0+\kappa_0)k^2]A_2 + i\kappa_0 kB_3 = 0\,, \tag{43}$$

$$i\kappa_0 kB_2 = 0\,.$$

This last equation indicates

$$B_2 = 0\,. \tag{44}$$

This indicates that microrotation waves do not propagate along the direction of B_2. Also Eq. (39) gives three Eqs. (45), (46), and (47):

$$(2\kappa_0 - \rho_0 j\omega^2 + \gamma_0 k^2) + (\alpha_0+\beta_0)k^2]B_1 = 0 \tag{45}$$

and

$$(2\kappa_0 - \rho_0 j\omega^2 + \gamma_0 k^2)B_2 = 0\,.$$

This indicates that $B_2 = 0$, but

$$2\kappa_0 - \rho_0 j\omega^2 + \gamma_0 k^2 \neq 0\,. \tag{46}$$

This confirms that there is no propagation along the direction of B_2. The third equation is

$$i\kappa_0 k A_2 - (2\kappa_0 - \rho_0 j\omega^2 + \gamma_0 k^2) B_3 = 0\,. \tag{47}$$

The dispersion equation for longitudinal waves propagating along the direction of $\vec{k}$ is represented by (42), that is, by

$$\left[\rho_0\omega^2 - (\lambda_0 + 2\mu_0 + \kappa_0)k^2\right] - \varepsilon^2(im_2 + \omega m_3)\frac{\omega\theta_0(1 - i\omega t_0\delta_{lk})m_2 k^2}{i\omega(1 - it_0\omega)\eta_0 - \nu_0 k^2} = 0\,. \tag{48}$$

This is a fourth degree equation in the wave number k. From Eq. (48) effects of randomness of the generalized thermal field determined by the presence of m_2, and m_3 is discernible to terms to the order of ε^2.

Equation (45) determines the propagation of microrotation waves along the direction of B_1; the wave number is determined by

$$k^2 = \frac{\rho_0 j\omega^2 - 2\kappa_0}{\alpha_0 + \beta_0 + \gamma_0}\,. \tag{49}$$

Waves having amplitudes A_2 and B_3 are coupled by Eqs. (43) and (47). Eliminating A_2 and B_3 one gets the dispersion equation for the propagation of coupled waves in the form

$$\frac{A_2}{B_3} = -\frac{i\kappa_0 k}{\rho_0\omega^2 - (\mu_0 + \kappa_0)k^2} = \frac{2\kappa_0 - \rho_0 j\omega^2 + \gamma_0 k^2}{i\kappa_0 k}\,,$$

or

$$\left[\rho_0\omega^2 - (\mu_0 + \kappa_0)k^2\right]\left[2\kappa_0 - \rho_0 j\omega^2 + \gamma_0 k^2\right] = \kappa_0^2 k^2\,. \tag{50}$$

This equation which is again a fourth degree equation in the wave number k however determines the dispersion equation of waves propagating in the non-thermal micropolar elastic medium. Equation (48) only includes one ε^2-order term which represents small generalized thermal effects. Equations (48), (49), and (50) can easily be solved numerically.

5 Analysis of dispersion equations

We proceed to analyze dispersion Eqs. (33) and (36). Each term of the form $\int\langle M_1 G_0 M_1'\rangle \vec{A}e^{i\vec{k}\cdot\vec{x}'}$ contains linear functions of the displacement amplitudes, A_1, A_2, A_3, and the microrotation amplitudes B_1, B_2, B_3. Each of the integrals involves correlation functions between different micropolar elastic and generalized thermal parameters including the generalized thermomechanical coupling parameters m and $m^\bullet$. It is observed that none of the integrands of the forms $\langle M_1 G_0 M_1'\rangle \vec{A}e^{i\vec{k}\cdot\vec{x}'}$ contains the perturbed operator S_1. Thus wave propagation in the coupled random medium is independent of the perturbation in the classical thermal parameters $\eta(\vec{x})$ and $\nu(\vec{x})$. Moreover the only integrand representing effects of random variation of generalized thermal field is $\langle K_1 G_4 R_1'\rangle \vec{A}e^{i\vec{k}\cdot\vec{x}'}$. The integrand involves the random coupling variable $m^\bullet$. In a latter section we will analyze (33) and (36) retaining the integral $\int\langle K_1 G_4 R_1'\rangle \vec{A}e^{i\vec{k}\cdot\vec{x}'}d\vec{x}'$ and making all other correlation functions vanish.

Now equations (36) and (33) give rise to six equations. Then terms of the order ε^2 in each of these equations are arranged as linear combinations of five amplitudes A_1, A_2, B_1, B_2, B_3, the coefficients of each of which being integrals involving different correlation functions. Rewriting one gets:

$$\begin{aligned}&\left[\rho_0\omega^2-(\lambda_0+2\mu_0+\kappa_0)k^2\right]A_1-\varepsilon^2\tfrac{\omega\theta_0(1-i\omega t_0\delta_{lk})m_2(im_2+\omega m_3)k^2}{i\omega(1-it_0\omega)\eta_0-\nu_0k^2}A_1\\&-\varepsilon^2\omega\theta_0(1-i\omega t_0\delta_{lk})m_2(im_2+\omega m_3)kA_1\int_0^\infty e^{i\beta r}\sin krdr\\&-\varepsilon^2[a_{11}A_1+a_{12}A_2+b_{11}B_1+b_{12}B_2+b_{13}B_3]=0\,,\end{aligned}\tag{51}$$

$$\begin{aligned}&[\rho_0\omega^2-(\mu_0+\kappa_0)k^2]A_2-i\kappa_0kB_3\\&\quad-\varepsilon^2[a_{21}A_1+a_{22}A_2+b_{21}B_1+b_{22}B_2+b_{23}B_3]=0\,,\end{aligned}\tag{52}$$

$$i\kappa_0kB_2-\varepsilon^2[a_{31}A_1+a_{32}A_2+b_{31}B_1+b_{32}B_2+b_{33}B_3]=0\,,\tag{53}$$

$$\begin{aligned}&[\rho_0j\omega^2-2\kappa_0-(\alpha_0+\beta_0+\gamma_0)k^2]B_1\\&\quad-\varepsilon^2[a_{41}A_1+a_{42}A_2+b_{41}B_1+b_{42}B_2+b_{43}B_3]=0\,,\end{aligned}\tag{54}$$

$$(\rho_0j\omega^2-2\kappa_0-\gamma_0k^2)B_2-\varepsilon^2[a_{51}A_1+a_{52}A_2+b_{51}B_1+b_{52}B_2+b_{53}B_3]=0\,,\tag{55}$$

$$\begin{aligned}&i\kappa_0kA_2+(\rho_0j\omega^2-2\kappa_0-\gamma_0k^2)B_3\\&\quad-\varepsilon^2[a_{61}A_1+a_{62}A_2+b_{61}B_1+b_{62}B_2+b_{63}B_3]=0\,.\end{aligned}\tag{56}$$

The integrands in the coefficients, a_{lj} and $b_{lk}(l = 1, 2, ..., 6; j = 1, 2; k = 1, 2, 3)$, are long expressions involving: (i) components of Green's tensor and their first and second order derivatives with respect to Cartesian coordinates, and (ii) various correlation functions (there are 49+2 in all, the last two being the auto-correlation function of the non-generalized thermo-mechanical coupling parameter and the cross-correlation function between the two thermo-mechanical coupling parameters) and their first and second order derivatives with respect to Cartesian coordinates.

6 Transformation to radial forms

The transformation of these integrals from Cartesian to radial forms are therefore carried out under the substitutions

$$\vec{r} = \vec{x} - \vec{x}' = (\xi, \eta, \zeta) = (r\cos\theta,\ r\sin\theta\cos\phi,\ r\sin\theta\sin\phi)$$

so that

$$\frac{\partial}{\partial x} = \frac{\partial}{\partial \xi} = -\frac{\partial}{\partial x'}\,, \quad \text{etc.} \tag{57}$$

The Green's tensor and the correlation functions are all functions of $r = |\vec{r}|$ alone. Thus 30 coefficients a_{lj} and b_{lk} are all functions of the wave number k alone. The expressions for $a_{11}, a_{22}, a_{62}, b_{23}, b_{51}, b_{63}$, which enter into the dispersion relations governing wave propagation in the medium are transformed into radial forms; the other coefficients which involve similar lengthy and cumbersome expressions are omitted. The expression for a_{11} dependent on thermal parameters is computed as

$$
\begin{aligned}
a_{11} = {} & 4\pi k \int_0^\infty r^2 [\{kR_1 - \frac{1}{k}\omega^2 (R_{\lambda\rho} + R_{\mu\rho})\}\{f'(G_1)''_{11} + \frac{(G_1)'_{11}}{r}(f + f'')\} - R'_1\{f'''(G_1)''_{11} \\
& - \frac{1}{r}(G_1)'_{11}(f' + f''')\} + \frac{1}{2}(R'_{\lambda\lambda} + R'_{\mu\lambda})\{G_1)''_{11} + (G_1)''_{33} - \frac{1}{r}((G_1)'_{11} + (G_1)'_{33})\}(f' + f''') \\
& + ((G_1)''_{11} + 2(G_1)'_{11})[\{\frac{1}{k}\omega^2 (R_{\mu\rho} + R_{\kappa\rho}) - kR_2\}f + \frac{1}{k}R'_2 f'] + (G_1)'_{11}[k\{(R'_1 + R'_2)f'' + \\
& R'_2(f + f'')\} - R''_{\lambda\lambda} f''' - \frac{1}{r}R'_{\lambda\lambda}(f' + f''')] + \frac{1}{2}[(R''_{\lambda\lambda} - \frac{1}{2}R'_{\lambda\lambda})((G_1)'_{11} + (G_1)'_{33}) + (R''_{\mu\lambda} - \frac{1}{r}R'_{\mu\lambda}) \\
& \{(G_1)'_{33} f' + (f' + f''')(G_1)'_{11}\}] + \frac{1}{r}R'_{\mu\lambda} f'((G_1)'_{11} + (G_1)'_{33}) + (R''_2 - \frac{1}{r}R'_2)(G_1)'_{11}(f' + f''') \\
& - \omega^2[\frac{1}{k}(G_1)'_{11}\{f''(R'_{\lambda\rho} + 2R'_{\mu\rho} + R'_{\kappa\rho}) + (R_{\mu\rho} + R_{k\rho})(f + f'')\} - (G_1)_{11}\{\frac{1}{k}f\omega^2 R_{\rho\rho} \\
& - kf(R_{\rho\lambda} + 2R_{\rho\mu} + R_{\rho\kappa}) + f'(R'_{\rho\lambda} + 2R'_{\rho\mu} + R'_{\rho\kappa})\}] dr \\
& - 4i\pi k\omega\theta_0(1 - i\delta_{lk}t_0\omega k)\int_0^\infty [(R_{mm} - i\omega R_{mm\bullet})G'_4 + (R'_{mm} - i\omega R'_{mm\bullet})G_4]r^2 f' dr.
\end{aligned}
\tag{58}
$$

where

$$
\begin{aligned}
R_1(r) &= \langle(\lambda_1 + \mu_1)(\lambda'_1 + 2\mu'_1 + \kappa'_1)\rangle\ , \\
R_2(r) &= \langle(\mu_1 + \kappa_1)(\lambda'_1 + 2\mu'_1 + \kappa'_1)\rangle\ , \\
R_{\lambda\rho}(r) = \langle\lambda_1\rho'_1\rangle, R_{mm}(r) &= \langle mm'\rangle, R_{mm\bullet}(r) = \langle mm^{\bullet\prime}\rangle, \text{etc.} \\
\lambda_1 = \lambda_1(\vec{x}), \lambda'_1 &= \lambda'_1(\vec{x}'), \\
m_1 = m_1(\vec{x}),\ m_1^\bullet &= m_1 t = m_1^\bullet(\vec{x}), \\
m'_1 = m_1(\vec{x}'),\ m_1^{\bullet\prime} &= m_1 t = m_1^\bullet(\vec{x}'), \text{etc.}
\end{aligned}
\tag{59}
$$

and

$$
\begin{aligned}
f &= \frac{\sin kr}{kr},\ f' = \frac{df}{d(kr)} \\
(G_1)'_{11} &= \frac{d(G_1)_{11}}{dr}\ ,\quad R'_1 = \frac{dR_1}{dr},\ etc. \\
R_7(r) &= \left\langle(\alpha_1 + \beta_1)(2\kappa'_1 - j\omega^2\rho'_1)\right\rangle\ .
\end{aligned}
\tag{60}
$$

The radial expressions for coefficients $a_{22}, a_{62}, b_{23}, b_{51}, b_{63}$, which are independent of thermal field can be found in [18]. However the expression for b_{63} is reproduced illustratively as also as a ready reference for the analysis given below.

$$
\begin{aligned}
b_{63} = 4\pi k\int_0^\infty r^2[&\{R_{\kappa\kappa}f' + \frac{1}{k}R'_{\kappa\kappa}f'' + \frac{1}{2k}R'_{\kappa\kappa}(f+f')\}(G_1)'_{11} - \frac{1}{2k}\{k^2(R_{\alpha\gamma}+R_{\beta\gamma})+R_7\}\\
&\{\frac{2}{r}f(G_4)'_{33} + (f+f'')(\frac{1}{r}(G_4)'_{33} - (G_4)''_{33})\} + \frac{1}{2}(R'_{\alpha\beta}+R'_{\beta\beta})((G_4)''_{11} - (G_4)'_{11})\\
&(f'+f'') + (R'_{\alpha\gamma}+R'_{\beta\gamma})\{\frac{1}{r}f'(G_4)'_{33} + \frac{1}{2}(f'+f''')((G_4)''_{33} - \frac{1}{r}(G_4)'_{33})\} + \frac{1}{2k}(k^2R'_{\alpha\gamma}\\
&+2R'_{\alpha\kappa} - j\omega^2R_{\alpha\rho})(f+f'')(G_4)'_{33} + \{\frac{1}{2}(R''_{\alpha\beta}-R'_{\alpha\beta})(f'+f''') + R'_{\alpha\beta}f'\}(G_4)'_{11}\\
&+\frac{1}{2}(R''_8 - R'_8)(f'+f''')(G_4)'_{33} + \{R'_{\gamma\gamma}f' - \frac{1}{k}(R_{\gamma\gamma}k^2 + 2R_{\gamma\kappa} - j\omega^2R_{\gamma\rho})f\}\{(G_4)''_{33} + \frac{2}{r}(G_4)'_{33}\}\\
&+\frac{1}{2k}(G_4)'_{33}[f''\{R_9 + k^2(R'_{\beta\gamma}+4R'_{\gamma\gamma})\} + \{k^2(R'_{\beta\gamma}+2R'_{\gamma\gamma})+R_{10}\}f] + \frac{1}{2}(R''_{\beta\beta} - \frac{1}{r}R'_{\beta\beta})\\
&(G_4)'_{11}(f'+f''') + (G_4)'_{33}[R''_{\gamma\gamma}f + \frac{1}{2}(f'+f''')(R''_{\beta\gamma} - \frac{1}{r}R'_{\beta\gamma})] + [k(2R_{\kappa\gamma} - j\omega^2R_{\beta\gamma}) + \frac{1}{k}R_{11}]\\
&\times f(G_4)_{33} - (G_4)'_{33}f'(2R'_{\kappa\beta} - j\omega^2R'_{\rho\beta})]dr
\end{aligned}
\tag{61}
$$

where

$$
\begin{aligned}
R_7(r) &= \langle(\alpha_1+\beta_1)(2\kappa'_1 - j\omega^2\rho'_1)\rangle,\\
R_8(r) &= \langle(\alpha_1+\beta_1+\gamma_1)\gamma'_1\rangle,\\
R_9(r) &= \langle(\beta_1+4\gamma_1)(2\kappa'_1 - j\omega^2\rho'_1)\rangle,\\
R_{10}(r) &= \langle(\beta_1+2\gamma_1)(2\kappa'_1 - j\omega^2\rho'_1)\rangle,\\
R_{11}(r) &= \langle(2\kappa_1 - j\omega^2\rho_1)(2\kappa'_1 - j\omega^2\rho'_1)\rangle =\\
&= 4\langle\kappa_1\kappa'_1\rangle - 2j\omega^2[\langle\rho_1\kappa'_1\rangle + \langle\rho'_1\kappa'_1\rangle] + j^2\omega^4\langle\rho_1\rho'_1\rangle.
\end{aligned}
\tag{62}
$$

7 Analysis of equations (51)–(56)

(i) Let

$$
k^2 = k_l^2 + \varepsilon^2\delta_l\,, \tag{63}
$$

where

$$
k_l^2 = \frac{\rho_0\omega^2}{\alpha_0+\beta_0+\gamma_0} \tag{64}
$$

be taken as a solution of Eqs. (51)–(56). Substituting in (54) one gets the equation

$$
\begin{aligned}
&\{-[2\kappa_0 - \rho_0 j\omega^2 + (\alpha_0+\beta_0+\gamma_0)]k_l^2\}B_1\\
&-\varepsilon^2\{[a_{41}A_1 + a_{42}A_2 + [b_{41} + (\alpha_0+\beta_0+\gamma_0)\delta_l]B_1 +\\
&b_{42}B_2 + b_{43}B_3]_{k=k_l}\} = 0.
\end{aligned}
$$

Hence

$$B_1 \approx O(\varepsilon^2) \ . \tag{65}$$

Similarly it can be shown from Eq. (57) that

$$B_2 \approx O(\varepsilon^2) \ . \tag{66}$$

From (52) one gets

$$\begin{aligned}&\left[\rho_0\omega^2 - (\mu_0+\kappa_0)k_l^2\right]A_2 - i\kappa_0 k_l B_3\\ &-\varepsilon^2\left[a_{21}A_1 + \left\{a_{22} + (\mu_0+\kappa_0)\delta_l\right\}A_2 + b_{21}B_1 + b_{22}B_2 + \right.\\ &\left.\left\{b_{23} - \tfrac{i\kappa_0}{2k_l}\right\}B_3\right]_{k=k_l} = 0 \ .\end{aligned}$$

Similarly from (56) one gets

$$\begin{aligned}&i\kappa_0 k_l A_2 + (\rho_0 j\omega^2 - 2\kappa_0 - \gamma_0 k_l^2)B_3\\ &-\varepsilon^2\left[a_{61}A_1 + (a_{62} + \tfrac{i\kappa_0}{2k_l})A_2 + b_{61}B_1 + b_{62}B_2 + (\gamma_0\delta_l + b_{63})B_3\right]_{k=k_l} = 0.\end{aligned}$$

Thus from these two equations it can be concluded that for finite A_1

$$A_2 \approx O(\varepsilon^2) \ \text{ and } \ B_3 \approx O(\varepsilon^2) \ . \tag{67}$$

Lastly the first Eq. (51) becomes, on neglecting A_2, B_1, B_2, and B_3, as these amplitudes are small to the order ε^2 only:

$$\begin{aligned}&\left[\rho_0\omega^2 - (\lambda_0+2\mu_0+\kappa_0)(k_l^2+\varepsilon^2\delta_l)\right]A_1\\ &-\varepsilon^2\tfrac{\omega\theta_0(1-i\omega t_0\delta_{lk})m_2(im_2+\omega m_3)k_l^2}{i\omega(1-it_0\omega)\eta_0-\nu_0 k_l^2}A_1\\ &-\varepsilon^2\omega\theta_0(1-i\omega t_0\delta_{lk})m_2(im_2+\omega m_3)k_l A_1\int_0^{\infty} e^{i\beta r}\sin k_l r\,dr\\ &-\varepsilon^2[a_{11}]_{k=k_l}A_1 = 0.\end{aligned}$$

Rewriting, one obtains, assuming A_1 to be finite,

$$-(\lambda_0+2\mu_0+\kappa_0)\varepsilon^2\delta_l A_1 + \varepsilon^2 D_3 A_1 + \varepsilon^2 D_4 A_1 - \varepsilon^2 a_{11}(k_l)A_1 = 0 \ ,$$

where

$$\begin{aligned}D_3(k_l) &= -\frac{\omega\theta_0(1-i\omega t_0\delta_{lk})m_2(im_2+\omega m_3)k^2}{i\omega(1-it_0\omega)\eta_0-\nu_0 k^2} \ ,\\ D_4(k_l) &= -\omega\theta_0(1-i\omega t_0\delta_{lk})m_2(im_2+\omega m_3)k_l\int_0^{\infty} e^{i\beta r}\sin k_l r\,dr \ .\end{aligned}$$

Hence

$$\delta_l = \frac{D_3(k_l) + D_4(k_l) - a_{11}(k_l)}{\lambda_0 + 2\mu_0 + \kappa_0} \,. \tag{68}$$

where

$$\begin{aligned} D_3(k_l) &= -\frac{\omega\theta_0(1 - i\omega t_0\delta_{lk})m_2(im_2 + \omega m_3)k^2}{i\omega(1 - it_0\omega)\eta_0 - \nu_0 k^2} \\ &= \frac{-\omega\theta_0 m_2^2 k^2(1 - it_0\omega)\left[(\omega\eta_0 - \nu_0 k^2) + it_0\omega\eta_0\right]}{(\omega\eta_0 - \nu_0 k^2)^2 + (t_0\omega\eta_0)^2}, t_1 = 0, \delta_{lk} = 1, (L - S), \\ &= \frac{-\omega\theta_0 m_2 k^2\left[(m_2 - i\omega m_3)(\omega\eta_0 - \nu_0 k^2) + it_0\omega\eta_0\right]}{(\omega\eta_0 - \nu_0 k^2)^2 + (t_0\omega\eta_0)^2}, \delta_{lk} = 0, t_1 > 1, (G - L). \end{aligned} \tag{69}$$

and

$$\begin{aligned} &D_4(k_l) = -\omega\theta_0(1 - i\omega t_0\delta_{lk})m_2(im_2 + \omega m_3)k_l \int_0^\infty e^{i\beta r} \sin k_l r dr \\ &= -\omega\theta_0 m_2^2 k_l[t_0\omega + i] \int_0^\infty e^{i\beta r} \sin k_l r dr,\ t_1 = 0, \delta_{lk} = 1, (L - S), \\ &= -\omega\theta_0 m_2 k_l[\omega m_3 + im_2] \int_0^\infty e^{i\beta r} \sin k_l r dr,\ t_1 > 0, \delta_{lk} = 0, (G - L). \end{aligned} \tag{70}$$

Thus Eq. (68) determines δ_l given by (63). The integral in D_4 can be easily evaluated. The change in wave number δ_l which is small therefore depends upon the random variation of the generalized thermal field and measured in terms of statistical means, m_2, m_3, for both L-S and G-L theories. For L-S, the change depends upon m_2 only, and for G-L upon m_2, m_3, (for, L-S, $t_1 = 0, \delta_{lk} = 1, k = 1$, and for G-L, $t_1 > 0, \delta_{lk} = 0, k = 2$. Generalized thermal relaxation times t_0 and t_1 satisfy ([10,21,29,42]) the inequalities $t_1 \geq t_0 \geq 0$).

Thus it is observed that for waves for which the wave number k satisfies Eqs. (63)–(64), the amplitude A_1 is important in comparison to other amplitudes A_2, B_1, B_2, and B_3. Therefore Eq. (63), which represents longitudinal type of displacement waves, is modified due to random fluctuation of inhomogeneities of the medium such that the wave number is increased by $\varepsilon^2 \frac{\delta_l}{2k_l}$.

(ii) Next let us consider waves for which

$$k^2 = k_n^2 + \varepsilon^2\delta_n, \quad \text{where } k_n^2 = \frac{\rho_0 j\omega^2 - 2\kappa_0}{\alpha_0 + \beta_0 + \gamma_0} \,. \tag{71}$$

From (51) one gets

$$[\rho_0\omega^2 - (\lambda_0 + 2\mu_0 + \kappa_0)k_n^2]A_1 - \varepsilon^2(\lambda_0 + 2\mu_0 + \kappa_0)\delta_n A_1$$
$$-\varepsilon^2 \frac{\omega\theta_0(1 - i\omega t_0\delta_{lk})m_2(im_2 + \omega m_3)k_n^2}{i\omega(1 - it_0\omega)\eta_0 - \nu_0 k^2} A_1$$
$$-\varepsilon^2\omega\theta_0(1 - i\omega t_0\delta_{lk})m_2(im_2 + \omega m_3)k_n A_1 \int_0^\infty e^{i\beta r}\sin k_n r dr$$
$$-\varepsilon^2[a_{11}A_1 + a_{12}A_2 + b_{11}B_1 + b_{12}B_2 + b_{13}B_3]_{k=k_n} = 0\ .$$

This shows that

$$A_1 \approx O(\varepsilon^2)\ . \tag{72}$$

From (53) it follows that

$$\left[i\kappa_0 + \frac{\varepsilon^2\delta_n}{2k_n^2}i\kappa_0\right]k_n B_2 - \varepsilon^2\left[a_{31}A_1 + a_{32}A_2 + b_{31}B_1 + b_{32}B_2 + b_{33}B_3\right] = 0.$$

This shows that

$$B_2 \approx O(\varepsilon^2)\ . \tag{73}$$

Also from (52) and (56) it can be shown that for finite B_1,

$$[\rho_0\omega^2 - (\mu_0 + \kappa_0)k_n^2]A_2 - i\kappa_0 k_n B_3 - \varepsilon^2\delta_n(\mu_0 + \kappa_0)A_2 - \tfrac{\varepsilon^2\delta_n}{2k_n^2}i\kappa_0 k_n B_3$$
$$-\varepsilon^2\left[a_{21}A_1 + a_{22}A_2 + b_{21}B_1 + b_{22}B_2 + b_{23}B_3\right] = 0 \tag{73a}$$

and

$$i\kappa_0 k_n A_2 + (\rho_0 j\omega^2 - 2\kappa_0 - \gamma_0 k_n^2)B_3 + \tfrac{\varepsilon^2\delta_n}{2k_n^2}i\kappa_0 k_n A_2 - \varepsilon^2\delta_n\gamma_0 B_3$$
$$-\varepsilon^2\int\left[a_{61}A_1 + a_{62}A_2 + b_{61}B_1 + b_{62}B_2 + b_{63}B_3\right] = 0\ , \tag{73b}$$

respectively. From these two Eqs. (73a) and (73b) it is clear that

$$A_2 \approx O(\varepsilon^2) \ \text{ and } \ B_3 \approx O(\varepsilon^2)\ . \tag{74}$$

Equation (54) however, determines δ_n, since

$$-\varepsilon^2\delta_n(\alpha_0 + \beta_0 + \gamma_0)B_1$$
$$-\varepsilon^2\int\left[a_{41}A_1 + a_{42}A_2 + b_{41}B_1 + b_{42}B_2 + b_{43}B_3\right] = 0$$

and $(A_1, A_2, B_2, B_3) \approx O(\varepsilon^2)$. Hence, if B_1 is finite, then

$$\delta_n = \frac{-b_{41}}{\alpha_0 + \beta_0 + \gamma_0}\ . \tag{75}$$

Therefore, $\delta_n = 0$ if $b_{41} = 0$ and amplitude B_1 is finite.

It is observed that for the waves represented by (71), the amplitude B_1 is important in comparison to the amplitudes A_1, A_2, B_2, and B_3. These are amplitudes of longitudinal type microrotation waves propagating in the random generalized thermoelastic micropolar field but are scarcely affected by the random inhomogeneities of the medium.

(iii) Next let us examine the propagation of elastic waves for which

$$k^2 = k_c^2 + \varepsilon^2\delta_c, \quad k_c^2 = \frac{\rho_0\omega^2}{\lambda_0 + 2\mu_0}, \tag{76}$$

and

$$k^2 = k_s^2 + \varepsilon^2\delta_s, k_s^2 = \frac{\rho_0\omega^2}{\mu_0}\ . \tag{77}$$

Substituting (76) in (51) one observes

$$\begin{aligned}
&[-\kappa_0\rho_0\omega^2 - \varepsilon^2(\lambda_0 + 2\mu_0 + \kappa_0)(\lambda_0 + 2\mu_0)\delta_c]A_1 \\
&-\varepsilon^2\frac{\omega\theta_0(1 - i\omega t_0\delta_{lk})m_2(im_2 + \omega m_3)k_c^2}{i\omega(1 - it_0\omega)\eta_0 - \nu_o k_c^2}(\lambda_0 + 2\mu_0)A_1 \\
&-\varepsilon^2\omega\theta_0(1 - i\omega t_0\delta_{lk})m_2(im_2 + \omega m_3)(\lambda_0 + 2\mu_0)k_cA_1\int_0^{\infty} e^{i\beta r}\sin krdr \\
&-\varepsilon^2(a_{11}A_1 + a_{12}A_2 + b_{11}B_1 + b_{12}B_2 + b_{13}B_3)(\lambda_0 + 2\mu_0) = 0\ .
\end{aligned}$$

Hence

$$A_1 \approx O(\varepsilon^2)\ . \tag{78a}$$

Substituting (76) in (55) it can be similarly shown that

$$B_2 \approx O(\varepsilon^2)\ . \tag{78b}$$

From (54) one can similarly conclude that

$$B_1 \approx O(\varepsilon^2)\ . \tag{79}$$

Two equations (52) and (56) are coupled with the transverse amplitudes A_2 and B_3 such that

$$[\rho_0\omega^2 - (\mu_0 + \kappa_0)k^2]A_2 - i\kappa_0 kB_3 - \varepsilon^2(b_{22}B_2 + b_{23}B_3) = 0$$

and

$$i\kappa_0 kA_2 + (\rho_0 j\omega^2 - 2\kappa_0 - \gamma_0 k^2)B_3 - \varepsilon^2(b_{62}B_2 + b_{63}B_3) = 0\ .$$

Eliminating A_2 and B_3 one obtains the dispersion equation for two sets of transverse type of displacement and microrotation waves propagating in the uncoupled micropolar elastic medium and independent of thermal field, as no thermal parameter is involved in any of the integrals b_{22}, b_{23}, b_{62}, and b_{63}, given by

$$\begin{aligned}&[\rho_0\omega^2-(\mu_0+\kappa_0)k^2](\rho_0 j\omega^2-2\kappa_0-\gamma_0k^2)-\kappa_0^2k^2\\&-\varepsilon^2\Big[a_{22}(\rho_0 j\omega^2-2\kappa_0-\gamma_0k^2)+b_{63}[\rho_0\omega^2-(\mu_0+\kappa_0)k^2]\\&+i\kappa_0k(a_{62}-b_{23})\Big]=0.\end{aligned}\tag{80}$$

This equation involves integrals a_{22}, a_{62}, b_{23}, and b_{63} each involving correlation functions between non-thermal medium-parameters only. Substituting (76) in (80) and neglecting terms to the order ε^2, the deviation δ_c can be computed from:

$$\begin{aligned}&[\rho_0\omega^2-(\mu_0+\kappa_0)k_c^2](\rho_0 j\omega^2-2\kappa_0-\gamma_0k_c^2)-\kappa_0^2k_c^2\\&-\varepsilon^2\gamma_0\delta_c[\rho_0\omega^2-(\mu_0+\kappa_0)k_c^2]-\varepsilon^2(\mu_0+\kappa_0)\delta_c(\rho_0 j\omega^2-2\kappa_0-\gamma_0k_c^2)-\varepsilon^2\kappa_0^2\delta_c\\&-\varepsilon^2\Big[a_{22}(\rho_0 j\omega^2-2\kappa_0-\gamma_0k_c^2)+b_{63}[\rho_0\omega^2-(\mu_0+\kappa_0)k_c^2]\\&+i\kappa_0(a_{62}-b_{23})k_c\Big]=0\,.\end{aligned}$$

If $\varepsilon^2=0$, then we know

$$[\rho_0\omega^2-(\mu_0+\kappa_0)k_c^2](\rho_0 j\omega^2-2\kappa_0-\gamma_0k_c^2)-\kappa_0^2k_c^2=0\,.$$

Hence δ_c and similarly δ_s are obtained in the forms:

$$\delta_c\approx-\frac{b_{63}[\rho_0\omega^2-(\mu_0+\kappa_0)k_c^2]+a_{22}(\rho_0 j\omega^2-2\kappa_0-\gamma_0k_c^2)+(a_{62}-b_{23})i\kappa_0k_c}{\gamma_0[\rho_0\omega^2-(\mu_0+\kappa_0)k_c^2]+(\mu_0+\kappa_0)(\rho_0 j\omega^2-2\kappa_0-\gamma_0k_c^2)+\kappa_0^2},\tag{81}$$

and

$$\delta_s\approx-\frac{b_{63}[\rho_0\omega^2-(\mu_0+\kappa_0)k_s^2]+a_{22}(\rho_0 j\omega^2-2\kappa_0-\gamma_0k_s^2)+(a_{62}-b_{23})i\kappa_0k_s}{\gamma_0[\rho_0\omega^2-(\mu_0+\kappa_0)k_s^2]+(\mu_0+\kappa_0)(\rho_0 j\omega^2-2\kappa_0-\gamma_0k_s^2)+\kappa_0^2}\,.\tag{82}$$

Both δ_c and δ_s are complex quantities. Computing real and imaginary parts one can write:

$$k=k_c+\frac{\varepsilon^2\delta_c}{2k_c}=k_c+\varepsilon^2\frac{\mathrm{Re}\delta_c}{2k_c}+i\varepsilon^2\frac{\mathrm{Im}\delta_c}{2k_c}\,,\tag{83}$$

and

$$k = k_s + \frac{\varepsilon^2 \delta_s}{2k_s} = k_c + \varepsilon^2 \frac{\mathrm{Re}\delta_s}{2k_s} + i\varepsilon^2 \frac{\mathrm{Im}\delta_s}{2k_s} \,. \tag{84}$$

Hence for longitudinal waves

$$i\vec{k}\,\vec{x} = ikx = ix\left[k_c + \frac{\varepsilon^2 \delta_c}{2k_c}\right] = ix\left[k_c + \varepsilon^2 \frac{\mathrm{Re}\delta_c}{2k_c} + i\varepsilon^2 \frac{\mathrm{Im}\delta_c}{2k_c}\right] ,$$

and for transverse waves

$$i\vec{k}\,\vec{x} = ikx = ix\left[k_s + \frac{\varepsilon^2 \delta_s}{2k_s}\right] = ix\left[k_s + \varepsilon^2 \frac{\mathrm{Re}\delta_s}{2k_s} + i\varepsilon^2 \frac{\mathrm{Im}\delta_s}{2k_s}\right] .$$

Thus change in the wave number and attenuation occurs in both cases, having attenuation factors of the forms

$$\exp\left[-\frac{\varepsilon^2 x}{2}\mathrm{Im}\left(\frac{\delta_c}{k_c}\,,\frac{\delta_s}{k_s}\right)\right]. \tag{85}$$

It may be recalled here that the only term in Eq. (36) that might contribute to some effect of thermal parameters on $\delta_{c,s}$ is

$$\begin{aligned}
&\int \langle K_1 G_4 R_1' \rangle (\vec{A} e^{i\vec{k}\cdot\vec{x}'}) d\vec{x}' \\
&= -\omega\theta_0(1 - i\delta_{lk} t_0 \omega)(\vec{k}\,\vec{A}) e^{i\vec{k}\,\vec{x}} \int \{\vec{\nabla}[G_4(r) R_{mm}(r)] \\
&- i\omega\vec{\nabla}[G_4(r) R_{mm\bullet}]\} e^{-i\vec{k}'\cdot\vec{r}} d\vec{r} \,.
\end{aligned}$$

This term clearly does not add anything to a_{22} since in our case $\vec{k}\,\vec{A} = (kA_1, 0, 0)$. Therefore the integrals a_{22}, a_{62}, b_{23} and b_{63} are all independent of the thermal field. However the integral $\int \langle K_1 G_4 R_1' \rangle (\vec{A} e^{i\vec{k}\cdot\vec{x}'}) d\vec{x}'$ contributes an additional term to a_{11} which is

$$-4i\pi\omega\theta_0(1 - i\delta_{lk} t_0 \omega) k \int_0^\infty [(R_{mm} - i\omega R_{mm\bullet}) G_4' + (R_{mm}' - i\omega R_{mm\bullet}') G_4] r^2 f' dr \,.$$

This term has already been included in the radial expression for a_{11} in (58).

8 Attenuation of high frequency nonthermal waves in a particular case

This topic has already been discussed in [18]. However for the sake of continuity of discussion, the salient features are briefly enumerated below.

It may be noted that the expressions derived for δ_c and δ_s do not depend on generalized thermal parameters. Hence the phenomenon of propagation of transverse type of displacement and microrotation waves in the random micropolar elastic medium is considered taking

$$R_{\rho\rho}(r) = \langle \rho_1^2 \rangle e^{\frac{-r}{a}} \neq 0, a \rangle 0 \ , \tag{86}$$

and making all other auto- and cross-correlation functions vanish. (Auto-correlation functions $\langle \kappa_1 \kappa_1' \rangle, \langle \beta_1 \beta_1' \rangle, \langle \gamma_1 \gamma_1' \rangle$, signifying effects of random variation of micropolar elastic properties of the medium appear several times in b_{63} making calculations unmanageably lengthy and cumbersome and hence are omitted). Then

$$b_{63}(k_c) = \frac{4j\pi\omega^2 \langle \rho_1^2 \rangle}{k_c} \int_0^{\infty.} r e^{-\frac{r}{a}} \left[G_4(r) \right]_{33} \sin(k_c r) dr \tag{87}$$

and

$$a_{22}(k_c) = a_{62}(k_c) = b_{23}(k_c) = 0 \ . \tag{88}$$

where $[G_4(r)]_{33}$ has already been evaluated [18]. Components including $[G_4(r)]_{33}$ of the associated Green's tensor have been reproduced in the App. III for ready-reference.

For large ω the approximate values of k_c^2, k_s^2, k_m^2, and k_n^2 were computed to show that transverse type of displacement waves attenuate. In a similar way it was shown that high frequency transverse type microrotation waves attenuate if $j > 1$. Results indicate that body waves of these types attenuate due to randomness as they propagate through the medium, only in the non-thermal environment.

9 Computation of the dispersion of the field from the mean field

In this section we propose to give an outline of the procedure to evaluate an expression for dispersion of the field from the mean field. It is assumed that $v_0(\vec{x})$ and $v(\vec{x})$ represent solutions of operator equations $L_0 v_0(\vec{x}) = 0$ and $Lv(\vec{x}) = 0$ respectively, where $L = L_0 + \varepsilon L_1 + \varepsilon^2 L_2 + O(\varepsilon^3)$.

Following Karal and Keller ([23], Eq. (5)) it can be easily shown that

$$v = v_0 + \varepsilon L_0^{-1} L_1 v_0 + \varepsilon^2 (L_0^{-1} L_1 L_0^1 l_1 + L_0^{-1} l_2) v_0 + O(\varepsilon^2) \ . \tag{89a}$$

Hence

$$\bar{v}^T = \bar{v}_0^T + \varepsilon\overline{(L_0^{-1}L_1v_0)}^T + \varepsilon^2\left[\overline{(L_0^{-1}L_1L_0^{-1}L_1v_0)}^T + \overline{(L_0^{-1}L_2v_0)}^T\right] + O(\varepsilon^3)\,, \tag{89b}$$

where v^T is the transpose of v and $\bar{v}^T$ is the complex conjugate of v^T. Therefore

$$\begin{aligned}\bar{v}^T v = \bar{v}_0^T v_0 &+ \varepsilon\left[\overline{(L_0^{-1}L_1v_0)}^T v_0 + \bar{v}_0^T(L_0^{-1}L_1v_0)\right]\\ &+\varepsilon^2\left[\overline{(L_0^{-1}L_1v_0)}^T(L_0^{-1}L_1v_0) + \overline{(L_0^{-1}L_1L_0^{-1}L_1v_0)}^T v_0\right.\\ &\left.+\overline{(L_0^{-1}L_2v_0)}^T v_0 + \bar{v}_0^T(L_0^{-1}L_1L_0^{-1}L_1v_0) + \bar{v}_0^T(L_0^{-1}L_2v_0)\right] + O(\varepsilon^3)\end{aligned}$$

We take expectation of this equation taking that $\langle L_1\rangle = 0$, so that

$$\left\langle \bar{v}_0^T(L_0^{-1}L_1v_0)\right\rangle = \bar{v}_0^T L_0^{-1}\langle L_1\rangle v_0 = 0$$

and

$$\left\langle (L_0^{-1}L_1v_0)^T v_0\right\rangle = \left(L_0^{-1}\langle L_1\rangle v_0\right)^T v_0 = 0\,.$$

The condition $\langle L_1\rangle = 0$ with the help of Eq. (23), leads to

$$m_2 = i\omega m_3 \;\text{ and }\; 1 = it_0\omega,$$

taking $\delta_{lk} = 1$ and assuming ω to be complex. Combining these two relations one gets

$$m_2 = im_3 \times \frac{1}{it_0}\,.$$

Hence

$$m_3 = t_0 m_2\,. \tag{90}$$

Therefore

$$\begin{aligned}\bar{v}^T v \;=\; \bar{v}_0^T v_0 \;&+\; \varepsilon^2\left[\left\langle\overline{(L_0^{-1}L_1v_0)}^T(L_0^{-1}L_1v_0)\right\rangle \;+\; \left\langle\overline{(L_0^{-1}L_1L_0^{-1}L_1v_0)}^T v_0\right\rangle\right.\\ &+\left\langle\overline{(L_0^{-1}L_2v_0)}^T v_0\right\rangle \;+\; \left\langle\bar{v}_0^T(L_0^{-1}L_1L_0^{-1}L_1v_0)\right\rangle\\ &\left.+\left\langle\bar{v}_0^T(L_0^{-1}L_2v_0)\right\rangle\right] \;+\; O(\varepsilon^3)\,.\end{aligned} \tag{91}$$

From (89a) we obtain on taking the expectation

$$\langle v\rangle \;=\; v_0 \;+\; \varepsilon^2\Big[\Big\langle L_0^{-1}L_1L_0^{-1}L_1v_0\Big\rangle \;+\; \Big\langle L_0^{-1}L_2v_0\Big\rangle\Big] \;+\; O(\varepsilon^3)\,.$$

Hence

$$v_0 \;=\; \langle v\rangle \;-\; \varepsilon^2\Big[\Big\langle L_0^{-1}L_1L_0^{-1}L_1v_0\Big\rangle \;+\; \Big\langle L_0^{-1}L_2v_0\Big\rangle\Big] \;+\; O(\varepsilon^3)\,.$$

and by iteration it follows that

$$v_0 \;=\; \langle v\rangle \;-\; \varepsilon^2\Big[\Big\langle L_0^{-1}L_1L_0^{-1}L_1\Big\rangle\langle v\rangle \;+\; \Big\langle L_0^{-1}L_2\Big\rangle\langle v\rangle\Big] \;+\; O(\varepsilon^3) \tag{92}$$

and

$$\bar{v}_0^T \;=\; \Big\langle \bar{v}^T\Big\rangle \;-\; \varepsilon^2\left[\Big\langle\overline{\Big(L_0^{-1}L_1L_0^{-1}L_1\langle v\rangle\Big)}^T\Big\rangle \;+\; \Big\langle\overline{\Big(L_0^{-1}L_2\langle v\rangle\Big)}^T\Big\rangle\right] \;+\; O(\varepsilon^3) \tag{93}$$

Thus

$$\begin{aligned}\bar{v}_0^Tv_0 = \Big\langle \bar{v}^T\Big\rangle\langle v\rangle \;-\; \varepsilon^2\Big[&\Big\langle\overline{\Big(L_0^{-1}L_1L_0^{-1}L_1\langle v\rangle\Big)}^T\Big\rangle\langle v\rangle \;+\; \Big\langle \bar{v}^T\Big\rangle\\ &\times\Big\langle\Big(L_0^{-1}L_1L_0^{-1}L_1\langle v\rangle\Big)\Big\rangle + \Big\langle\overline{\Big(L_0^{-1}L_2\langle v\rangle\Big)}^T\Big\rangle\langle v\rangle\\ &+\Big\langle \bar{v}^T\Big\rangle\Big\langle\Big(L_0^{-1}L_2\langle v\rangle\Big)\Big\rangle\Big] \;+\; O(\varepsilon^3)\end{aligned} \tag{94}$$

Substituting Eqs. (92)–(94) into (91) we obtain the expression

$$\Big\langle \bar{v}^Tv\Big\rangle \;-\; \Big\langle \bar{v}^T\Big\rangle\langle v\rangle \;=\; \varepsilon^2\left[\Big\langle\overline{(L_0^{-1}L_1\langle v\rangle)}^T(L_0^{-1}L_1\langle v\rangle)\Big\rangle\right] \;+\; O(\varepsilon^3)\,, \tag{95}$$

which is equal to sum of variances of real and imaginary parts of all the components of v. This relation holds only under the condition that $m_3 = t_0m_2$. Taking in general

$$L = (M_{lj}), \quad (lj) = 1,2,3 \tag{96}$$

$$L_0^{-1}f \;=\; \int (G_{lj})e^{i\vec{k}\cdot\vec{x}'}\,d\vec{x}'\,, \tag{97}$$

$$\langle v(\vec{x})\rangle \;=\; [A_j]e^{i\vec{k}\cdot\vec{x}}\,, \tag{98}$$

$$\vec{k} = \vec{k}_1 + i\vec{k}_2\,, \quad k_1\,, k_2 \equiv \text{real}\,, \qquad \langle L_1 \rangle = 0\,, \tag{99}$$

it has been shown that

$$\begin{aligned} \left\langle \bar{v}^T v \right\rangle - \left\langle \bar{v}^T \right\rangle \langle v \rangle &= \varepsilon^2 e^{-2Im\vec{k}\cdot\vec{x}} \left(\sum |C_l|^2\right) \\ &= \varepsilon^2 e^{-2Im\vec{k}\ \vec{x}}\, \ell\,(A_l)\,. \end{aligned} \tag{100}$$

where $\ell\,(A_l) \geq 0$ is seen from (92) to be a bilinear function of the amplitudes A_l. Then Eq. (100) shows that the dispersion ($\sqrt{variance}$) of the field from the mean field represented by the plane wave (98), is a small quantity of order ε and that it decays as the wave propagates in those cases where $\mathrm{Im}\, k > 0$. It follows that [18] the field may differ from the plane wave mean field by a quantity of order ε with finite probability.

10 Variance for micropolar generalized thermoelastic wave propagation in the random medium

This analysis is next applied to the waves in the random micropolar generalized thermoelastic medium. In this case

$$\begin{aligned} (L_0^{-1} L_1 < v. >)^T &= [e^{i\vec{k}\cdot\vec{x}} \int \begin{bmatrix} G_0 & G_1 & 0 \\ G_2 & G_3 & 0 \\ 0 & 0 & G_4 \end{bmatrix} \begin{bmatrix} M_1 & P_1 & K_1 \\ N_1 & Q_1 & 0 \\ R_1 & 0 & S_1 \end{bmatrix} \begin{bmatrix} \vec{A} \\ \vec{B} \\ C \end{bmatrix} e^{-i\vec{k}\cdot(\vec{x}-\vec{x}')}]^T\, d\vec{x}' \\ &= [e^{i\vec{k}\cdot\vec{x}} \int \begin{bmatrix} G_0 & G_1 & 0 \\ G_2 & G_3 & 0 \\ 0 & 0 & G_4 \end{bmatrix} \begin{bmatrix} M_1\vec{A} + P_1\vec{B} + K_1 C \\ N_1\vec{A} + Q_1\vec{B} \\ R_1\vec{A} + S_1 C \end{bmatrix} e^{-i\vec{k}\cdot(\vec{x}-\vec{x}')}]^T\, d\vec{x}' \\ &= [e^{i\vec{k}\cdot\vec{x}} \int \begin{bmatrix} G_0(M_1\vec{A} + P_1\vec{B} + K_1 C) + G_1(N_1\vec{A} + Q_1\vec{B}) \\ G_2(M_1\vec{A} + P_1\vec{B} + K_1 C) + G_3(N_1\vec{A} + Q_1\vec{B}) \\ G_4(R_1\vec{A} + S_1 C) \end{bmatrix} e^{-i\vec{k}\cdot(\vec{x}-\vec{x}')}]^T\, d\vec{x}' \end{aligned} \tag{101}$$

where

$$M\vec{u} = \rho\frac{\partial^2\vec{u}}{\partial t^2} - (\lambda+\mu)\vec{\nabla}(\vec{\nabla}\vec{u}) - (\mu+\kappa)\nabla^2\vec{u} - \vec{\nabla}\lambda(\vec{\nabla}\vec{u}) - \vec{\nabla}\mu\times(\vec{\nabla}\times\vec{u}) - (\vec{\nabla}(2\mu+\kappa)\vec{\nabla})\vec{u}$$

$$M_1(\vec{A}e^{i\vec{k}\cdot\vec{x}}) = [-\rho_1\omega^2\vec{A} + (\lambda_1+\mu_1)(\vec{k}\,\vec{A})\vec{k} + (\mu_1+\kappa_1)k^2\vec{A}$$

$$-i(\vec{k}\,\vec{A})\vec{\nabla}\lambda_1 - i\vec{\nabla}\mu_1\times(\vec{k}\times\vec{A}) - i(\vec{\nabla}(2\mu_1+\kappa_1)\vec{k})\vec{A}]e^{i\vec{k}\cdot\vec{x}}$$

$$P_1(\vec{B}e^{i\vec{k}\cdot\vec{x}}) = -\vec{\nabla}\times(\kappa_1\vec{B}e^{i\vec{k}\cdot\vec{x}}) = -[\vec{\nabla}k_1\times\vec{B} + i\kappa_1\vec{k}\times\vec{B}]e^{i\vec{k}\cdot\vec{x}},$$

$$K_1(Ce^{i\vec{k}\cdot\vec{x}}) = [\vec{\nabla}(m_1) - i\omega\vec{\nabla}m_1^{\bullet}]Ce^{i\vec{k}\cdot\vec{x}} = [\vec{\nabla}m_1 + im_1\vec{k} - i\omega(\vec{\nabla}m_1^{\bullet} + im_1^{\bullet})]Ce^{i\vec{k}\cdot\vec{x}},$$

$$N_1(\vec{A}e^{i\vec{k}\cdot\vec{x}}) = -\kappa_1(\vec{\nabla}\times)(\vec{A}e^{i\vec{k}\cdot\vec{x}}) = -i\kappa_1(\vec{k}\times\vec{A})e^{i\vec{k}\cdot\vec{x}}$$

$$Q_1(\vec{B}e^{i\vec{k}\cdot\vec{x}}) = [(-\rho_1 j\omega^2 + 2\kappa_1)\vec{B} + (\alpha_1+\beta_1)(\vec{k}\cdot\vec{B})\vec{k} - i(\vec{k}\,\vec{B})(\vec{\nabla}\alpha_1)$$

$$+\gamma_1 k^2\vec{B} - i(\vec{\nabla}\beta_1)\times(\vec{k}\times\vec{B}) - i\{\vec{\nabla}(\beta_1+\gamma_1)\vec{k}\}\vec{B}]e^{i\vec{k}\cdot\vec{x}}$$

$$R_1(\vec{A}e^{i\vec{k}\cdot\vec{x}}) = -i\omega\theta_0(1-i\delta_{1k}t_0\omega)m_1(\vec{k}\,\vec{A})e^{i\vec{k}\cdot\vec{x}},$$

$$S_1(Ce^{i\vec{k}\cdot\vec{x}}) = [-i\omega(1-it_0\omega)\eta_1 Ce^{i\vec{k}\cdot\vec{x}}] - iC\vec{\nabla}\{\nu_1\vec{\nabla}(e^{i\vec{k}\cdot\vec{x}})\}$$

$$= -i[\omega(1-it_0\omega)\eta_1 + (\vec{\nabla}\nu_1 + i\nu_1\vec{k})\vec{k}]Ce^{i\vec{k}\cdot\vec{x}}$$

and $\langle L_1\rangle = 0$.

Let us write

$$\left(L_0^{-1}L_1\langle v\rangle\right)^T = e^{i\vec{k}_2\cdot\vec{x}}\, e^{i\vec{k}_1\cdot\vec{x}}(c_1 + id_1\ ,\ c_2 + id_2)\ , \qquad (102)$$

where c_i, d_i, are linear functions of A_1, A_2, B_1, B_2, and B_3. Then it can be shown as before that

$$\overline{\left(L_0^{-1}L_1\langle v\rangle\right)}^T\left(L_0^{-1}L_1\langle v\rangle\right) = e^{-2(\mathrm{Im}k)x}\,\ell\,(A_l\,,B_l)$$

where $\ell(A_l\,,B_l)$ is clearly a non-negative, bilinear function of A_l and B_l. Hence the amount of dispersion of waves from the mean field comes out to be $\varepsilon e^{-(\mathrm{Im}k)x}\sqrt{\ell}$.

It may be concluded that the dispersion of the wave field from the mean field may be obtained following this procedure in many other cases examined by employing Keller's perturbation theory.

11 The uncoupled problem

This section proposes to outline, approximately following Chow [25] the method of examining the uncoupled random micropolar generalized-thermal problem. With this end in view the $\vec{u}-$term is dropped from the temperature Eq. (7), so that the reduced temperature equation becomes

$$\eta(\vec{x})[\dot{\theta}(\vec{x},t) + t_0\ddot{\theta}(\vec{x},t)] = \vec{\nabla}\{\nu(\vec{x})\vec{\nabla}[\theta(\vec{x},t)]\} + q\ .$$

The objective is to study the random elasticity-displacement Eq. (5) independently. The three dispersion equations (29)–(31) now become:

$$\left[\rho_0\omega^2\vec{A}-(\lambda_0+\mu_0)(\vec{k}\,\vec{A})\vec{k}-(\mu_0+\kappa_0)k^2\vec{A}\right]+i\kappa_0(\vec{k}\times\vec{B})-\varepsilon(im_2+\omega m_3)C\vec{k}$$

$$+\varepsilon^2\left[\omega\theta_0(1-\omega t_0\delta_{lk})m_2(m_2-i\omega m_3)(\vec{k}\,\vec{A})\right]\int\left[(\vec{\nabla}G_4)\right]e^{-i\vec{k}\,\vec{r}}d\vec{r}$$

$$-\varepsilon^2\int\left[\begin{array}{l}\langle[M_1\{G_0(M_1'\vec{A}+P_1'\vec{B}+K_1'C)+G_1(N_1'\vec{A}+Q_1'\vec{B})\}\\+P_1\{G_2(M_1'\vec{A}+P_1'\vec{B}+K_1'C)+G_3(N_1'\vec{A}+Q_1'\vec{B})\}\\+K_1G_4(R_1'\vec{A}+S_1'C)]\rangle\end{array}\right]e^{-i\vec{k}\cdot\vec{r}}d\vec{r}=0\,, \tag{103}$$

$$i\kappa_0(\vec{k}\times\vec{A})-\left[(2\kappa_0-\rho_0j\omega^2+\gamma_0k^2)\vec{B}+(\alpha_0+\beta_0)(\vec{k}\,\vec{B})\vec{k}\right]$$

$$-\varepsilon^2\int\left[\begin{array}{l}\langle[N_1\{G_0(M_1'\vec{A}+P_1'\vec{B}+K_1'C)+G_1(N_1'\vec{A}+Q_1'\vec{B})\}\\+Q_1\{G_2(M_1'\vec{A}+P_1'\vec{B}+K_1'C)+G_3(N_1'\vec{A}+Q_1'\vec{B})\}]\rangle\end{array}\right]e^{-i\vec{k}\cdot\vec{r}}d\vec{r}=0 \tag{104}$$

and

$$\left[i\omega(1-it_0\omega)\eta_0-\nu_0k^2\right]C=0\,. \tag{105}$$

Simplified Case I. Equation (105) is easily solvable since $C\neq 0$. The first two equations can be analyzed as before or otherwise. Considering equations up to ε-order terms one gets

$$\left[\rho_0\omega^2\vec{A}-(\lambda_0+\mu_0)(\vec{k}\,\vec{A})\vec{k}-(\mu_0+\kappa_0)k^2\vec{A}\right]+i\kappa_0(\vec{k}\times\vec{B})-\varepsilon(im_2+\omega m_3)C\vec{k}=0$$

and

$$i\kappa_0(\vec{k}\times\vec{A})-\left[(2\kappa_0-\rho_0j\omega^2+\gamma_0k^2)\vec{B}+(\alpha_0+\beta_0)(\vec{k}\,\vec{B})\vec{k}\right]=0\,.$$

The six equations are

$$\left[\rho_0\omega^2-(\lambda_0+2\mu_0+\kappa_0)k^2\right]A_1-\varepsilon(im_2+\omega m_3)Ck=0\,,$$

$$\left[\rho_0\omega^2-(\mu_0+\kappa_0)k^2\right]A_2+i\kappa_0kB_3=0\,,$$

$$i\kappa_0kB_2=0$$

and

$$\left[(2\kappa_0-\rho_0j\omega^2)+(\alpha_0+\beta_0+\gamma_0)k^2\right]B_1=0\,,$$

$$(2\kappa_0-\rho_0j\omega^2+\gamma_0k^2)B_2=0\,,$$

$$i\kappa_0 k A_2 - (2\kappa_0 - \rho_0 j\omega^2 + \gamma_0 k^2)B_3 = 0 \ .$$

It is clear that the amplitude ratio

$$\frac{A_1}{C} = \frac{\varepsilon(im_2 + \omega m_3)k}{\rho_0\omega^2 - (\lambda_0 + 2\mu_0 + \kappa_0)k^2} = O(\varepsilon)$$

and is dependent upon expectation values of generalized thermal parameters m and $m^\bullet = t_1 m$. Moreover A_1 is finite but small such that $A_1 = O(\varepsilon)$. Also $B_2 = 0$ indicates that there is no propagation along B_2. Further $B_1 \neq 0$ and $B_1 \equiv$ finite, indicates that waves with wave number given by

$$k^2 = \frac{\rho_0 j\omega^2 - 2\kappa_0}{\alpha_0 + \beta_0 + \gamma_0}$$

propagate in the medium. Finally the coupled dispersion equation for waves propagating along A_2 and B_3 directions is represented by

$$\frac{A_2}{B_3} = -\frac{i\kappa_0 k}{\rho_0\omega^2 - (\mu_0 + \kappa_0)k^2} = \frac{2\kappa_0 - \rho_0 j\omega^2 + \gamma_0 k^2}{i\kappa_0 k} \ ,$$

$$\left[\rho_0\omega^2 - (\mu_0 + \kappa_0)k^2\right]\left[2\kappa_0 - \rho_0 j\omega^2 + \gamma_0 k^2\right] = \kappa_0^2 k^2 \ .$$

Case II. Unlike Chow ([25], cf. Eq. (4.3)), we retain the ε-order term in (31) to get

$$\left[i\omega(1 - it_0\omega)\eta_0 - \nu_0 k^2\right]C - \varepsilon\omega\theta_0(1 - i\omega t_0\delta_{lk})m_2(\vec{k}\,\vec{A}) = 0 \ . \qquad (106)$$

Then Eqs. (103), (104), and (105) can be analyzed as in Sec. 4 or otherwise.

12 Summary and conclusions

1. The integrand of a_{11} only is dependent on generalized thermal parameters including thermomechanical auto-correlation function and the cross-correlation function between thermomechanical and generalized thermomechanical coupling parameters. This dependence holds good both for L-S and G-L thermoelastic fields.

2. Numerical solutions can be easily obtained by setting

$$R_{mm}(r) = \langle\rho_1^2\rangle e^{-\frac{r}{b}}, \quad R_{mm}(r) = \langle\rho_1^2\rangle e^{-\frac{r}{b}}.$$

3. On the other hand integrands of a_{22}, a_{62}, b_{23}, and b_{63} are clearly independent of auto- and cross-correlation functions $R_{mm}(r)$ and $R_{mm\bullet}(r)$.

4. The three vector wave equations considered up to first order perturbation only leads to the dispersion equation for the wave propagation in the deterministic micropolar elastic medium. However effects of generalized thermal field are discernible only if the second order perturbation term is retained in this dispersion equation. This will be evident from the Eq. (48) of Sec. 4.

5. Equation (64) shows that longitudinal type displacement waves get modified due to random fluctuation of inhomogeneities of the micropolar medium under generalized thermoelasticity such that the wave number is increased by $\varepsilon^2 \frac{\delta_l}{2k_l}$, where δ_l is a function of $R_{mm}(r)$ and $R_{mm\bullet}(r)$. These results are valid for both L-S and G-L generalized thermoelasticity.

6. Equation (68) shows that the change in wave number δ_l depends upon the random variation of the generalized thermal field and measured in terms of statistical means, m_2 and m_3, for both L-S and G-L theories. For L-S, the change depends upon m_2 only, and for G-L upon m_2 and m_3.

7. Equation (100) shows that the dispersion ($\sqrt{\text{variance}}$) of the field from the mean field is a small quantity of order ε and that it decays as the wave propagates in those cases where $\operatorname{Im} k > 0$. This result holds good only if $m_3 = t_0 m_2$.

8. It is quite clear from Eqs. (70) and (75) that longitudinal type microrotation waves propagate in the random generalized thermoelastic micropolar medium but are scarcely affected by the random inhomogeneities of the medium, at least up to the domain of second order perturbation. In this case the amplitude B_1 is important in comparison to the amplitudes A_1, A_2, B_2, and B_3.

   The study of micropolar materials and micropolar generalized-thermoelasticity in particular has been enormously drawing the interest of applied mathematicians and engineers in recent times. Micropolar materials include fibrous and granular or composite substances. The domain of micropolarity is therefore expanding in time.

The study of micropolar properties in relation to wave propagation in coupled media therefore has been gaining importance from the perspective of probable applications in industry, engineering and to a great extent in earthquake prediction and seismology. Research studies are being carried out through various methodologies. The present paper has introduced the smooth perturbation technique [21] in examining the phenomenon of wave propagation in an infinite random generalized thermoelastic micropolar medium. In future certain other methods, *viz.*, iterative perturbation method [31] or the method of scatters [37] may be employed in measuring effects of random variation of parameters. The domain decomposition method developed by Adomian [43] may also be employed to study micropolar elasticity in coupled dynamic problems. There is possibility of solving micropolar coupled elastic problems with the help of fractional calculus theories [44,45].

Acknowledgement The authors sincerely thank the reviewers for making a number of excellent suggestions towards improving the manuscript.

Received 11 October 2016

References

[1] Eringen A.C.: *Linear theory of micropolar elasticity.* J. Math. Mech. **15**(1966), 6, 909–922.

[2] Eringen A.C.: *Theory of thermo-microstretch elastic solids.* Int. J. Eng. Sci. **28**(1990), 12, 1291–1301.

[3] Eringen A.C.: *Theory of thermo-microstretch fluids and bubbly liquids.* Int. J. Eng. Sci. **28**(1990), 2, 133–143.

[4] Eringen A.: *Microcontinuum Field Theories.* Springer Science + Business Media, New York 1999.

[5] Marin M.: *Some basic theorems in elastostatics of micropolar materials with voids.* J. Comput. Appl. Math. **70**(1996), 1, 115–126.

[6] Marin M.: *A domain of influence theorem for microstretch elastic materials.* Nonlinear Analysis: Real World Applications **11**(2010), 5, 3446–3452.

[7] Marin M., Lupu M.: *On harmonic vibrations in thermoelasticity of micropolar bodies.* J. Vib. Control **4**(1998), 5, 507–518.

[8] Marin M., Marinescu C.: *Thermoelasticity of initially stressed bodies, asymptotic equipartition of energies.* Int. J. Eng. Sci. **36**(1998), 1, 73–86.

[9] Kumar R.: *Wave propagation in micropolar viscoelastic generalized thermoelastic solid*. Int. J. Engg. Sci. **38**(2000), 1377–1395.

[10] Singh B.: *Wave propagation in an anisotropic generalized thermoelastic solid*. Indian J. Pure Appl. Math. **34**(2003), 10, 1479–1485.

[11] Singh B., Kumar R.: *Reflection and Refraction of plane waves at an interface between micropolar elastic solid and viscoelastic solid*. Int. J. Eng. Sci. **36**(1998), 2, 119–135.

[12] Kumar R., Deswal S: *Surface wave propagation in a micropolar thermoelastic medium without energy dissipation*. J. Sound Vibration **256**(2002), 1, 173–178.

[13] Kumar R., Singh B.: *Wave propagation in a micropolar generalized thermoelastic body with stretch*. Proc. Indian Acad. Sci. (Math. Sci), **106**(1996), 2, 183–199.

[14] Kumar R., Tomar S.K.: *Propagation of micropolar waves at boundary surface*. Indian J. Pure Appl. Math. **27**(1996), 8, 821–835.

[15] Aouadi M.: *The coupled theory of micropolar thermoelastic diffusion*. Acta Mechanica **208**(2009), 181–203.

[16] Suiker A.S.J., Borst R. de, Chang C.S.: *Micro-mechanical modelling of granular material: Part I: Derivation of a second-gradient micro-polar constitutive theory*. Part II: *Plane wave propagation in infinite media* Acta Mechanica **149**(2001), 161–2001.

[17] Majewski E.: *Earthquake Source Asymmetry, Structural Media and Rotation Effects,* Chapter 19 (R.Teisseyre, M. Takeo, and E. Majewski, Eds.). Springer Verlag, 2006.

[18] Mitra M, Bhattacharyya R.K.: *On wave propagation in a random micropolar thermoelastic medium, second soments and associated Green's tensor*. Wave Random Complex **25**(2015), 4, 506–535.

[19] Lord H.W., Shulman Y.A.: *Generalized dynamical theory of thermoelasticity*. J. Mech. Phys. Solids **15**(1967), 299–309.

[20] Green A.E.,Lindsay K.A.: *Thermoelasticity*. J. Elasticity **2**(1972), 1–7.

[21] Ignaczak J., Ostoja-Starzewski M.: *Thermoelasticity with Finite Wave Speeds*. Chap. 6. Oxford University Press, Oxford 2010.

[22] Keller J.B.: *Stochastic equations and wave propagation in random media*. Proc. Symp. App. Math. **16**(1964), 145–170.

[23] Karal F.C., Keller J.B.: *Elastic, electro-magnetic and other waves in a random medium*. J. Mathematical Phys. **5**(1964), 537–547.

[24] Keller J.B., Karal F.C.: *Effective dielectric constant, permeability and conductivity of a random medium and the velocity and attenuation of coherent waves*. J. Math. Phys. **7**(1966), 661–670.

[25] Chow P.L.: *Thermoelastic wave propagation in a random medium and some related problems*. Int. J. Eng. Sci **11**(1973), 953–971.

[26] Chen Y.M., Tien C.L.: *Penetration of temperature waves in a random medium*. J. Maths. Physics XLVI, 2, 1967.

[27] Bhattacharyya R.K.: *On wave propagation in a Random magneto-thermo-viscoelastic medium*. Indian J. Pure appl. Math. **17**(1986), 705–725.

[28] Bhattacharyya R.K.: *On reflection of waves from the boundary of a random elastic semi-infinite medium*. Pure App. Geophysics (PAGEOPH) **146**(1996), 3-4, 677–688.

[29] Bera R.K.: *Propagation of waves in a random magneto-thermoelastic medium*. Computers and Mathematics with Applications **36**(1998), 9, 85–102.

[30] Chernov L.A.: *Wave Propagation in a Random Medium*. McGraw Hill, 1960.

[31] Beran M.J., McCoy J.J.: *Mean field variation in random media*. Quart. App. Math. **28**(1970), July, 245–258.

[32] Beran M.J., Frankenthal S., Deshmukh V., Whitman A.M.: *Propagation of radiation in time-dependent three-dimensional random media*. Wave Random Complex **18**(2008), 3, 435–460.

[33] Sobczyk K.: *Elastic wave propagation in a discrete random medium*. Acta Mechanica **25**(1976), 13–18.

[34] Wenzel A.R.: *Radiation and attenuation of waves in a random medium*. J. Acoust Soc. Am. **71**(1982), 1, 26–35.

[35] Sobczyk K., Wedrychowicz S., Spencer B.F. Jr: *Dynamics of structural systemswith spatial randomness*. Int. J. Solids Struct. **33**(1996), 11, 1651–1669.

[36] Frankenthal S., Beran M.J.: *Propagation in one-dimensionally stratified time-independent scattering media*. Wave Random Complex **17**(2007), 2, 189–212.

[37] Uscinski B.J.: *Intensity fluctuations in a moving random medium*. Wave Random Complex **15**(2005), 4, 437–450.

[38] Frisch U.: *Wave Propagation in Random Media*. In: Probabilistic Methods in Applied Mathematics (A.T. Bharucha-Reid, Ed.), 1, 76–198, Academic Press, New York 1968.

[39] Chen K.K., Soong T.T.: *Covariance properties of waves propagating in a random medium*. J. Acoustical. Society of America **49**(1971), 5(2), 1639–1642.

[40] Soong T.T.: *Random Differential Equations in Science and Engineering*. Academic Press, New York 1973.

[41] Ishimaru A.: *Wave Propagation and Scattering in Random Media,* Oxford University Press, Oxford 1978.

[42] Choudhury M., Basu U., Bhattacharyya R.K.: *Wave propagation in a rotating randomly varying granular generalized thermoelastic medium*. Comput. Math. Appl. **70**(2015), 2803–2821.

[43] Adomian George: *Non-Linear Stochastic Operator Equations*. Academic Press, Harcourt Brace Jovanovich, New York, London 1986.

[44] Podlubny I.: *Fractional Differential Equations*. Academic Press. San Diego, New York, London 1999.

[45] Povstenko Y.Z.: *Fractional heat conduction equation and associated thermal stress*. J. Thermal Stresses **28**(2004), 83–102.

[46] Lavoine J.: *Methods de Calcul II, Calcul Symbolique Distributions et pseudo-fonctions*. Centre National de la Recherche Scientifique, Paris 1959.

Appendix I

Components of the associated Green's tensor

The 36+9 components of the Green's tensor

$$G = \begin{vmatrix} G_1 & G_2 & 0 \\ G_3 & G_4 & 0 \\ 0 & 0 & G_5 \end{vmatrix},$$

where G_i, $i = 1, 2, 3, 4$, are 3×3 matrices, are then obtained and given by (for $\omega^2 >> \kappa_0(\kappa_0 + 2\mu_0)$):

$$(G_j)_{kl} = (G_j)_{kk}\delta_{kl} \tag{1}$$

with $(G_1)_{11} = (G_1)_{22}$ for $j = 1, 4$;

$$(G_j)_{kl} = 0 \quad \text{if } (k,l) \neq (1,2),(2,1); \tag{2}$$

with $(G_1)_{12} = -(G_1)_{21}$, $j = 2, 3$;
and $(G_3)_{kl} = -(G_2)_{kl}$.
Components of G_5 have been defined in (27) and (28).

The independent components $(G_1)_{11}, (G_1)_{33}, (G_2)_{12}, (G_4)_{11}$ and $(G_4)_{33}$ are given by:

$$\begin{aligned}(G_1)_{11} &= \frac{i\kappa_0^2}{2\pi\gamma_0(\mu_0+\kappa_0)^2 r^3}\left[\frac{r^2-(i+k_m r)}{(k_m^2-k_c^2)(k_m^2-k_s^2)}e^{ik_m r}\right. \\ &+ \frac{r^2-(i+k_c r)}{(k_c^2-k_m^2)(k_c^2-k_s^2)}e^{ik_c r} + \left.\frac{r^2-(i+k_s r)}{(k_s^2-k_m^2)(k_s^2-k_c^2)}e^{ik_s r}\right] \\ &- \frac{1}{4\pi r^3}\left[\frac{r^2k_{s'}^2+irk_{s'}-1}{\mu_0 k_{s'}^2}e^{ik_{s'}r} - \frac{ik_{c'}r-1}{(\lambda_0+2\mu_0)k_{c'}^2}e^{ik_{c'}r}\right]\end{aligned}$$

$$\begin{aligned}(G_1)_{33} &= \frac{-i\kappa_0}{\pi\gamma_0(\mu_0+\kappa_0)^2 2r^3}\left[\frac{i+k_m r}{(k_m^2-k_c^2)(k_m^2-k_s^2)}e^{ik_m r} + \frac{i+k_c r}{(k_c^2-k_m^2)(k_c^2-k_s^2)}e^{ik_c r}\right. \\ &+ \left.\frac{i+k_s r}{(k_s^2-k_m^2)(k_s^2-k_c^2)}e^{ik_s r}\right] + \frac{1}{4\pi r^3}\left[\frac{2(ik_{s'}r-1)}{\mu_0 k_{s'}^2}e^{ik_{s'}r} - \frac{k_{c'}^2r^2+2ik_{c'}r-2}{(\lambda_0+2\mu_0)k_{c'}^2}e^{ik_{c'}r}\right]\end{aligned}$$

$$(G_2)_{12} = \frac{-k_0}{2\pi\gamma_0(k_c^2 - k_s^2)(\mu_0 + k_0)r^2}\left[(i + k_c r)e^{iK_c r} - (i + k_s r)e^{iK_s r}\right]$$

The other 9 components have been computed in the text.

$$(G_4)_{11} = \frac{-1}{2\pi\gamma_0(\mu_0+\kappa_0)(k_c^2-k_s^2)r}\left[\left\{(\mu_0+\kappa_0)k_c^2-\rho_0\omega^2\right\}e^{ik_cr}-\left\{(\mu_0+\kappa_0)k_s^2-\rho_0\omega^2\right\}e^{ik_sr}\right]$$
$$+\frac{1}{2\pi\gamma_0(\mu_0+\kappa_0)(\alpha_0+\beta_0+\gamma_0)r^3}\left[\frac{[(\alpha_0+\beta_0)\left\{(\mu_0+\kappa_0)k_c^2-\rho_0\omega^2\right\}+\kappa_0^2](1-ik_cr)}{(k_c^2-k_s^2)(k_c^2-k_n^2)}e^{ik_cr}\right.$$
$$+\frac{[(\alpha_0+\beta_0)\left\{(\mu_0+\kappa_0)k_s^2-\rho_0\omega^2\right\}+\kappa_0^2](1-ik_sr)}{(k_s^2-k_c^2)(k_s^2-k_n^2)}e^{ik_sr}$$
$$\left.+\frac{[(\alpha_0+\beta_0)\left\{(\mu_0+\kappa_0)k_n^2-\rho_0\omega^2\right\}+\kappa_0^2](1-ik_nr)}{(k_n^2-k_c^2)(k_n^2-k_s^2)}e^{ik_nr}\right]$$

$$(G_4)_{33} = \frac{-1}{2\pi\gamma_0(\mu_0+\kappa_0)(k_c^2-k_s^2)r}\left[\left\{(\mu_0+\kappa_0)k_c^2-\rho_0\omega^2\right\}e^{ik_cr}-\left\{(\mu_0+\kappa_0)k_s^2-\rho_0\omega^2\right\}e^{ik_sr}\right]$$
$$+\frac{1}{2\pi\gamma_0(\mu_0+\kappa_0)(\alpha_0+\beta_0+\gamma_0)r^3}\left[\frac{[(\alpha_0+\beta_0)\left\{(\mu_0+\kappa_0)k_c^2-\rho_0\omega^2\right\}+\kappa_0^2](k_c^2r^2+2ik_cr-2)}{(k_c^2-k_s^2)(k_c^2-k_n^2)}e^{ik_cr}\right.$$
$$+\frac{[(\alpha_0+\beta_0)\left\{(\mu_0+\kappa_0)k_s^2-\rho_0\omega^2\right\}+\kappa_0^2](k_s^2r^2+2ik_sr-2)}{(k_s^2-k_c^2)(k_s^2-k_n^2)}e^{ik_sr}$$
$$\left.+\frac{[(\alpha_0+\beta_0)\left\{(\mu_0+\kappa_0)k_n^2-\rho_0\omega^2\right\}+\kappa_0^2](k_n^2r^2+2ik_nr-2)}{(k_n^2-k_c^2)(k_n^2-k_s^2)}e^{ik_nr}\right]$$

Appendix II

Method of forming products and taking expectation values $\langle M_1G_0M_1'\rangle(\vec{A}e^{i\vec{k}\cdot\vec{x}'})$, etc.

$$\langle N_1G_0M_1'\rangle(\vec{A}e^{i\vec{k}\,\vec{x}'})$$
$$=\kappa_1\vec{\nabla}\times G_0[-(\lambda_1'+\mu_1')(\vec{k}\,\vec{A})\vec{k}-(\mu_1'+\kappa_1')k^2\vec{A}+$$
$$i\vec{\nabla}'\lambda_1'(\vec{k}\,\vec{A})+i\vec{\nabla}'\mu_1'\times(\vec{k}\times\vec{A})+i[\vec{\nabla}'(2\vec{\mu'}+\kappa_1')\,\vec{k}]\vec{A}+\rho_1'\omega^2\vec{A}]e^{i\vec{k}\,\vec{x}'}$$

$$=[-(R_{\kappa\lambda}+R_{\kappa\mu})A_1k^2(0,\frac{\partial(G_0)_{11}}{\partial z},-\frac{\partial(G_0)_{11}}{\partial y})-k^2(R_{\kappa\mu}+R_{\kappa\kappa})(-A_2\frac{\partial(G_0)_{22}}{\partial z},A_1\frac{\partial(G_0)_{11}}{\partial z},$$
$$A_2\frac{\partial(G_0)_{22}}{\partial x}-A_1\frac{\partial(G_0)_{11}}{\partial y})+ikA_1(\frac{\partial R_{\kappa\lambda}}{\partial z'}\cdot\frac{\partial(G_0)_{33}}{\partial y}-\frac{\partial R_{\kappa\lambda}}{\partial y'}\cdot\frac{\partial(G_0)_{22}}{\partial z},$$
$$\frac{\partial R_{\kappa\lambda}}{\partial x'}\cdot\frac{\partial(G_0)_{11}}{\partial z}-\frac{\partial R_{\kappa\lambda}}{\partial z'}\cdot\frac{\partial(G_0)_{22}}{\partial x},\frac{\partial R_{\kappa\lambda}}{\partial y'}\cdot\frac{\partial(G_0)_{22}}{\partial x}-\frac{\partial R_{\kappa\lambda}}{\partial x'}\cdot\frac{\partial(G_0)_{11}}{\partial y})+ikA_2(\frac{\partial R_{\kappa\mu}}{\partial x'}\cdot\frac{\partial(G_0)_{22}}{\partial z},$$
$$A_2\frac{\partial(G_0)_{22}}{\partial x}-A_1\frac{\partial(G_0)_{11}}{\partial y})\frac{\partial(2R_{\kappa\mu}+R_{\kappa\kappa})}{\partial x'}.$$

$$\frac{\partial R_{\kappa\mu}}{\partial y'}\cdot\frac{\partial (G_0)_{11}}{\partial z},-\frac{\partial R_{\kappa\mu}}{\partial x'}\cdot\frac{\partial (G_0)_{22}}{\partial x}-\frac{\partial R_{\kappa\mu}}{\partial y'}\cdot\frac{\partial (G_0)_{11}}{\partial y})+ik(-A_2\frac{\partial (G_0)_{22}}{\partial z},A_1\frac{\partial (G_0)_{11}}{\partial z},$$

$$+\omega^2 R_{\kappa\rho}(-A_2\frac{\partial (G_0)_{22}}{\partial z},A_1\frac{\partial (G_0)_{11}}{\partial z},A_2\frac{\partial (G_0)_{22}}{\partial x}-A_1\frac{\partial (G_0)_{11}}{\partial y})]e^{i\vec{k}\cdot\vec{x}'}.$$

Appendix III

A note on transforming to radial forms

$\vec{r}=\vec{x}-\vec{x}'=(\xi,\eta,\varsigma)=(r\cos\theta,r\sin\theta\cos\phi,r\sin\theta\sin\phi);$

$\frac{\partial}{\partial x}=\frac{\partial}{\partial\xi},\frac{\partial}{\partial y}=\frac{\partial}{\partial\eta},\frac{\partial}{\partial z}=\frac{\partial}{\partial\varsigma};\frac{\partial}{\partial x'}=-\frac{\partial}{\partial\xi},\frac{\partial}{\partial y'}=-\frac{\partial}{\partial\eta},\frac{\partial}{\partial z'}=-\frac{\partial}{\partial\varsigma};$

$r^2=\xi^2+\eta^2+\varsigma^2;\ \ r\frac{\partial r}{\partial\xi}=\xi;\therefore\frac{\partial r}{\partial\xi}=\frac{\xi}{r},\frac{\partial r}{\partial\eta}=\frac{\eta}{r},\frac{\partial r}{\partial\varsigma}=\frac{\varsigma}{r};$

$\frac{\partial}{\partial x}=\frac{\partial}{\partial\xi}=(\frac{\partial}{\partial r})\frac{\partial r}{\partial\xi}=\frac{\xi}{r}\frac{\partial}{\partial r}=\cos\theta\frac{\partial}{\partial r};$

$\frac{\partial}{\partial y}=\frac{\eta}{r}\frac{\partial}{\partial r}=\sin\theta\cos\phi\frac{\partial}{\partial r};\frac{\partial}{\partial z}=\frac{\varsigma}{r}\frac{\partial}{\partial r}=\sin\theta\sin\phi\frac{\partial}{\partial r};$

$\frac{\partial^2}{\partial x^2}=\frac{\xi}{r}\frac{\partial}{\partial r}(\frac{\xi}{r}\frac{\partial}{\partial r})=\cos^2\theta\frac{\partial^2}{\partial r^2};\frac{\partial^2}{\partial y^2}=\frac{\eta}{r}\frac{\partial}{\partial r}(\frac{\eta}{r}\frac{\partial}{\partial r})=\sin^2\theta\cos^2\phi\frac{\partial^2}{\partial r^2};$

$\frac{\partial^2}{\partial z^2}=\frac{\varsigma}{r}\frac{\partial}{\partial r}(\frac{\varsigma}{r}\frac{\partial}{\partial r})=\sin^2\theta\sin^2\phi\frac{\partial^2}{\partial r^2}.$

1. $\int_0^{2\pi}\cos^2\phi d\phi=.\int_0^{2\pi}\sin^2\phi d\phi=\pi;$
2. $f(r)=\frac{\sin kr}{kr}$
3. $f'(r)=\frac{d}{d(kr)}\frac{\sin kr}{kr};f''(r)=\frac{d^2}{d(kr)^2}\frac{\sin kr}{kr}$
4. $\int_0^{\pi}e^{-ikr\cos\theta}\sin\theta d\theta=2\frac{\sin kr}{kr}=2f(r)=\int_{-1}^{1}e^{-ikrx}dx$
5. $\int_0^{\pi}e^{-ikr\cos\theta}\sin\theta\cos\theta d\theta=2if'(r)=\int_{-1}^{1}xe^{-ikrx}dx$
6. $\int_0^{\pi}e^{-ikr\cos\theta}\sin\theta\cos^3\theta d\theta=-2if'''(r)$

7. $\int_0^\pi e^{-ikr\cos\theta}\sin^3\theta\cos\theta d\theta = 2i[f'(r)+f'''(r)]$

8. $\int_0^\pi e^{-ikr\cos\theta}\sin\theta\cos^2\theta d\theta = -2f''(r)$

9. $\int_0^\pi e^{-ikr\cos\theta}\sin^3\theta d\theta = -2[f(r)+f''(r)]$

10. $\int_0^{2\pi}\cos^3\phi d\phi = \left|\sin\phi - \frac{1}{3}\sin^3\phi\right|_0^{2\pi} = 0.$

Appendix IV

Finite parts of some integrals [46]

(i) $Pf\int_0^\infty \frac{e^{-pt}}{t}dt = -\log p - \gamma = -\log Cp,\ \ \mathrm{Re}p > 0,$
where $\gamma = \log C = .577$ (Euler's constant) .

(ii) $Pf\int_0^\infty \frac{e^{-pt}}{t^2}dt = p(\log p + \gamma - 1)$.

(iii) $\int_0^\infty e^{-pt}\frac{\sin bt}{t}dt = \tan^{-1}\frac{b}{p}, |\arg p| < \pi/2$.

(iv) $Pf\int_0^\infty e^{-pt}\frac{\cos bt}{t}dt = -\frac{1}{2}\log(p^2+b^2) - \gamma,\ |\arg p| < \pi/2$.

(v) $Pf\int_0^\infty e^{-pt}\frac{\sin bt}{t^2}dt = \frac{-r}{1}[\theta\cos\theta + \{\log r - \Psi(2)\}\sin\theta,\ |\arg p| < \pi/2$,

$\theta = \tan^{-1}\frac{b}{p}, r = \sqrt{p^2+b^2}.$

(vi) $Pf\int_0^\infty e^{-pt}\frac{\cos bt}{t^2}dt = \frac{-r}{1}\Big\{[\log r - \Psi(2)]\cos\theta - \theta\sin\theta\Big\},\ |\arg p| < \pi/2,$

$\Psi(2) = -\gamma + 1 + \frac{1}{2}$.

archives
of thermodynamics
Vol. **38**(2017), No. 2, 61–79
DOI: 10.1515/aoter-2017-0010

System effects of primary energy reduction connected with operation of the CHP plants

ANDRZEJ ZIĘBIK*
PAWEŁ GŁADYSZ

Silesian University of Technology, Institute of Thermal Technology,
Konarskiego 22, 44-100 Gliwice

Abstract The paper is devoted to explication of one of the advantages of heat and electricity cogeneration, rarely considered in technical literature. Usually attention is paid to the fact that heat losses of the heat distribution network are less severe in the case of cogeneration of heat in comparison with its separate production. But this conclusion is also true in other cases when the internal consumption of heat is significant. In this paper it has been proved in the case of two examples concerning trigeneration technology with an absorption chiller cooperating with a combined heat and power (CHP) plant and CHP plant integrated with amine post-combustion CO_2 processing unit. In both considered cases it might be said that thanks to cogeneration we have to do with less severe consequences of significant demand of heat for internal purposes.

Keywords: Cogeneration; Trigeneration; Amine CO_2 capture; System effects

Nomenclature

E	–	energy
fg	–	flue gases
Q	–	heat
q	–	unit consumption of heat

*Corresponding Author. Email andrzej.ziebik@polsl.pl

Greek symbols

α	–	coefficient of the share of cogeneration
Δ	–	increase
$\lvert-\Delta\rvert$	–	savings (reduction, decrease)
ε	–	index of internal electricity or heat consumption
η	–	efficiency
σ	–	power to heat ratio

Subscripts

a	–	absorption chiller
c	–	cooling agent
ch	–	chemical
com	–	compressors
con	–	consumers
ct	–	cooling agent transmission
E	–	energy
el	–	electrical
G	–	gross
h	–	heat
hp	–	heat-generating plant
ht	–	heat transport
int	–	integrated
los	–	losses
N	–	net
pp	–	power plant
rec	–	recovery
ref	–	reference
reg	–	regenerative
sb	–	steam boiler
sep	–	separate production
sys	–	systems
tt	–	transformation and transmission

Abbreviations

CCS	–	CO_2 capture and storage
CHP	–	combined heat and power
COP	–	coefficient of performance
CPU	–	CO_2 processing unit

1 Introduction

The municipal and industrial thermal processes can be usually provided with heat from the combined heat and power (CHP) units or heat-generating plants by means of heat distribution network. Losses of heat during transmission as well as consumption of heat in additional installations as for instance absorption chiller in trigeneration (or combined cooling, heat and

power – CCHP) technology or desorber in amine CO_2 processing unit cause the increase of internal consumption of heat and in consequence increase of fuel consumption. Partial compensation of the increased internal consumption of heat takes place in the CHP units because electricity is cogenerated as a by-product deciding about the system effects of the reduction of primary energy consumption. This problem has been highlighted in [1], where heat losses during transmission of heat from the CHP plants or heat-generating plants by heat distribution network have been analysed. The essence of this problem is a perception of the fact that although heat losses cause additional consumption of the chemical energy of fuels in the CHP plant (local effect), on the other hand, however, the production of electricity grows and increases primary energy savings thanks to cogeneration (system effects). Thus the final result is positive. This effect does not take place in the case of the production of heat in a heat-generating plant. It should also be stressed that the system effect of primary energy reduction thanks to cogeneration is recorded not directly in the CHP plant but on the level of the national energy system.

The first author of this considerations paid attention in his earlier papers to the fact that the same effect can also be observed in the case of trigeneration technology with the absorption chiller [2,3]. Similarly as in the previous case, this effect is caused by the production of electricity in cogeneration with the production of heat for the absorption chiller. The index of the savings of chemical energy of fuel in the trigeneration system grows with decreasing of the coefficient of performance (COP) of the absorption chiller. It should not however be understood that the worse COP, leads to elevated savings. It means, however, that cooperation of the absorption chiller with the cogeneration system (CHP plant) causes less severe consequences of the worse COP of the absorption chiller if the demand for driving heat is realized by the CHP plant [3].

Large internal users of heat are systems of CO_2 capture and storage (CCS), particularly with post-combustion CO_2 capture [4]. In the case of CHP-CCS systems the internal demand for regeneration heat in CO_2 capture unit is realized by the bleeders of the extraction-condensing turbine or outlet steam from the back-pressure turbine. Due to this, a growth of gross production of electricity in cogeneration has been observed. But on the other hand, the internal consumption of electricity increases because of driving the CO_2 compressors as well as pumps and fans in CO_2 processing unit. Finally, the net production of electricity in cogeneration has been

decreased but this reduction is lower, the greater is the demand for heat concerning regeneration of solvent. This is also a system effect of primary energy reduction due to cogeneration technology [5,6].

The algorithms of the aforesaid above three cases of system effects of primary energy reduction connected with power and heat cogeneration technology are presented in this paper. For each case the results of exemplary calculations confirming the thesis described in algorithmic part of the paper have also been presented. It should be noticed that generally the useful effect of heat and electricity cogeneration being a primary energy savings is not observed locally in a CHP plant because this is a system effect [7,8]. Direct savings of the chemical energy of fuels takes place in a system power plant in which some part of electricity production has been replaced by production of the CHP plant. Including consumption of energy during extraction, processing and transport of fuels we can evaluate cumulative energy savings on the level of national energy system [8].

2 Partial compensation of chemical energy consumption of fuel charging the heat losses in heat distribution network supplied from CHP plant

Every loss of heat in the heat distribution network cooperating with a heat-generating plant or a CHP plant causes a growth of the gross production of heat. In consequence, the consumption of chemical energy of fuel increases. In the case of heat-generating plant the increase of the consumption of the chemical energy of fuel connected with additional production of heat due to heat losses is as follows:

$$\Delta E_{ch\ hp} = \frac{Q_{los}}{\eta_{E\ hp\ G}}\ , \tag{1}$$

where:

- $\Delta E_{ch\ hp}$ – additional consumption of the chemical energy of fuels in heat-generating plant due to heat losses,
- Q_{los} – heat losses in heat distribution network,
- $\eta_{E\ hp\ G}$ – gross energy efficiency of heat-generating plant.

Thus, when heat distribution network are fed from the heat-generating plant the heat losses cause directly the increase of the consumption of

chemical energy of fuels.

Heat losses in the heat distribution network cooperating with CHP plant also lead to increasing the consumption of chemical energy of fuel locally in CHP plant but simultaneously increase the cogeneration of electricity and in result we can observe decreasing the consumption of the chemical energy of fuels in the replaced power plant due to substituting the some part of its electricity production by the CHP plant. The system effect of these operations is calculated by means of the equation

$$\Delta E_{ch\ sys} = \Delta E_{ch\ CHP} - |-\Delta E_{ch\ pp}| \ , \tag{2}$$

where:

$\Delta E_{ch\ sys}$ – system effect of increasing the consumption of the chemical energy of fuels in the case of CHP plant cooperating with heat distribution network,

$\Delta E_{ch\ CHP}$ – increase of the consumption of the chemical energy of fuel in the CHP plant,

$|-\Delta E_{ch\ pp}|$ – decrease of the chemical energy of fuel consumption in the replaced power plant due to cogeneration of heat and electricity.

The increase of the consumption of the chemical energy of fuels due to heat losses, concerning CHP plant, is as follows:

$$\Delta E_{ch\ CHP} = \frac{Q_{los} + \Delta E_{el\ CHP\ G}}{\eta_{E\ CHP\ G}} \ , \tag{3}$$

where:

$\Delta E_{el\ CHP\ G}$ – increase of gross electricity production in cogeneration of heat covering the heat losses,

$\eta_{E\ CHP\ G}$ – gross energy efficiency of a CHP plant.

Assuming that the efficiencies of transformation and transmissions of electricity are the same in the case of power plant and CHP unit the decrease of the consumption of the chemical energy of fuels in a system power plant due to replacing the part of electricity production by a CHP plant results from the equation

$$|-\Delta E_{ch\ pp}| = \frac{\Delta E_{el\ CHP\ G}\,(1 - \varepsilon_{CHP})}{\eta_{E\ pp\ N}} \ , \tag{4}$$

where:

$\eta_{E\ pp\ N}$ – net energy efficiency of the replaced power plant,

ε_{CHP} – index of internal electricity consumption concerning CHP plant.

Including Eqs. (3) and (4) into Eq. (2) we get a formula concerning system increase of the chemical energy of fuels in the case of cogeneration:

$$\Delta E_{ch\ sys} = Q_{los}\left[\frac{1+\sigma}{\eta_{E\ CHP\ G}} - \frac{\sigma\,(1-\varepsilon_{CHP})}{\eta_{E\ pp\ N}}\right], \tag{5}$$

where σ denotes power to heat ratio.

Reduction of the consumption of chemical energy of fuels, charging the heat losses in heat distribution network, due to cogeneration of heat and electricity in comparison with the separate production of heat results from the equation:

$$|-\Delta E_{ch}| = \Delta E_{ch\ hp} - \Delta E_{ch\ sys}\ , \tag{6}$$

where $|-\Delta E_{ch}|$ denotes energy savings of the chemical energy of fuels due to cogeneration.

In Eq. (6) it was assumed that the change of electricity consumption for heat transmission due to the change of heat losses is nearly the same in both considered cases, namely cogeneration and separate production of heat in heat generating plant. As the partial efficiency of electricity production in a CHP plant is the same as efficiency of electricity production in system power plant [8,9] the changes of the consumption of the chemical energy of fuel in the case of heat transmission from heat generating plant and in the case of CHP plant are the same. Therefore both these items included into Eq. (6) are reduced.

Introducing Eqs. (1) and (5) into Eq. (6) and referring energy savings to heat losses we have

$$\frac{|-\Delta E_{ch}|}{Q_{los}} = \frac{1}{\eta_{E\ hp\ G}} - \frac{1}{\eta_{E\ CHP\ G}} + \sigma\left(\frac{1-\varepsilon_{CHP}}{\eta_{E\ pp\ N}} - \frac{1}{\eta_{E\ CHP\ G}}\right). \tag{7}$$

The following input data have been assumed in the analysis: $\eta_{E\ hp\ G} = 0.85$, $\eta_{E\ pp\ N} = 0.43$, and $\varepsilon_{CHP} = 0.11$. The analysis has been carried out in the following ranges of $\eta_{E\ CHP\ G}$ and σ: 0.75–0.85, and 0.3–0.5, respectively. Figure 1 presents the reduction of consumption of chemical energy of fuels covering the heat losses in heat distribution network supplied from CHP plant. This effect of partial compensation of chemical energy of fuels connected with heat losses depends on the gross energy efficiency of CHP plant and power to heat ratio. The higher values of those parameters the higher system effects (reduction of chemical energy consumption) thanks to cogeneration. Generally we can say that heat losses connected with the

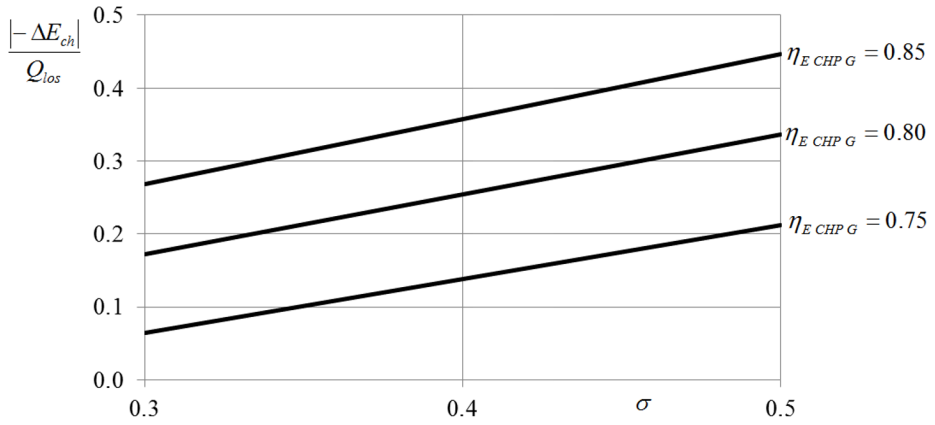

Figure 1: Reduction of the consumption of chemical energy of fuels covering heat losses by cogeneration.

transmission of heat by means of heat distribution network are less severe in the case of its cooperation with CHP plant in comparison with supply the heat distribution network from heat generating plant [9].

3 System effects of primary energy reduction in trigeneration installations

Combination of a CHP plant with centralized system of cooling agent production [10] is called 'trigeneration'. This consideration is devoted to an installation equipped with absorption chiller driven by heat from CHP plant. Figure 2 presents a scheme of a classical CHP plant cooperating with the centralized system of cooling agent production.

The additional gross production of heat dedicated to production of cooling agent in a CHP plant and additional gross cogeneration of electricity are charged by the additional consumption of the chemical energy of fuels:

$$\Delta E_{ch\,CHP} = \frac{Q_{c\,con}\,(1+\sigma)}{\eta_{E\,CHP\,G}\eta_{ct}\,(1-\varepsilon_c)\,COP_a}\,, \tag{8}$$

where:

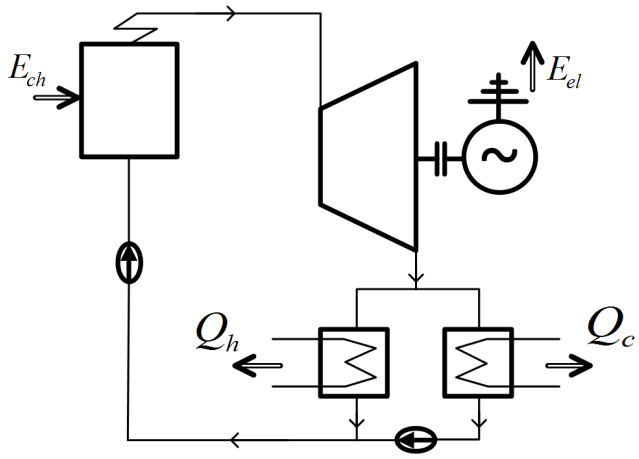

Figure 2: Scheme of a CHP unit with a centralized system of providing the cooling agent: E_{ch} – chemical energy of fuel, E_{el} – production of electricity, Q_h – production of heat, Q_c – production of cooling agent.

$\Delta E_{ch\,CHP}$	–	additional consumption of the chemical energy of fuels in a CHP plant due to production of cooling agent,
$Q_{c\,con}$	–	amount of cooling agent by the consumers,
σ	–	power to heat ratio,
$\eta_{E\,CHP\,G}$	–	gross energy efficiency of a CHP plant,
η_{ct}	–	efficiency of cooling agent transmission from CHP plant,
ε_c	–	own consumption of cooling agent in a CHP plant,
COP_a	–	coefficient of performance of absorption chiller.

In the case of separate production of the cooling agent in cooperation with a heat-generating plant and electricity production in the system power plant the consumption of chemical energy of fuels is as follows:

$$E_{ch\,sep} = \frac{Q_{c\,con}}{\eta_{E\,hp\,G}\eta'_{ct}\,(1-\varepsilon'_c)\,COP_a} + \frac{\sigma\,Q_{c\,con}\,(1-\varepsilon_{el})\,\eta_{tt}}{\eta_{E\,pp\,N}\eta_{ct}\,(1-\varepsilon_c)\,COP_a\eta'_{tt}}\,, \qquad (9)$$

where:

$E_{ch\,sep}$	–	consumption of chemical energy of fuels charging the separate production of cooling agent and electricity,
$\eta_{E\,hp\,G}$	–	gross energy efficiency of heat-generating plant,
η_{ct}, η'_{ct}	–	efficiency of cooling agent transmission from CHP plant and heat generating plant,

ε_c' – own consumption of cooling agent in heat-generating plant,
$\eta_{E\ pp\ N}$ – net energy efficiency of a systems power plant,
ε_{el} – own consumption of electricity in a CHP plant,
η_{tt}, η_{tt}' – efficiency of transformation and transmission of electricity from CHP plant and systems power plant.

Assuming that $\eta_{tt} = \eta_{tt}'$ and neglecting the own consumption of the cooling agent and its losses during transmission the savings of chemical energy of fuel results from the comparison of 'trigeneration' system with a separate production of heat, cooling agent and electricity is as follows:

$$\frac{|-\Delta E_{ch}|}{Q_{c\ con}} = \frac{1}{COP_a}\left[\frac{1}{\eta_{E\ hp\ G}} - \frac{1}{\eta_{E\ CHP\ G}} + \sigma\left(\frac{1-\varepsilon_{el}}{\eta_{E\ pp\ N}} - \frac{1}{\eta_{E\ CHP\ G}}\right)\right]. \tag{10}$$

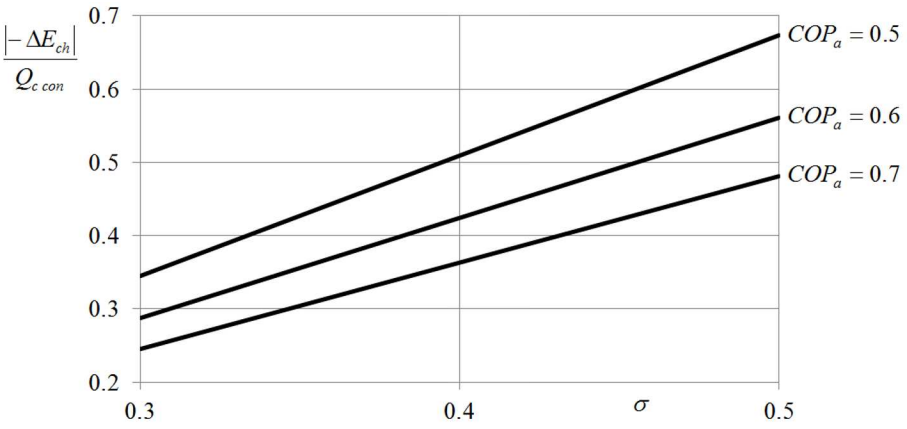

Figure 3: Energy savings of the chemical energy of fuels due to trigeneration.

Figure 3 presents energy savings of chemical energy of fuel thanks to the production of cooling agent in the absorption chiller in cooperation with the CHP plant (trigeneration technology). These savings result from replacing the electricity production in a system power plant, thanks to additional production of electricity in cogeneration, with additional heat demand for absorption chiller. It is natural that the energy savings increase with increasing power to heat ratio but the growth with the decreasing COP_a of the absorption chiller needs explanation. This tendency cannot be interpreted that the worse efficiency is better. It merely means that the production of

heat in cogeneration with electricity partially compensates worse COP_a of the absorption chiller [2,3].

4 System effect of partial compensation of the increased own consumption of heat in a CHP plant integrated with an amine CO_2 processing unit

The post-combustion CO_2 capture based on amine solvent belongs at present to the most technically mature ways of CO_2 removal [11–14]. The weak side of this method is a high demand for heat in order to regenerate the solvent. Figure 4 presents scheme of CHP plant integrated with CO_2 processing unit (CPU) and installation of waste heat recovery. CPU consists of CO_2 absorption column and desorption column [13]. Desorption column serves to the regeneration of aqueous solution of mixture containing monoethanoloamine, dieethanoloamine and methyldieethanoloamine. This process in desorber requires additional production of heat for internal consumption. The process heat for this purpose is transported from the bleeds of the extraction-condensing steam turbine or from the outlet of back-pressure turbine with a pressure of about 0.2 MPa. It provides required range of temperature regeneration. In [12] attention has been paid to the considerable consumption of heat concerning amine regeneration. In this consideration, the unit consumption of heat for regenerative purposes has been assumed: 4, 3.4, and 3.15 MJ/kg CO_2. The first value concerns traditional installations existing up to now whereas the second one is treated as a value possible to be achieved today. The third value can be treated as a value in the nearest future confirmed by several research works [15–19].

It should be stressed that the CPU installation is not only consumer of process heat but also is a source of waste heat in which recovery may cover partially the demand for system of the heat distribution network (district or industrial). The source of waste heat is the process of CO_2 desorption in which the condensation of H_2O takes place. Also, the installation of interstage cooling of CO_2 compressors are sources of waste heat.

Similarly as in previous subsections the growth of internal consumption of heat for the purpose of solvent regeneration in the CHP plant leads to an increase of the electricity production. But in this case the situation is more complicated because simultaneously the demand for electricity growths due

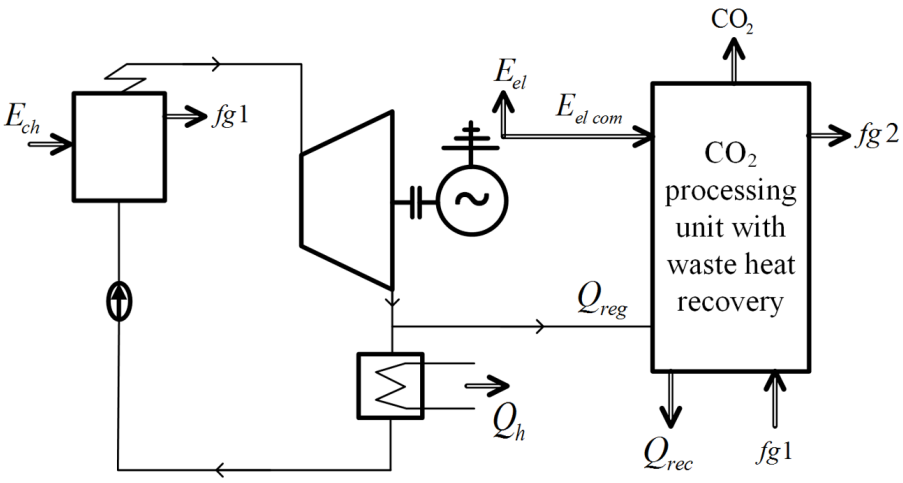

Figure 4: Scheme of a CHP plant integrated with CO_2 processing unit and installation of waste heat recovery: E_{ch} – chemical energy of fuel, fg – flue gases, E_{el} – electricity for external consumers, E_{elcom} – electricity for CO_2 compressors, Q_{reg} – regenerative heat, Q_h – heat for external consumers, Q_{rec} – heat from waste energy recovery.

to driving the CO_2 compressors in CPU. Additionally, waste heat recovery from CPU leads to a reduction of the demand for low-pressure heating steam from the turbine and in consequence the production of electricity cogenerated with low-pressure heating steam has been decreased. Such the thermodynamic analysis characterizes the greater complexity than in the cases presented previously. That is why simulation models were prepared by means of the commercial engineering software Thermoflex [20]. This software allows to construct requisite models of the analysed energy system based on predefined components available in the library of Thermoflex. The components are among others group of turbine stages, compressors, pumps, heat exchangers of regeneration and heat engineering and also for instance the installation of CO_2 processing unit. Simulation models have been constructed not only as a design mode but also as off-design one. Annual duration curve of outdoor temperature and the characteristics of the heat distribution network have been applied in the simulation calculations [5,6].

First of all the reference CHP plant with an extraction-back-pressure turbine and CFB peak boiler (without CPU) has been modeled. In this case the index of savings of chemical energy of fuel is calculated from the

formula [6]

$$\left(\frac{\left|-\Delta\dot{E}_{ch}\right|}{\dot{Q}_{con}}\right)_{ref} = \frac{\alpha_{cog}}{\eta_{ht}}\left[\frac{1}{(1-\varepsilon_{h\ hp})\ \eta_{E\ hp\ G}}+\frac{\sigma_{ref}\,(1-\varepsilon_{el\ ref})}{(1-\varepsilon_{h\ ref})\ \eta_{E\ pp\ N}}-\frac{1+\frac{\sigma_{ref}}{\eta_{me}}}{(1-\varepsilon_{h\ ref})\ \eta_{E\ sb}}\right], \quad (11)$$

where:

- $\left|-\Delta\dot{E}_{ch}\right|$ – savings of the chemical energy of fuel,
- $\dot{Q}_{con}$ – demand of heat flux by consumers,
- α_{cog} – coefficient of the share of cogeneration,
- η_{ht} – efficiency of heat transmission,
- $\varepsilon_{h\ hp}$ – relative internal consumption of heat concerning heat-generating plant,
- $\eta_{E\ hp\ G}$ – gross energy efficiency of heat-generating plant,
- σ_{ref} – power to heat ratio concerning the reference CHP plant,
- $\varepsilon_{el\ ref}$ – relative internal consumption of electricity in concerned reference CHP plant,
- $\varepsilon_{h\ ref}$ – relative internal consumption of heat concerning reference CHP plant,
- $\eta_{E\ pp\ N}$ – net energy efficiency of replaced power plant,
- η_{me} – electromechanical efficiency,
- $\eta_{E\ sb}$ – energy efficiency of steam boiler.

Next, the model of the CHP plant with back-pressure turbine and CO_2 processing unit has been elaborated. The additional desulphurization system must be installed due to requirement of amine CO_2 processing unit. The compressors station of CO_2 has been equipped with four units. Waste heat from interstage cooling of CO_2 compressors has been utilized in the basic heat exchanger of district heating system. In order to regenerate the amine solution, the CO_2 processing unit is fed by the process steam from the outlet of back-pressure turbine. The index of savings of chemical energy of fuel is as follows [6]:

$$\left(\frac{\left|-\Delta\dot{E}_{ch}\right|}{\dot{Q}_{con}}\right)_{int} = \frac{\alpha_{cog}}{\eta_{ht}}\left[\frac{1}{(1-\varepsilon_{h\ hp})\,\eta^{int}_{E\ hp\ G}}-\frac{1}{(1-\varepsilon_{h\ int})\,\eta^{int}_{E\ cog\ G}}\right]+ \\ +\sigma_{int}\left[\frac{\alpha_{cog}}{(1-\varepsilon_{h\ int})\,\eta_{ht}}-\frac{\dot{Q}_{rec}}{\dot{Q}_{con}}+\frac{\dot{Q}_{reg}}{\dot{Q}_{con}}\right]\left[\frac{(1-\varepsilon_{el\ int})}{\eta^{int}_{E\ pp\ N}}-\frac{1}{\eta^{int}_{E\ cog\ G}}\right] \quad (12)$$

where:

$\left(\frac{|-\Delta \dot{E}_{ch}|}{\dot{Q}_{con}}\right)_{int}$ – index of the chemical energy savings concerning CHP integrated with CPU and installation of waste heat recovery,

$\eta^{int}_{E\ hp\ G}$ – gross energy efficiency of integrated heat-generating plant,

$\eta^{int}_{E\ cog\ G}$ – gross energy efficiency of integrated CHP plant,

$\varepsilon_{h\ int}$ – relative internal consumption of heat concerning integrated CHP plant,

σ_{int} – power to heat ratio of integrated CHP plant,

$\dot{Q}_{rec}$ – flux of heat from installation of waste heat recovery,

$\dot{Q}_{reg}$ – flux of heat from regeneration of solvent,

$\varepsilon_{el\ int}$ – relative internal consumption of electricity concerning integrated CHP plant,

$\eta^{int}_{E\ pp\ N}$ – net energy efficiency of replaced integrated power plant.

Table 1 presents the results of simulation analysis concerning the CHP plant integrated with amine CO_2 processing unit and waste heat recovery installation [5,6]. The following additional input data have been used in an analysis:

- unit consumption of the chemical energy of fuel and production of electricity in a reference CHP plant (without CO_2 removal) with reference to heat by consumers – $E_{ch\ ref}/Q_{con} = 1.1665$ J/J and $E_{el\ ref}/Q_{con} = 0.3446$ J/J,
- net efficiency of replaced integrated power plant – $\eta^{int}_{E\ pp\ N} = 0.334$,
- index of the chemical energy savings concerning the reference CHP plant with reference to heat by the consumers – $|-\Delta E_{ch\ ref}|/Q_{con} = 0.381$ J/J.

The additional demand for internal consumption of heat in CPU installation connected with the regeneration of the solvent in CPU installation causes, of course, an additional consumption of the chemical energy of fuel but on the other hand the electricity additionally cogenerated with heat for regeneration of solvent influences the reduction of the chemical energy consumption concerning systems power plant due to decrease of its electricity production (effect of replacement). The CPU installation operates together with the CO_2 compressor station. Therefore, besides the increase of inter-

nal consumption of heat due to regeneration of the solvent also internal consumption of electricity increases due to driving CO_2 compressors.

Table 1: Selected results of simulative analysis of CHP plant integrated with CO_2 processing unit and waste heat recovery installation [5,6]*).

Unit consumption of heat for regeneration of solvent, q_{reg}, MJ/kg CO_2	4.0	3.4	3.15
Unit consumption of chemical energy of fuel with reference to heat by the consumers, $E_{ch\ int}/Q_{con}$, J/J	1.3499	1.2395	1.2006
Increase of unit consumption of chemical energy of fuel in comparison with reference CHP plant, $(E_{ch\ int} - E_{ch\ ref})/Q_{con}$, J/J	0.1834	0.0730	0.0341
Unit production of electricity with reference to heat by the consumers, $E_{el\ int}/Q_{con}$, J/J	0.3898	0.3579	0.3467
Increase of unit production of electricity in comparison with reference CHP plant, $(E_{el\ int} - E_{el\ ref})/Q_{con}$, J/J	0.0452	0.0133	0.0021
Increase of internal unit consumption of electricity due to CO_2 processing unit, $(\varepsilon_{el\ int}E_{el\ int} - \varepsilon_{el\ ref}E_{el\ ref})/Q_{con}$, J/J	0.0537	0.0493	0.0478
Deficit of the electricity production in the integrated CHP plant, $\lvert-\Delta E_{el\ int}\rvert/Q_{con}$, J/J	-0.0085	-0.0360	-0.0457
Increase of the consumption of chemical energy of fuel charging the production of electricity in replaced power plant, $\Delta E_{ch\ pp}/Q_{con}$, J/J	0.0254	0.1078	0.1368
Index of chemical energy savings with reference to heat by the consumers, $\lvert-\Delta E_{ch\ int}\rvert/Q_{con}$, J/J	0.342	0.323	0.308

*) All values in Tab. 1, except the unit consumption of heat for regeneration of solvent, have been calculated with reference to heat by the consumers.

Basing on the results of simulation analysis of power plant integrated with post-combustion CO_2 capture the increase of internal consumption of electricity due to compression of CO_2, as well as the increase of additional production of electricity in cogeneration with heat have been evaluated. The differences between them for the particular unit consumption of regenerative heat (4.0, 3.4, 3.15) are negative values (Tab. 1). It means that

by the assumption of E_{elcon} = idem (demand for electricity by consumers must be kept, similarly as demand for heat by consumers Q_{con} = idem) the balance of electricity requires additional production in a replaced system power plant, causing the additional consumption of chemical energy of fuel.

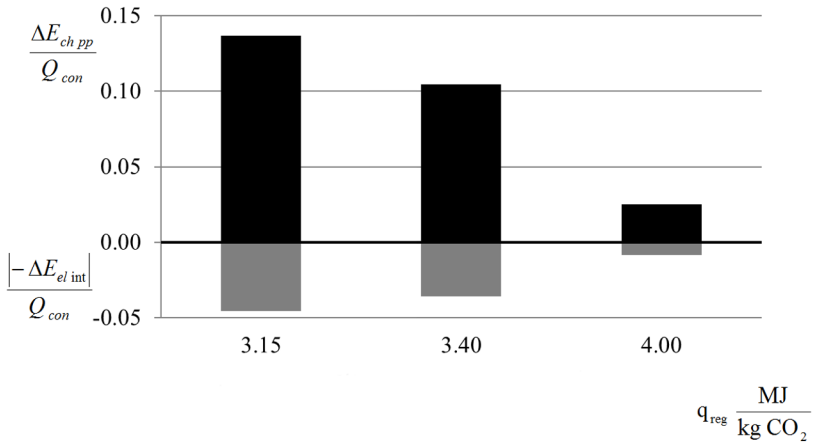

Figure 5: System effect of decreasing the deficit of the electricity production in the CHP plant: ΔE_{chpp} – chemical energy of fuel in replaced integrated power plant charging the production of electricity closing the balance, Q_{con} – heat loco consumers, -ΔE_{elCHP} – deficit of electricity production, q_{reg} – unit consumption of heat for regeneration of solvent.

Figure 5 presents both deficit of electricity concerning CHP plant (the least value concerns q_{reg}= 4.0 MJ/kg CO_2) and additional consumption of chemical energy of fuels charging the production of electricity in replaced power plant closing its balance. Similarly as in the previous cases it is clear that thanks to cogeneration we may observe a partial compensation of severe consequences of the worse coefficient of the unit consumption for regenerative purpose. In the case of the highest value of unit consumption of heat regeneration of solvent the deficit of electricity is the lowest. The lowest is also the increase of additional consumption of chemical energy of fuel in replaced integrated power plant.

Additional argument concerning the partial compensation of the increased internal consumption of heat thanks to cogeneration is showed in Fig. 6, where the relative reduction of the index of chemical energy savings in comparison with the reference CHP plant is presented. The lowest relative reduction of primary energy savings corresponds with the highest unit

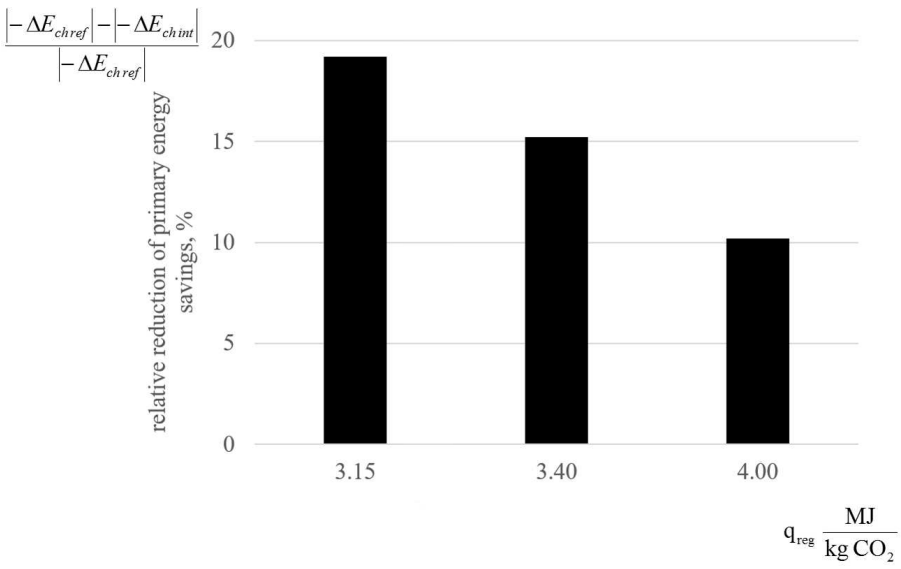

Figure 6: Relative reduction of primary energy savings due to additional consumption of heat for regeneration of solvent in the CO_2 processing unit: $|-\Delta E_{chref}|$– energy savings of fuel concerning reference CHP plant, $|-\Delta E_{chint}|$– energy savings of fuel corresponding the CHP plant integrated with CPU, q_{reg} – unit consumption of heat for regeneration of solvent.

consumption of heat for the solvent regeneration. It does not indicate that the worse amine CPU (q_{reg}= 4.0 MJ/kg CO_2) the better, because in this case the consumption of chemical energy of fuel in the CHP integrated with amine CPU is the largest ($E_{ch\,int}/Q_{con}$ = 1.3499J/J – Tab. 1). It may only indicate that thanks to cogeneration of heat production we may observe less severe consequences of the worse energy efficiency of CPU installation. This effect does not take place in the separate production of heat.

5 Conclusions

The presented problem, characterizing additional positive effects of CHP plants, is rarely exposed as an advantage of cogeneration technology. Already the first example concerning the partial compensation of heat losses during transmission of heat to industrial or municipal consumers, mentioned in literature [1], indicates clearly that heat losses during the transmission of heat from the CHP plant are less severe in comparison with the

transmission from the heat-generating plant. Generally the positive effects of cogeneration are observed not locally in a CHP plant but within the frame of the national energy system. It means that the index of savings of chemical energy of fuel in comparison with separate production of heat and electricity is an adequate measure of the effectiveness in the case of heat and electricity cogeneration. At this point two additional remarks have to be mentioned. First of all, the system effects of primary energy reduction connected with cogeneration should be investigated for the CHP plants that have been already internally optimized, e.g., by means of the coefficient of the share of cogeneration [21]. Secondly, the proposed within the paper methodology concerning heat losses during the transmission of heat can only be used for the centralized cogeneration systems, thus within the wide range of small-scale cogeneration solution (e.g., micro-CHP based on the gas boiler with ORC module [22]) the presented approach cannot be applied.

Trigeneration realized in cooperation with absorption chiller is the second example in which system approach is needed for interpreting the useful effects. The savings of the chemical energy of fuel growth with the grows of the power to heat ratio and with decreasing the COP of absorption chiller. If the first reason is natural, the second one has a system character and results from the production of electricity in cogeneration with heat delivering the absorption chiller which partially replaces the production of electricity in the system power plant. The growing tendency of energy savings with the decreasing of COP of absorption chiller should explain that thanks to cogeneration we have less severe consequences due to the worse coefficient of performance of absorption chiller.

In a CHP plant integrated with amine post-combustion CO_2 processing unit there is not only an increase of internal consumption of heat but also an increase of the internal consumption of electricity. Therefore, on the one hand we have an increase of electricity cogeneration due to additional demand for heat delivered to regeneration of solvent and on the other hand the increase of internal consumption of electricity concerning the driving of the CO_2 compressors. In the considered case this causes the deficit in electricity balance of the CHP plant covered by the system power plant. Similarly as in trigeneration thanks to cogeneration of heat and electricity there is to be observed an effect of less severe consequences due to high value of the coefficient of unit consumption of heat for regeneration purposes of the solvent.

Summing up these considerations it can be noticed that thanks to combined heat and power plants the increase of internal consumption of heat relates to the system effect of less severe consequences in comparison with separate production of heat and electricity. Examples presented in this paper confirm this conclusion.

Acknowledgements This work was carried out and financed within the frame of statutory research fund of the Faculty of Power and Environmental Engineering of the Silesian University of Technology in Gliwice (Poland).

Received 24 February 2017

References

[1] Szargut J.: *Influence of the efficiency of heat transmission on energy effectiveness of CHP plant.* Gospodarka Paliwami i Energią **4**(1992), 3–5 (in Polish).

[2] Ziębik A.: *Cogeneration of heat and power combined with production of cooling agent.* Gospodarka Paliwami i Energią **11**(2003), 2–6(in Polish).

[3] Ziębik A., Hoinka K.: *Energy Systems of Complex Buildings.* Springer Verlag, London 2013.

[4] Lund H., Vad Mathiesen B.: *The role of carbon capture and storage in a future sustainable energy system.* Energy **44**(2012), 469–476.

[5] Ziębik A., Budnik M., Liszka M.: *Thermodynamic indices assessing the integration of coal- fired CHP plants with post-combustion CO2 processing unit (CPU).* Energ. Convers. Manage. **73**(2013), 389–397.

[6] Ziębik A., Budnik M., Liszka M.: *Energy effectiveness of heat and electricity cogeneration integrated with amine processing unit.* Energetyka, **68**(2015), 5, 331–339.

[7] Horlock J.H.: *Cogeneration – Combined Heat and Power(CHP). Thermodynamics and Economics.* Krieger Publishing Company, Malabar 1997.

[8] Szargut J., Ziębik A.: *Fundamentals of Thermal Engineering.* PWN, Warszawa 2000 (in Polish).

[9] Szargut J., Ziębik A.: *Cogeneration of heat and electricity – CHP.* Polish Academy of Sciences. Division Katowice. Katowice – Gliwice 2007 (in Polish).

[10] Recknagel H., Sprenger E., Honman W., Schramek E.R.: *Heating and Air Conditioning. Guidebook.* EWFE, Gdańsk 1994 (in Polish).

[11] Fisher K. S., Searcy K. *et al.*: *Advanced amine solvent formulations and process integration for near-zero CO_2 capture success.* Grant No.: De-FG02-06ER84625 US Department of Energy – National Energy Technology Laboratory. Trimeric Corporation, Buda 2007.

[12] Mangalapally H.P., Hasse H.: *Pilot plant experiments for post combustion carbon dioxide capture by reactive absorption with novel solvents*. Energy Proced. **4**(2011), 1–8.

[13] Ogawa T., Ohashi Y., Yamanaka S., Miyaike K.: *Development of carbon dioxide removal system from the flue gas of coal fired power plant*. Energy Proced 2009, **1**(2009), 1, 721–724.

[14] Kuramochi T., Ramírez A., Faaij A., Turkenburg W: *Post-combustion CO2 capture from part-load industrial NGCC-CHPs: Selected results*. Energy Proced. **1**(2009), 1, 1395–1402.

[15] *Global CCS Institute: CO2 capture technologies*. Post Combustion Capture, 2011. www.cdn.globalccsinstitute.com/sites/default/files/publications/29721/co2-capture-technologies-pcc.pdf (accessed 21 Nov.15).

[16] *MHI's Energy Efficiency flue gas CO_2 Capture Technology and Large Scale CCS Demonstration test at coal-fired Power Plants in USA*. Mitsubishi Heavy Industries, Techn. Rev. **48**(2011), 1.

[17] Eswaran S., Wu S., Nicolo R.: *Advanced Amine-based CO_2 Capture for Coal-fired Power Plants*. Coal-Gen 2010. www.hitachipowersystems.us/technical_-papers/index.html (accessed 21.Nov.16)

[18] *Final Report CASTOR (CO2 from Capture to Storage): Project report*, Apr. 2011. www.cordis.europa.eu/documents/documentlibrary/12477 2011EN6.pdf (accessed 21.Nov.16).

[19] *Advanced Coal Power Systems with CO_2 Capture: EPRI's CoalFleet for Vision*, 2011. Update, a summary of Technology Status and Research, Development and Demonstrations, 2011 Technical Report. www.epri.com/abstracts/Pages/ProductAbstract.aspx?productIdij000000000001023468 (accessed 21.Nov.16).

[20] *Thermoflex* version 22. Thermoflex Inc., www.thermoflex.com

[21] Ziębik A., Gładysz P.: *Optimal coefficient of the share of cogeneration in the district heating system cooperating with thermal storage*. Arch. Thermodyn. **32**(2011), 3, 71–87.

[22] Wajs J., Mikielewicz D., Bajor M., Kneba Z.: *Experimental investigation of domestic micro-CHP based on the gas boiler fitted with ORC module*. Arch. Thermodyn. **37**(2016), 3, 79–94.

archives
of thermodynamics
Vol. **38**(2017), No. 2, 81–100
DOI: 10.1515/aoter-2017-0011

Non-linear unsteady inverse boundary problem for heat conduction equation

MAGDA JOACHIMIAK*
MICHAŁ CIAŁKOWSKI

Poznań University of Technology, Chair of Thermal Engineering, Piotrowo 3, 60-965 Poznań

Abstract Direct and inverse problems for unsteady heat conduction equation for a cylinder were solved in this paper. Changes of heat conduction coefficient and specific heat depending on the temperature were taken into consideration. To solve the non-linear problem, the Kirchhoff's substitution was applied. Solution was written as a linear combination of Chebyshev polynomials. Sensitivity of the solution to the inverse problem with respect to the error in temperature measurement and thermocouple installation error was analysed. Temperature distribution on the boundary of the cylinder, being the numerical example presented in the paper, is similar to that obtained during heating in the nitrification process.

Keywords: Inverse problem; Sensitivity of the solution to the inverse problem; Application of Chebyshev polynomials

Nomenclature

a	–	thermal diffusivity, m^2/s
c	–	specific heat, J/kgK
f	–	temperature on the cylinder boundary, °C
Fo	–	Fourier number
g	–	distance between the thermocouple and cylinder boundary, m
MINUS	–	values calculated with the thermocouple installation error of δr^*into the direction of the axis of cylinder

*Corresponding Author. Email magda.joachimiak@put.poznan.pl

PLUS	–	values calculated with the thermocouple installation error of δr^*into the direction of cylinder boundary
r	–	radius, m
R	–	maximum radius, m
random	–	values calculated with stochastic disturbance of temperature measurement
t	–	time, s
T	–	temperature, °C
dp	–	values calculated with the use of the direct problem
ip	–	values calculated with the use of the inverse problem

Greek symbols

β	–	coefficient in the assumed temperature function on the cylinder boundary
δ	–	absolute error
Δ	–	difference, Laplacian
∇	–	gradient
ϑ	–	temperature in non-dimensional coordinates
λ	–	heat conduction coefficient for the cylinder, W/mK
ξ	–	radius in non-dimensional coordinates
ρ	–	density, kg/m^3
τ	–	time in non-dimensional coordinates

Subscripts

0	–	start time (for $t = 0$)
max	–	maximum value during heating
$+\,\delta\xi^*$	–	inexact thermocouple location by $\delta\xi^*$ towards the boundary
$-\,\delta\xi^*$	–	inexact thermocouple location by $\delta\xi^*$ further from the boundary
$\delta\vartheta$	–	the error in temperature measurement of $\delta\vartheta$
m	–	measuring

Superscripts

*	–	measuring

1 Introduction

Realization of thermal field fulfilling the set criteria is required in processes of heating machine's components. To control body heating, it is important to know the temperature on the boundary of the region. However, it is not always possible to measure the boundary temperature, as, for example, in the burning chamber or on the inner surface of gas-turbine casing. It is extremely difficult when radiation constitutes a great part of heating process (heat treatment processes). In such cases, the boundary temperature can be determined from solution of the inverse problem based on temperature measurement at inner points in the body, arranged close to the boundary

where the course of temperature is not known [1,21]. Some methods of solving one-dimensional inverse problem of thermal field distribution for a cylinder were presented in [3]; and for the cylindrical layer – in [2]. Solution of the inverse problem based on Laplace's transform was discussed in [2,3,10,12]. Inverse problem for the heat conduction equation was solved with the use of sequential method and described in papers [2,22]. Analysis of thermal fields during unsteady heat transfer for an irregular geometry was described in [4]. Method of inverse problem finds a wide application in technical issues. In [24], a substitute calculation model for the inverse heat conduction problem was discussed. Boundary condition for a heated beam was sought for using this model and the finite element method. Paper [5] presents the algorithm for solving the inverse heat flow problems, which use the finite element method. The concept of this algorithm consists in solving the Neumann problem, where the heat flux on the inner boundary is sought. Algorithm gave smooth, non-oscillating and stable solution. It was used to analyse heat transfer in the region with holes. Paper [6] presents a method of solving the inverse heat conduction problem, comprising the solution of the Poisson's equation for simpler and linked with each other regions instead of the Laplace's equation for multiply-connected region, such as the gas-turbine blade with cooling channels. In paper [17], by means of solving the heat equation for 2D model in a steady-state with the use of the inverse problem, thermal conductivity of material as the polynomial depending on temperature was sought for. Paper [14] discusses heat flow in high-temperature industrial furnaces. Solving direct and inverse problems with the use of the conjugate gradient method for the changes of phase of metal solidification were analysed. Trefftz methods as well as the method of fundamental solutions are often used for solving direct and inverse problems for the equation of heat conduction [13,18, 23]. Paper [8] presents the solution of direct and inverse non-Fourier heat conduction problems with the use of Trefftz functions and Trefftz method. Paper [9] presents the method of solving nonlinear direct and inverse heat conduction problems with the use of Trefftz functions. Paper [16] discusses the solution of the inverse problem for the Poisson equation with the use of fundamental solution method and Tikhonov regularization. Application of the fundamental solutions method for solving the inverse problem of heat source determination in an unsteady heat conduction is presented in [15].

Heat treatment and thermo-chemical treatment processes comprise wide ranges of temperature. For nitrification process, heating temperature ranges from an ambient temperature up to the temperature of approx. 550 °C. Considering such range of temperature for steel, any change of heat conduction coefficient, λ, and specific heat, c, is significant. For the analysed range of temperature, the heat conduction coefficient changes from 52 W/(mK) to 36 W/(mK), and specific heat changes from 440 J/(kgK) to 750 J/(kgK) [11]; it is 30.8% and 70.5% of their initial values, respectively Heat conduction equation includes the change of thermal diffusivity $a = \lambda/\rho c$. Hence, the increase of λ and decrease of c causes the change of thermal diffusivity coefficient a from 0.000015 m^2/s to 0.000007 m^2/s, what is 53.3%. Such significant change of thermal diffusivity for temperature ranging from 20 °C to 550 °C in heat treatment processes requires application of mathematical model in which λ and c are functions depending on temperature (non-linear problem). Knowledge of temperature distribution during heating enables precise analysis of heat treatment processes and stresses arising during heating. Therefore, non-linear and unsteady heat conduction equation was solved in this paper with the use of the method of inverse problem.

2 Direct problem

Solution of direct problem enables determining temperature distribution in a cylinder with the known temperature on its boundary. For the heat conduction equation

$$\rho(T)\, c(T) \frac{\partial T}{\partial t} = \operatorname{div}(\lambda(T)\, \nabla T) \tag{1}$$

the following initial condition was assumed

$$T(r, t = 0) = T_0 = 0\ . \tag{2}$$

Kirchhoff's substitution [7] was applied

$$\vartheta = \frac{1}{\lambda_0} \int_{T_0}^{T} \lambda(u)\, du = \frac{1}{\lambda_0} \int_{0}^{T} \lambda(u)\, du \tag{3}$$

and

$$\vartheta + \delta\vartheta = \frac{1}{\lambda_0} \int_{0}^{T+\delta T} \lambda(u)\, du\ . \tag{4}$$

After substracting (3) from (4), we obtain

$$\delta\vartheta = \frac{1}{\lambda_0}\left(\int_0^{T+\delta T}\lambda\left(u\right)du - \int_0^{T}\lambda\left(u\right)du\right) = \frac{1}{\lambda_0}\int_T^{T+\delta T}\lambda\left(u\right)du\ . \tag{5}$$

It was hence obtained [7]

$$\frac{\partial\vartheta}{\partial t} = a\left(\vartheta\left(T\right)\right)\Delta\vartheta\ . \tag{6}$$

Equation (1) in polar coordinates reads

$$\frac{\partial\vartheta}{\partial t} = a\left(\vartheta\left(T\right)\right)\left(\frac{\partial^2\vartheta}{\partial r^2} + \frac{1}{r}\frac{\partial\vartheta}{\partial r}\right) \tag{7}$$

and when the non-dimensional coordinate

$$\bar{\xi} = \frac{r}{R} \in \langle 0,1\rangle \tag{8}$$

is introduced the Eq. (2) is transformed to the form

$$\frac{\partial\vartheta}{\partial t} = a(\vartheta\left(T\right))\frac{1}{R^2}\left(\frac{\partial^2\vartheta}{\partial\bar{\xi}^2} + \frac{1}{\bar{\xi}}\frac{\partial\vartheta}{\partial\bar{\xi}}\right)\ . \tag{9}$$

It was assumed that density changes a little during the heating process, and heat conduction coefficient and specific heat depend on temperature

$$\frac{\partial\vartheta}{\partial t} = \frac{\lambda\left(\vartheta\left(T\right)\right)}{\rho_0 c\left(\vartheta\left(T\right)\right)}\frac{1}{R^2}\left(\frac{\partial^2\vartheta}{\partial\bar{\xi}^2} + \frac{1}{\bar{\xi}}\frac{\partial\vartheta}{\partial\bar{\xi}}\right)\ . \tag{10}$$

When the non-dimensional time coordinate $\tau = \mathrm{Fo} = \frac{at}{R^2} = \frac{\lambda_0 t}{\rho_0 c_0 R^2}$ was introduced, the following equation was obtained:

$$\frac{\partial\vartheta}{\partial\tau} = \frac{\lambda(\vartheta\left(T\right))}{\lambda_0}\frac{c_0}{c(\vartheta\left(T\right))}\left(\frac{\partial^2\vartheta}{\partial\bar{\xi}^2} + \frac{1}{\bar{\xi}}\frac{\partial\vartheta}{\partial\bar{\xi}}\right), \qquad \bar{\xi}\in(0,1)\ . \tag{11}$$

Since the variable $\bar{\xi}\in\langle 0,1\rangle$, therefore substitution $\xi = 2\bar{\xi}-1$ is done. Then [19]

$$\bar{\xi} = \frac{\xi+1}{2}, \quad \frac{\partial\vartheta}{\partial\bar{\xi}} = 2\frac{\partial\vartheta}{\partial\xi}, \quad \frac{\partial^2\vartheta}{\partial\bar{\xi}^2} = 4\frac{\partial^2\vartheta}{\partial\xi^2}\ . \tag{12}$$

Hence

$$\frac{\partial \vartheta}{\partial \tau} = 4\frac{\lambda(\vartheta(T))}{\lambda_0}\frac{c_0}{c(\vartheta(T))}\left(\frac{\partial^2 \vartheta}{\partial \xi^2} + \frac{1}{\xi+1}\frac{\partial \vartheta}{\partial \xi}\right) . \tag{13}$$

Approximating the derivative with respect to time by the backward difference quotient, we have obtained the following linear equation:

$$\frac{\tilde{\vartheta}(\tau_i) - \tilde{\vartheta}(\tau_{i-1})}{\Delta\tau} \approx 4\frac{\lambda\left(\tilde{\vartheta}_{i-1}\right)}{\lambda_0}\frac{c_0}{c\left(\tilde{\vartheta}_{i-1}\right)}\left(\frac{d^2\tilde{\vartheta}}{d\xi^2} + \frac{1}{\xi+1}\frac{d\tilde{\vartheta}}{d\xi}\right) . \tag{14}$$

Solution to Eq. (11) is sought in the form of the linear combination of Chebyshev polynomials

$$\tilde{\vartheta} = \sum_{k=0}^{N} \alpha_k W_k(\xi), \quad \xi \in \langle -1, 1\rangle , \tag{15}$$

where $W_k(\xi)$ denotes the Chebyshev polynomials of the first type [20].

Assuming that $\beta^2 = \frac{1}{\Delta\tau}$, $Q = \vartheta(\tau_{i-1})$ and taking substitution (15) into account, we obtain the following system of linear equations

$$\beta^2 \sum_{k=0}^{N} \alpha_k W_k(\xi) - \beta^2 Q = 4\frac{\lambda\left(\tilde{\vartheta}_{i-1}\right)}{\lambda_0}\frac{c_0}{c\left(\tilde{\vartheta}_{i-1}\right)}\left(\sum_{k=0}^{N} \alpha_k W_k''(\xi) + \frac{1}{\xi+1}\sum_{k=0}^{N} \alpha_k W_k'(\xi)\right) . \tag{16}$$

Let $q(\xi,\tau) = 4\frac{\lambda(\vartheta_{i-1})}{\lambda_0}\frac{c_0}{c(\vartheta_{i-1})}$, thus we have

$$q(\xi,\tau)\sum_{k=0}^{N} \alpha_k W_k''(\xi) + \frac{1}{\xi+1} q(\xi,\tau)\sum_{k=0}^{N} \alpha_k W_k'(\xi) - \beta^2 \sum_{k=0}^{N} \alpha_k W_k(\xi) = -\beta^2 Q . \tag{17}$$

Therefore,

$$\sum_{k=0}^{N} \alpha_k q(\xi,\tau) W_k''(\xi) + \sum_{k=0}^{N} \alpha_k \frac{1}{\xi+1} q(\xi,\tau) W_k'(\xi) - \sum_{k=0}^{N} \alpha_k \beta^2 W_k(\xi) = -\beta^2 Q . \tag{18}$$

Hence, assuming $p(\xi) = \frac{1}{\xi+1}$ and $r(\xi,\tau) = -\beta^2 Q$, we have

$$\sum_{k=0}^{N} \alpha_k \left(q(\xi,\tau) W_k''(\xi) + p(\xi) q(\xi,\tau) W_k'(\xi) - \beta^2 W_k(\xi)\right) = r(\xi,\tau) . \tag{19}$$

To determine coefficients α_k, the collocation method is used, then for the radius ξ_i (for a period of time), we obtain the equation

$$\sum_{k=0}^{N} \alpha_k \left(q\left(\xi_i\right) W_k^{''}\left(\xi_i\right) + p\left(\xi_i\right) q\left(\xi_i\right) W_k^{'}\left(\xi_i\right) - \beta^2 W_k\left(\xi_i\right) \right) = r\left(\xi_i\right) \tag{20}$$

and demand that Eq. (20) is satisfied at all inner points ξ_i ($i = 1, 2, \ldots, N-1$). Hence we have N – 1 of equations, and the number of unknowns is N + 1, $\alpha_0, \alpha_1, \ldots, \alpha_N$; to close the system of equations, boundary conditions are joined

$$\left.\frac{\partial \tilde{\vartheta}}{\partial \xi}\right|_{\xi=-1} = 0 \ , \tag{21}$$

$$\left.\tilde{\vartheta}\right|_{\xi=1} = f\left(\tau\right) \ , \tag{22}$$

which, based on (15), has the form

$$\left.\frac{\partial \tilde{\vartheta}}{\partial \xi}\right|_{\xi=\xi_0=-1} = \sum_{k=0}^{N} \alpha_k W_k^{'}\left(\xi_0 = -1\right) = 0 \ , \tag{23}$$

$$\left.\tilde{\vartheta}\right|_{\xi=\xi_N=1} = \sum_{k=0}^{N} \alpha_k W_k\left(\xi_N = 1\right) = f\left(\tau\right) \ . \tag{24}$$

Equation (20) together with boundary conditions (23) and (24) creates the following matrix equation

$$A_{(N+1)\times(N+1)} \left\{ \begin{array}{c} \alpha_0 \\ \alpha_1 \\ \vdots \\ \alpha_{N-1} \\ \alpha_N \end{array} \right\} = \left\{ \begin{array}{c} 0 \\ r\left(\xi_1\right) \\ \vdots \\ r\left(\xi_{N-1}\right) \\ f \end{array} \right\} \ . \tag{25}$$

Elements of matrix $\mathbf{A}$ are expressed by the formulae

$$a_{0j} = W_j^{'}\left(\xi_0 = -1\right) \ , \tag{26}$$

$$a_{ij} = q\left(\xi_i\right) W_j^{''}\left(\xi_i\right) + p\left(\xi_i\right) q\left(\xi_i\right) W_j^{'}\left(\xi_i\right) - \beta^2 W_j\left(\xi_i\right) \ , \tag{27}$$

$$a_{Nj} = W_j\left(\xi_N = 1\right) \tag{28}$$

for $i = 1, 2, \ldots, N-1$, $j = 0, 1, 2, \ldots, N$. Multiplying the left side of Eq. (25) by the matrix A^{-1}, we obtain

$$\left\{ \begin{array}{c} \alpha_0 \\ \alpha_1 \\ \vdots \\ \alpha_{N-1} \\ \alpha_N \end{array} \right\} = A^{-1} \left\{ \begin{array}{c} 0 \\ r(\xi_1) \\ \vdots \\ r(\xi_{N-1}) \\ f \end{array} \right\}, \tag{29}$$

what can be noted as

$$\left\{ \begin{array}{c} \alpha_0 \\ \alpha_1 \\ \vdots \\ \alpha_{N-1} \\ \alpha_N \end{array} \right\} = \left[\begin{array}{ccccc} \tilde{a}_{00} & \tilde{a}_{01} & \ldots & \ldots & \tilde{a}_{0N} \\ \tilde{a}_{10} & \tilde{a}_{11} & \ldots & \ldots & \tilde{a}_{1N} \\ \vdots & \vdots & \ddots & & \vdots \\ \vdots & \vdots & & \ddots & \vdots \\ \tilde{a}_{N0} & \tilde{a}_{N1} & \ldots & \ldots & \tilde{a}_{NN} \end{array} \right] \left\{ \begin{array}{c} 0 \\ r(\xi_1) \\ \vdots \\ r(\xi_{N-1}) \\ f \end{array} \right\}, \tag{30}$$

where $\tilde{a}_{ij}$ are elements of the matrix $\mathbf{A}^{-1}$.

3 Inverse problem

The purpose of solving the inverse problem is to determine unknown temperature on the boundary of the cylinder f (in subsequent moments of time) based on temperature measurements inside the cylinder and on the form of the solution to the direct problem. On the basis of the Eq. (30) we have that

$$\left\{ \begin{array}{c} \alpha_0 \\ \alpha_1 \\ \vdots \\ \alpha_{N-1} \\ \alpha_N \end{array} \right\} = \left\{ \begin{array}{c} \sum_{i=1}^{N-1} \tilde{a}_{0i} r(\xi_i) + f\tilde{a}_{0N} \\ \sum_{i=1}^{N-1} \tilde{a}_{1i} r(\xi_i) + f\tilde{a}_{1N} \\ \vdots \\ \vdots \\ \sum_{i=1}^{N-1} \tilde{a}_{Ni} r(\xi_i) + f\tilde{a}_{NN} \end{array} \right\}. \tag{31}$$

Therefore,

$$\alpha_j = \sum_{i=1}^{N-1} \tilde{a}_{ji} r(\xi_i) + f\tilde{a}_{jN} \qquad \text{for} \qquad j = 0, 1, 2, \ldots, N\,. \tag{32}$$

Coefficients α_j were introduced into the solution (15). Hence,

$$\tilde{\vartheta}(\xi) = \sum_{k=0}^{N} \left(\sum_{i=1}^{N-1} \tilde{a}_{ki} r(\xi_i) + f\tilde{a}_{kN} \right) W_k(\xi)\,. \tag{33}$$

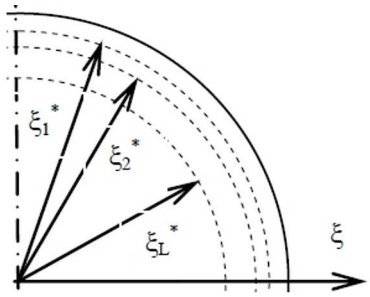

Figure 1: Measuring points.

For measuring points ξ_l^*, where $l = 1, 2, \ldots, L$ (Fig. 1), we have that

$$\tilde{\vartheta}\left(\xi_l^*\right) = \sum_{k=0}^{N} \left(\sum_{i=1}^{N-1} \tilde{a}_{ki} r\left(\xi_i\right) + f \tilde{a}_{kN} \right) W_k\left(\xi_l^*\right) \ . \tag{34}$$

To determine unknown parameters $\alpha_0, \alpha_1, \ldots, \alpha_N$, the functional should be minimized

$$I\left(f\right) = \sum_{l=1}^{L} \left(\tilde{\vartheta}\left(\xi_l^*, f\right) - \tilde{\vartheta}_m\left(\xi_l^*\right) \right)^2 \ . \tag{35}$$

Having substituted formula (33), for the value calculated at measuring points ξ_l^*, where $l = 1, 2, \ldots, L$, we have

$$I\left(f\right) = \sum_{l=1}^{L} \left[\sum_{k=0}^{N} \left(\sum_{i=1}^{N-1} \tilde{a}_{ki} r\left(\xi_i\right) + f \tilde{a}_{kN} \right) W_k\left(\xi_l^*\right) - \tilde{\vartheta}_m\left(\xi_l^*\right) \right]^2 \ . \tag{36}$$

Annihilation of the first derivative is the necessary condition of the functional (4) minimum

$$\frac{dI}{df} = 0 \ . \tag{37}$$

Including Eqs. (4) and (37), we obtained

$$\sum_{l=1}^{L} \left\{ \left[\sum_{k=0}^{N} \left(\sum_{i=1}^{N-1} \tilde{a}_{ki} r\left(\xi_i\right) + f \tilde{a}_{kN} \right) W_k\left(\xi_l^*\right) - \tilde{\vartheta}_m\left(\xi_l^*\right) \right] \sum_{k=0}^{N} W_k\left(\xi_l^*\right) \tilde{a}_{kN} \right\} = 0 \ . \tag{38}$$

Hence,

$$\sum_{l=1}^{L}\left\{\left[\sum_{k=0}^{N}W_k\left(\xi_l^*\right)\left(\sum_{i=1}^{N-1}\tilde{a}_{ki}r\left(\xi_i\right)\right)-\tilde{\vartheta}_m\left(\xi_l^*\right)\right]\sum_{k=0}^{N}W_k\left(\xi_l^*\right)\tilde{a}_{kN}+ f\left(\sum_{k=0}^{N}W_k\left(\xi_l^*\right)\tilde{a}_{kN}\right)^2\right\}=0\,. \tag{39}$$

Let

$$A_l=\left[\sum_{k=0}^{N}W_k\left(\xi_l^*\right)\left(\sum_{i=1}^{N-1}\tilde{a}_{ki}r\left(\xi_i\right)\right)-\tilde{\vartheta}_m\left(\xi_l^*\right)\right]\sum_{k=0}^{N}W_k\left(\xi_l^*\right)\tilde{a}_{kN}\,, \tag{40}$$

$$B_l=\left(\sum_{k=0}^{N}W_k\left(\xi_l^*\right)\tilde{a}_{kN}\right)^2\,, \tag{41}$$

then the Eq. (39) can be noted as

$$\sum_{l=1}^{L}\left\{A_l+fB_l\right\}=0\,. \tag{42}$$

Therefore,

$$f=\frac{-\sum_{l=1}^{L}A_l}{\sum_{l=1}^{L}B_l}\,. \tag{43}$$

In mathematical model, the heat conduction coefficient depends on temperature, and can be noted as the linear combination of Chebyshev polynomials

$$\lambda\left(T\right)=\sum_{i=0}^{n}a_iW_i(\tilde{T})\,, \tag{44}$$

where temperature $\tilde{T}=\frac{2T-T_{\max}-T_0}{T_{\max}-T_0}$, then $\tilde{T}\in\langle-1,1\rangle$. Applying the Kirchhoff's substitution (3), we obtain

$$\vartheta=\frac{1}{\lambda_0}\int_{T_0}^{T}\lambda\left(u\right)du=\frac{T_{\max}-T_0}{2\lambda_0}\int_{T_0}^{T}\sum_{i=0}^{n}a_iW_i(\tilde{T})d\tilde{T}\,. \tag{45}$$

Since $\vartheta=g\left(T\right)$, hence $T=g^{-1}\left(\vartheta\right)$. For the value $\vartheta\left(T\right)$, the interval $\langle T_i,T_{i+1}\rangle$ (Fig. 2), for which the following inequality is satisfied, is sought

$$\vartheta\left(T_i\right)\leq\vartheta\left(T\right)\leq\vartheta\left(T_{i+1}\right)\,. \tag{46}$$

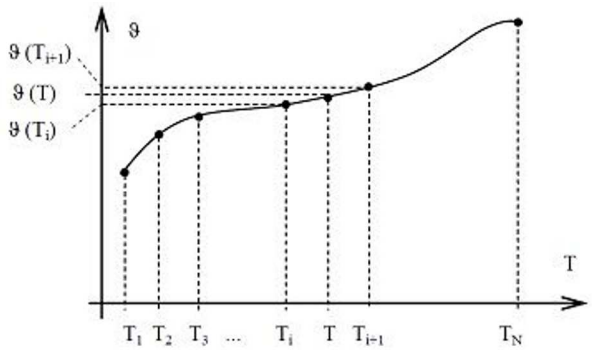

Figure 2: Determination of temperature $\vartheta(T)$ intermediate value in (T_i, T_{i+1}) interval in the function of k parameter, Eq. (48).

Then, on the basis of linear extrapolation

$$\vartheta\left(T\right) = k\vartheta\left(T_i\right) + \left(1-k\right)\vartheta\left(T_{i+1}\right) \ , \tag{47}$$

$$T = kT_i + \left(1-k\right)T_{i+1} \ . \tag{48}$$

Hence,

$$k = \frac{\vartheta\left(T\right) - \vartheta\left(T_{i+1}\right)}{\vartheta\left(T_i\right) - \vartheta\left(T_{i+1}\right)} \ . \tag{49}$$

Specific heat was also presented as the linear combination of Chebyshev polynomials

$$c\left(T\right) = \sum_{i=0}^{n} b_i W_i(\tilde{T}) \ , \tag{50}$$

where temperature $\tilde{T} \in \langle -1, 1\rangle$. Coefficients a_i and b_i were determined with the use of the least squares approximation method [14]. They are presented in Tab. 1.

4 Sensitivity of the solution to the inverse problem to errors in measurements

To determine the distribution of temperature on the cylinder boundary, it is necessary to measure temperature inside this cylinder as close to the boundary as possible. Sensitivity of the solution to the inverse problem comprises the impact of the thermocouple installation error $\pm\delta\xi_l^*$ as well

Table 1: Coefficients of polynomials approximating functions λ(T) and c(T).

i	a_i	b_i
0	41.519	660.920
1	-11.350	247.360
2	-0.90257	51.725
3	0.010553	18.980

as the error in temperature measurement $\delta\vartheta_l = h\left(\delta T_i\right)$ (5) on the sought distribution of temperature on the cylinder boundary. Non-dimensional temperature on the boundary is

$$f_{\pm\delta\xi_l^*,\delta\vartheta} = \frac{-\sum_{l=1}^{L} A_{l,\pm\delta\xi_l^*,\delta\vartheta_l}}{\sum_{l=1}^{L} B_{l,\pm\delta\xi_l^*,\delta\vartheta_l}}\,, \tag{51}$$

where

$$A_{l,\pm\delta\xi_l^*,\delta\vartheta_l} = \left[\sum_{k=0}^{N} W_k\left(\xi_l^*\right)\left(\sum_{i=1}^{N-1}\tilde{a}_{ki} r\left(\xi_i\right)\right) - \left(\tilde{\vartheta}_m\left(\xi_l^* \pm \delta\xi_l^*\right) + \delta\vartheta_l\right)\right]\sum_{k=0}^{N} W_k\left(\xi_l^*\right)\tilde{a}_{kN}\,, \tag{52}$$

$$B_{l,\pm\delta\xi_l^*,\delta\vartheta_l} = B_l = \left(\sum_{k=0}^{N} W_k\left(\xi_l^*\right)\tilde{a}_{kN}\right)^2\,. \tag{53}$$

5 Numerical example

To test the program, it was assumed that the distribution of temperature on the cylinder boundary can be described by the function of the form $f\left(\tau\right) = T_{\max}\left(1 - e^{-\beta\tau}\right)$, where $\beta = 1.1$. Calculations were performed for the cylinder of 100 mm diameter. The following values were assumed for calculations: $\lambda_0 = 52.531\frac{\mathrm{W}}{\mathrm{mK}}$, $c_0 = 429.331\frac{\mathrm{J}}{\mathrm{kgK}}$, and $\Delta\tau = 0.187$. Direct problem was solved and distributions of temperature on radii $r_1 = 48$ mm,

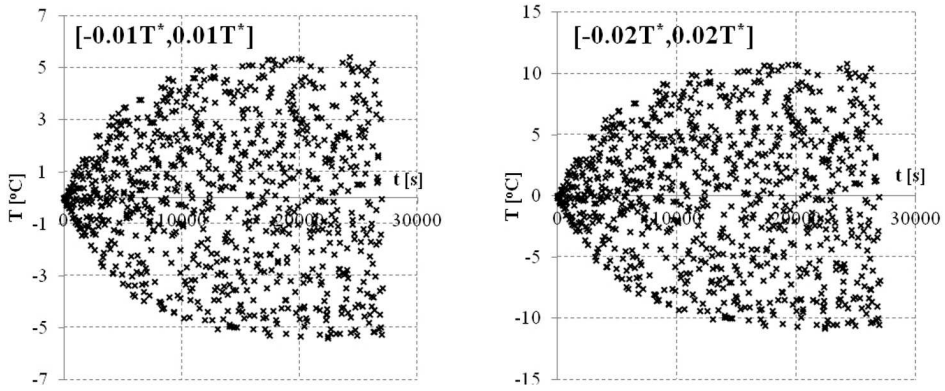

a) b)

Figure 3: Course of the random error in temperature measurement of values from the interval $[-0.01T^*, 0.01T^*]$ (a), and $[-0.02T^*, 0.02T^*]$ (b) for the temperature measurement at the distance of 2 mm from the boundary of the cylinder with the installation error $\delta r^* = -0.5$ mm.

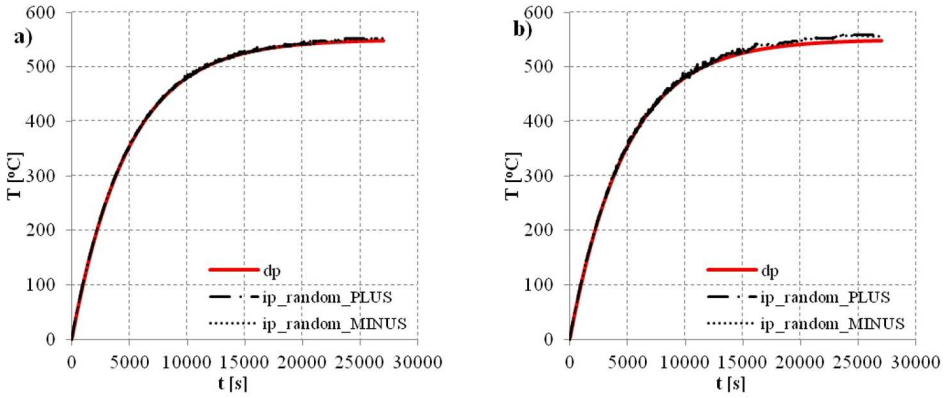

Figure 4: Distribution of temperature on the boundary of the cylinder assumed in the direct problem (*dp*) as well as calculated with the use of the inverse problem (*ip*) including error in thermocouple installation (PLUS, MINUS) and random error in temperature measurement (random): a) $0.01T^*$, b) $0.02T^*$.

$r_2 = 46$ mm and $r_3 = 44$ mm ($g_1 = 2$ mm, $g_2 = 4$ mm and $g_3 = 6$ mm) were determined. Obtained temperature values were input data for the solution of inverse problem and corresponded to the temperature measured by thermocouples. Analysis of solution sensitivity to errors in thermocouple installation was conducted. It was assumed that each of thermocouples may

be shifted into the direction of the cylinder boundary by $\delta r^* = 0.5$ mm, what was noted as PLUS in Fig. 3. Shifting thermocouple closer to the cylinder axis corresponds to the error in installation $\delta r^* = -0.5$ mm and is noted as MINUS (Fig. 4). In calculations, random error in temperature measurement δT^* was included, what is denoted as random in Fig. 3. This error was a random number from the interval $[-0.01T^*, 0.01T^*]$ or $[-0.02T^*, 0.02T^*]$. Figure 3 presents illustrative course of the random error in temperature measurement for the thermocouple located at the distance of 2 mm from the boundary with the installation error $\delta r^* = -0.5$ mm and with the maximal errors in temperature measurement $\delta T^* = 0.01T^*$ and $\delta T^* = 0.02T^*$.

Distributions of temperature on the boundary of the cylinder, assumed in the direct problem and calculated with the use of inverse problem, including the sensitivity of the solution were presented in Fig. 4. For the random error in temperature measurement $\delta T^* = 0.01\mathrm{T}^*$ and for thermocouples shifted into the direction of the cylinder axis by $|\delta r^*| = 0.5$ mm, the error of temperature distribution on the cylinder boundary was slightly above 6 °C (Fig. 5a, b). Larger differences between the assumed temperature and the calculated one with the use of the inverse problem were obtained when the random disturbance in temperature measurement was up to $0.02T^*$. Those values are up to 13 °C (Fig. 5c, d).

Temperature distributions in the cylinder, assumed in the direct problem and calculated with the use of the inverse problem method for the time of 900 s, 2100 s, 3000 s, 4200 s, 5100 s, and 8100 s are presented in Fig. 6. Calculations were made for thermocouples located at the distance of 2, 4 and 6 mm from the boundary. Installation error was $\delta r^* = -0.5$ mm. Random error in temperature measurement reached maximally 2% of the measured value, what correspond to values from the interval $[-0.02T^*, 0.02T^*]$.

Figure 7 presents the assumed distribution of temperature on the boundary of the cylinder as well as the distributions of temperature calculated with the use of the inverse problem for thermocouples located at the distance of 2, 4 and 6; 4, 6, and 8 as well as 6, 8, and 10 mm from the boundary. For random error in temperature measurement up to $0.02T^*$, when the distance of thermocouple location from the boundary increases, the maximal error in calculations on the cylinder boundary increases too.

Numerical tests, presented above, assumed greater measurement disturbances than those occurring real production conditions. Figure 8 presents distributions of temperature obtained as a result of solution of the in-

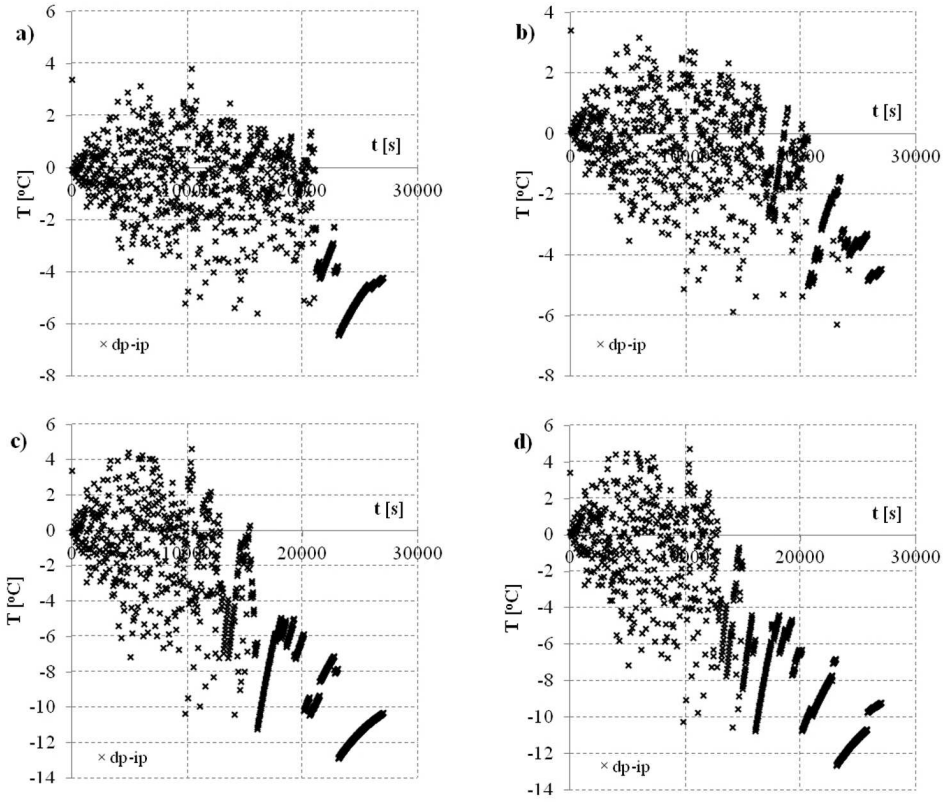

Figure 5: Difference in temperatures on the boundary of the cylinder assumed in the direct problem (*dp*) and calculated with the use of the inverse problem (*ip*), including the thermocouple installation errors $\delta r^* = 0.5$ mm (a, c) and $\delta r^* =$ -0.5 mm (b, d) as well as the random error in temperature measurement up to $0.01T^*$ (a, b) and $0.02T^*$ (c,d).

verse problem, with the installation error $\delta r^* = 0.5$ mm (PLUS) and $\delta r^* = -0.5$ mm (MINUS). Stable during the whole heating process error in temperature measurement of 3°C (PLUS) or $-3\,^\circ$C (MINUS) was assumed. These parameters correspond to heating conditions obtainable during the experiment. Errors in temperature distribution, obtained in this experiment, slightly exceeded $3\,^\circ$C.

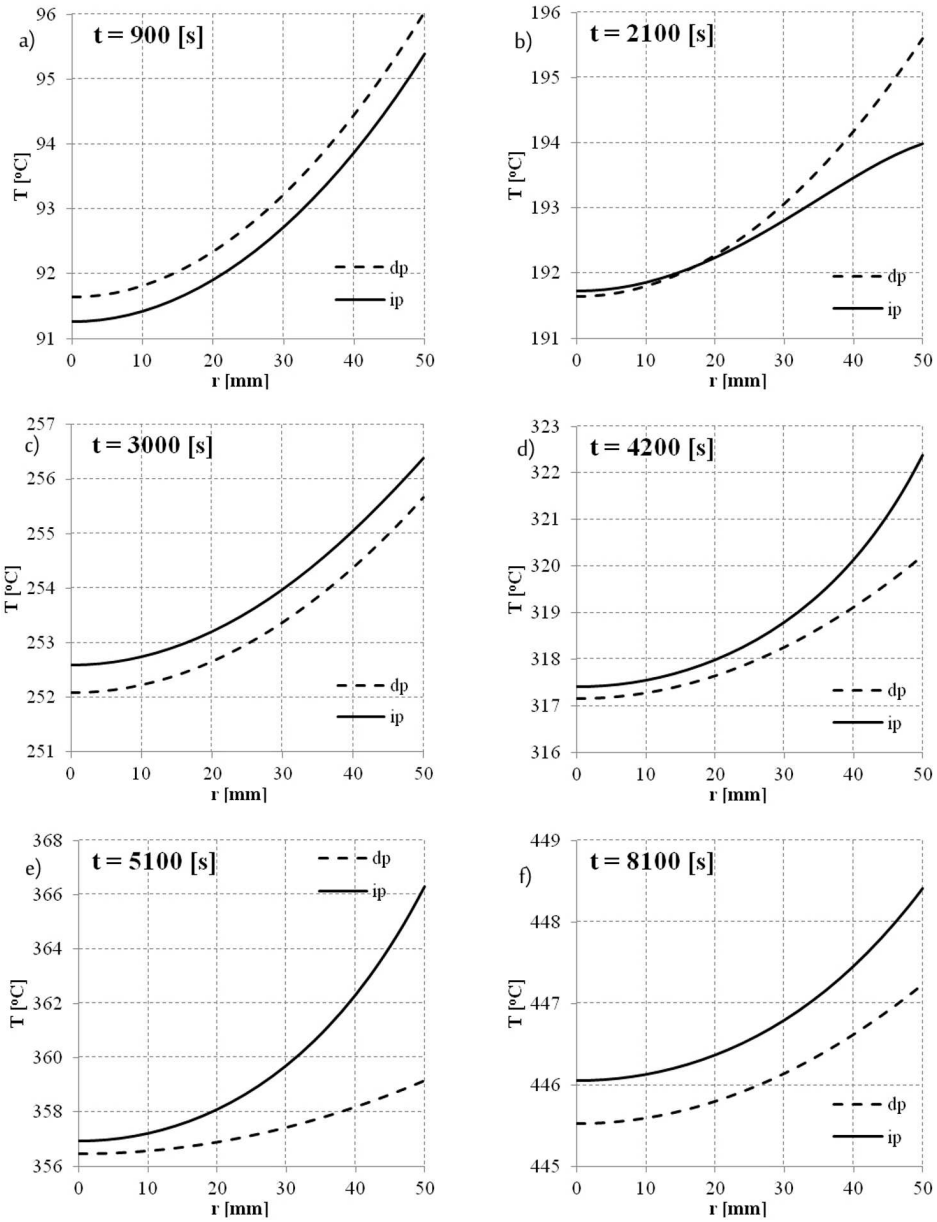

Figure 6: Temperature distribution along the radius of the cylinder for the time of a) $t = 900$ s, b) $t = 2100$ s, c) $t = 3000$ s, d) $t = 4200$ s, e) $t = 5100$ s, f) $t = 8100$ s with the maximal disturbance of $0.02\mathrm{T}^*$ and thermocouples located at the distance of 2, 4, and 6 mm from the boundary with the instalaltion error $\delta r^* = -0.5$ mm.

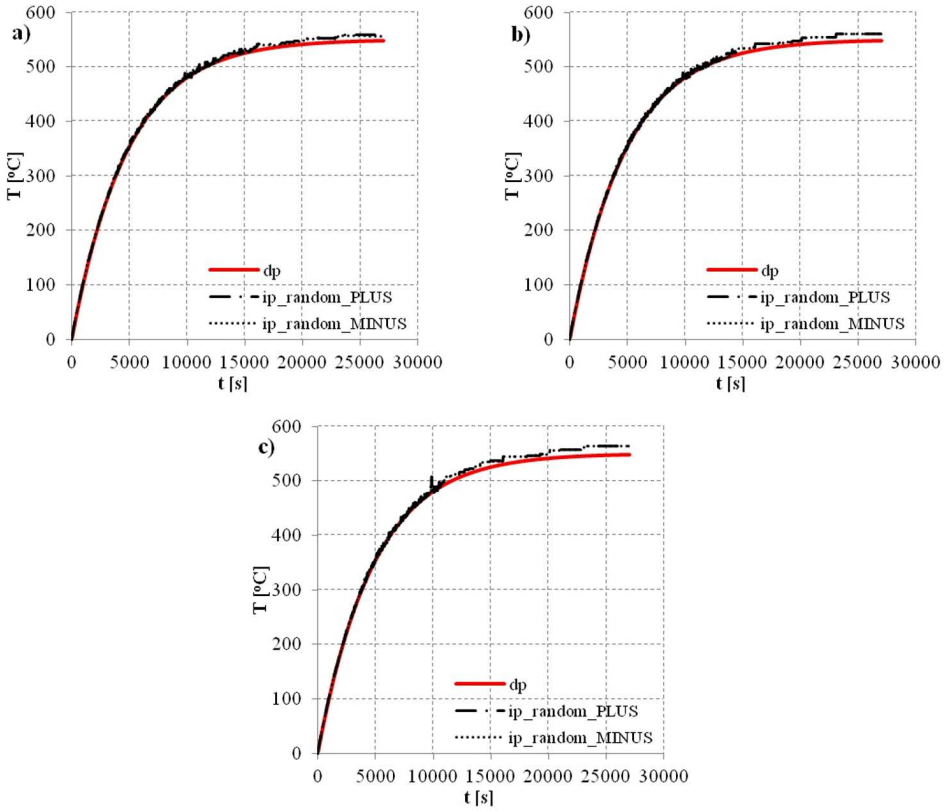

Figure 7: Temperature distribution on the boundary of the cylinder assumed in the direct problem (dp) and calculated with the use the inverse problem (ip) for installation errors $\delta r^* = 0.5$ mm (PLUS) and $\delta r^* = -0.5$ mm (MINUS) with the temperature measurement error up to $0.02T^*$ and thermocouples located at the distance of: a) 2, 4, 6 mm; b) 4, 6, 8 mm; c) 6, 8, 10 mm from the boundary of the cylinder.

6 Conclusion

In heat treatment processes, such as nitrification and carburising, heat conduction coefficient and specific heat change significantly during heating. In the computational model, described in this paper, the change in heat conduction coefficient and specific heat with respect of temperature were included. It enables temperature distribution on the boundary of the cylinder to be determined more precisely by solving the inverse problem and then by solving the direct problem inside the cylinder. It is a basis of pre-

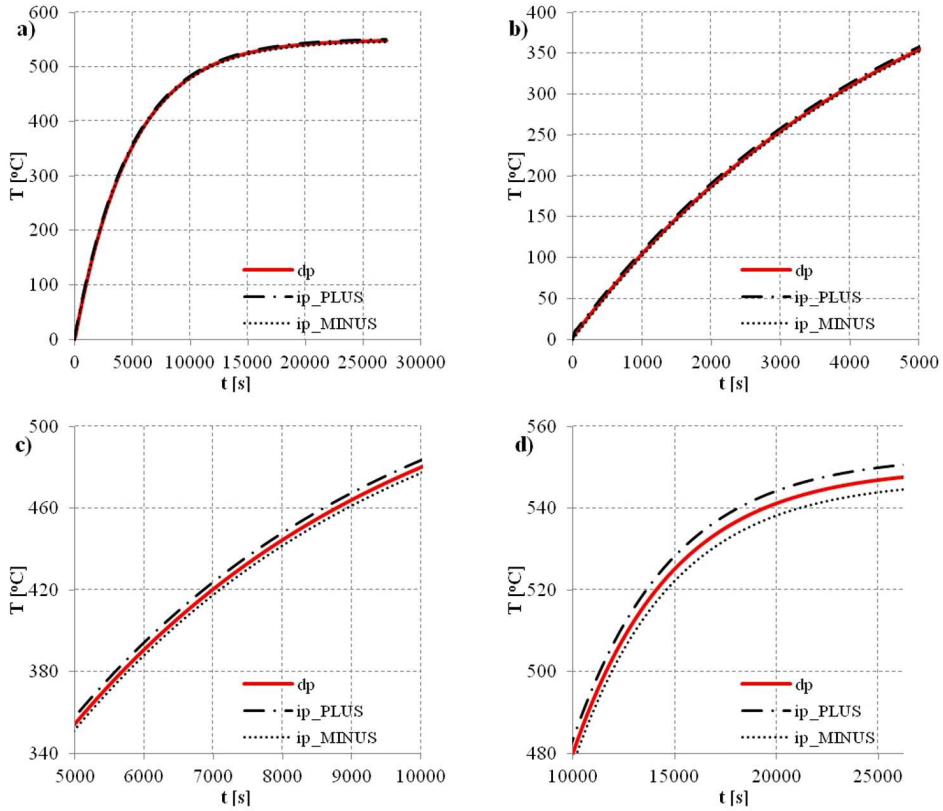

Figure 8: Distribution of temperatue on the boundary of the cylinder assumed in the direct problem (*dp*) and calculated with use of the inverse problem (*ip*) for installation errors $\delta r^* = 0.5$ mm (PLUS) and $\delta r^* =$ -0.5 mm (MINUS) with the error in temperature measurement $\delta T^* = 3\,^\circ$C (PLUS) and $\delta T^* = -3\,^\circ$C (MINUS) and thermocouples located at the distance of 2, 4 and 6 mm from the boundary of the cylinder.

cise analysis of structure of the layer, being the subject of heat treatment, and of stresses arising in the component being heat treated. Obtained results indicate low sensitivity of the solution to the inverse problem to the thermocouple installation and temperature measurement errors.

Received 9 June 2016

References

[1] Ciałkowski M.: *Selected methods and algorithms for solving inverse problems of heat conduction equation*. Wydawnictwo Politechniki Poznańskiej, Poznań 1996 (in Polish).

[2] Ciałkowski M., Grysa K.: *A sequential and global method of solving an inverse problem of heat conduction equation*. J. Theor. App. Mech-Pol. **48**(2010), 1, 111–134.

[3] Ciałkowski M.J., Grysa K.W.: *On a certain inverse problem of temperature and thermal stress fields*. Acta Mechanica **36**(1980),3-4169–185.

[4] Duda P., Taler J.: *Numerical method for the solution of non - linear two - dimensional inverse heat conduction problem using unstructured meshes*. Int. J. Numer. Meth. Engng. **48**(2000), 7, 881–899, 2000.

[5] Frąckowiak A., Botkin N.D., Ciałkowski M., Hoffmann K.H.: *A fitting algorithm for solving inverse problems of heat conduction*. Int. J. Heat Mass Trans. **53**(2010), 9-10, 2123–2127.

[6] Frąckowiak A., Wolfersdorf J.V., Ciałkowski M.: *Solution of the inverse heat conduction problem described by the Poisson equation for a cooled gas-turbine blade*. Int. J. Heat . Mass Trans. **54**(2011), 5-6, 1236–1243.

[7] Gdula S.: *Heat Conduction*. PWN, Warszawa 1984 (in Polish).

[8] Grysa K., Maciąg A., Adamczyk-Krasa J.: *Trefftz functions applied to direct and inverse non-fourier heat conduction problems*. J. Heat Trans. **136**(2014), 9, 1–9.

[9] Grysa K., Maciąg A., Pawinska A.: *Solving nonlinear direct and inverse problems of stationary heat transfer by using Trefftz functions*. Int. J. Heat Mass Trans. **55**(2012), 23-24, 7336–7340.

[10] Han-Taw Chen, Xin-Yi Wu: *Investigation of heat transfer coefficient in two-dimensional transient inverse heat conduction problems using the hybrid inverse scheme*. Int. J. Numer. Meth. Engng. **73**(2008), 1, 107–122.

[11] Incropera F.P., De Witt D.P.: *Fundamentals of Heat and Mass Transfer*. John Wiley & Sons, New York 1996.

[12] Joachimiak M., Ciałkowski M.: *Optimal choice of integral parameter in a process of solving the inverse problem for heat equation*. Arch. Thermodyn. **35**(2014), 3, 265–280.

[13] Maciąg A.: *Trefftz functions for selected direct and inverse problems of mechanics*. Polit. Świętokrzyska Publishers, Kielce 2009 (in Polish).

[14] Marois M.A., M. Désilets M., Lacroix M.: *What is the most suitable fixed grid solidification method for handling time-varying inverse Stefan problems in high temperature industrial furnaces?* Int. J. Heat Mass Trans. **55**(2012), 21-22, 5471–5478.

[15] Mierzwiczak M., Kołodziej J.A.: *Application of the method of fundamental solutions with the Laplace transformation for the inverse transient heat source problem*. J. Theor. App. Mech-Pol. **50**(2012), 4, 1011–1023.

[16] Mierzwiczak M., Kołodziej J.A.: *The determination of heat sources in two dimensional inverse steady heat problems by means of the method of fundamental solutions*. Inverse Prob. Sci. En. 1**9**(2011), 6, 777–792.

[17] Mierzwiczak M., Kołodziej J.A.: *The determination temperature-dependent thermal conductivity as inverse steady heat conduction problem*. Int. J. Heat Mass Trans. **54**(2011), 4, 790–796.

[18] Mierzwiczak M., Kołodziej J., Ciałkowski M., Frąckowiak A.: *Implementation of the method of fundamental solutions for heat conduction equation*. Poznań University of technology Publishers, Poznań 2011 (in Polish).

[19] Niedoba J., Niedoba W.: *Ordinary and partial differential equations. Mathematical problems*. (B. Choczewski, Ed.), Uczelniane Wydawnictwo Naukowo-Dydaktyczne, Kraków 2001 (in Polish).

[20] Paszkowski S.: *Numerical implementation of polynominals and Chebyshev*. PWN, Warszawa 1975 (in Polish).

[21] Taler J., Duda P.: *Solving direct and inverse problems of heat conduction*. WNT, Warszawa 2003 (in Polish).

[22] Taler J., Zima W.: *Solution of inverse heat conduction problems using control volume approach*. Int. J. Heat Mass Trans. **42**(1999), 1123–1140.

[23] Trefftz E.: *Ein Gegenstük zum Ritz'schen Verfahren*. Proc. 2nd Int. Cong. of Applied Mechanics, Zürich 1926, 131–137.

[24] Vakili S., Gadala M.S.: *Low cost surrogate model based evolutionary optimization solvers for inverse heat conduction problem*. Int. J. Heat Mass Trans. **56**(2013), 263–273.

archives
of thermodynamics
Vol. **38**(2017), No. 2, 101–122
DOI: 10.1515/aoter-2017-0012

Effect of rotation on a semiconducting medium with two-temperatures under L-S theory

MOHAMED I.A. OTHMAN[a,b]
RAMADAN S. TANTAWI[a]
EBTESAM E.M. ERAKI[a*]

[a] Department of Mathematics, Faculty of Science, P.O. Box 44519, Zagazig University, Zagazig, Egypt

[b] Department of Mathematics, Faculty of Science, Taif University 888, Saudi Arabia

Abstract The model of the equations of generalized thermoelasticity in a semi-conducting medium with two-temperature is established. The entire elastic medium is rotated with a uniform angular velocity. The formulation is applied under Lord-Schulman theory with one relaxation time. The normal mode analysis is used to obtain the expressions for the considered variables. Also some particular cases are discussed in the context of the problem. Numerical results for the considered variables are obtained and illustrated graphically. Comparisons are also made with the results predicted in the absence and presence of rotation as well as two-temperature parameter.

Keywords: Normal mode analysis; Lord-Shulman theory; Rotation; Conductive temperature; Semiconductors

Nomenclature

a^*	–	two temperature parameter
c_e	–	specific heat at constant strain
D_E	–	carrier diffusion coefficient

*Corresponding Author. Email ebtesam.eraki@yaho.com

E_g – energy gap of semiconductor
K – coefficient of thermal conductivity
N – carrier density
N_0 – carrier concentration at temperature T
T – thermodynamic temperature above the reference temperature T_0
u, v – displacement vector components

Greek symbols

α – thermal expansion coefficient
$\gamma = (3\lambda + 2\mu)\alpha$
δ_{ij} – thermal expansion coefficient
δ_n – difference of deformation potential of conduction and valence band such that $\delta_n = (3\lambda + 2\mu)d_n$
ε_{ij} – strain components
θ – conductive temperature
$\kappa = \frac{\partial N_0}{\partial T}\frac{1}{\tau}$
λ, μ – Lame' constants
τ – photo-generated carrier lifetime
τ_0 – thermal relaxation time
ρ – mass density
σ_y – stress components

1 Introduction

Thermoelasticity theories, which admit a finite speed for thermal signals, have received a lot of attention for the past four decades. In contrast to the coupled thermo-elasticity theory based on a parabolic heat equation [1], which predicts an infinite speed of the propagation of heat, these theories involve a hyperbolic heat equation and are referred to as generalized thermoelasticity theories. The theory of thermoelasticity with one relaxation time proposed by Lord and Shulman [2] arose as a result of the modification of equation of heat conduction in [1], originally proposed by Maxwell [3] in the context of theory of gases, and later by Cattaneo [4] and Vernotte [5] in the context of heat conduction in rigid bodies. Resulting from that theory heat equation of the wave type ensures the finite speed of wave propagation of heat and the displacement distributions. This theory was extended by Dhaliwal and Sherief [6] to include the anisotropic case. Othman and Said [7] used the normal mode analysis to study the effect of rotation on the two-dimensional problem of a fibre-reinforced thermoelastic with one relaxation time.

The first photothermal method was discovered by Gordon *et al.* [8] when they found the intracavity sample where a laser-based apparatus gave

rise to photothermal blooming, namely the photothermal lens. Sometime later, Kreuzer [9] showed that photoacoustic spectroscopy could be used for sensitive analysis when laser light sources were used. The photo-thermal generation during a photothermal process was studied by many authors. For semiconductor materials, the mechanism of this process includes two parts: two parts: part one: the propagation of a thermal wave causing elastic vibration in the medium; this is the thermoelastic (TE) mechanism of photothermal generation (Todorovic *et al.* [10]). Part two: the photoexcite free carriers produce directly a periodic elastic deformation that is, the electronic deformation (ED) in the sample (Todorovic *et al.* [10]). A general theoretical analysis of the (TE) and (ED) effects in a semi-conductor medium during a photo-thermal process consists in modeling the complex systems by simultaneous analysis of the coupled plasma, thermal, and elastic wave equations (Song *et al.* [11]). System of partially coupled plasma, thermal and elastic wave equations and conditions for neglecting the coupling between them is analyzed (Todorovic [12]). The treatment considers a semiconductor elastic medium for isotropic and homogeneous, thermal and elastic properties. Song *et al.* [13] used the coupled generalized thermoelastic with thermal relaxation time and plasma theories to study the reflection problem at the surface of a semi-infinite semiconducting medium during a photothermal process.

Some research in the past investigated different problems of rotating media. In a paper by Schoenberg and Censor [14], the propagation of plane harmonic waves in a rotating elastic medium without a thermal field has been studied. It was shown there that the rotation causes the elastic medium to be depressive and anisotropic. Many authors [15–25] studied the effect of rotation on elastic waves. These problems are based on the more realistic elastic model since earth, the moon and other planets have angular velocity.

Thermoelasticity with two temperatures is one of the nonclassical theories of thermoelasticity of elastic solids. The thermal dependence is the main difference of this theory with respect to the classical one. Chen and Gurtin [26], Chen *et al.* [27,28] have formulated a theory of heat conduction in deformable bodies, which depend on two distinct temperatures, the conductive temperature and thermodynamic temperature. For time independent situations, the difference between these two temperatures is proportional to the heat supply. For time dependent problems and with respect to wave propagation problem in particular, the two-temperatures

are in general different, regardless of the presence of heat supply. The two temperatures, T, and θ, and the strain are found to have representations in the form of a traveling wave plus a response, which occurs instantaneously throughout the body [29]. Warren and Chen [30] investigated the wave propagation in the two-temperature theory of thermoelasticity. Recently, Youssef [31,32], Abbas and Youssef [33] and Bijarnia and Singh [34] studied different problems under two temperature generalized thermoelastic theory.

This paper investigates the effect of two-temperature parameter and rotation in a semiconducting medium into the context of the two-temperature generalized thermoelasticity theory with one relaxation time.

2 Formulation of the problem and basic equations

Generally, theoretical analyses of the transport process in a semiconductor involve in the consideration of coupled plasma waves, thermal waves and elastic waves simultaneously. For a medium with isotropic and homogeneous properties, when the body forces are neglected, the governing equations are; Fig. 1:

1. Strain-displacement relations:

$$\varepsilon_{ij} = \frac{1}{2}(u_{i,j} + u_{j,i}), \quad i,j = 1,2\ , \tag{1}$$

   where the components of the displacement vector are $\mathbf{u} \equiv (u,\ v,\ 0)$.

2. Constitutive relations:

$$\sigma_{ij} = 2\mu\,\varepsilon_{ij} + [\lambda e - \gamma\,T - \delta_n\,N]\delta_{ij}\ . \tag{2}$$

3. Heat conduction equation (hyperbolic equation [35]):

$$K\nabla^2\theta + \frac{E_g}{\tau}N - \gamma T_0\left(1 + \tau_0\frac{\partial}{\partial t}\right)\dot{e} = \rho c_e\left(1 + \tau_0\frac{\partial}{\partial t}\right)\dot{T}\ , \tag{3}$$

   such that

$$T = \theta - a^*\nabla^2\theta\ . \tag{4}$$

4. Equation of motion:
   Since the medium is rotating uniformly with an angular velocity $\mathbf{\Omega} = \Omega n \equiv (0,\ 0,\ \Omega)$ where n is a unit vector representing the direction of

the axis of the rotation, the equation of motion in the rotating frame of reference has two additional terms (Schoenberg and Censor [14]): centripetal acceleration $\mathbf{\Omega} \times (\Omega \times \mathbf{u})$ due to time-varying motion only and Corioli's acceleration $2\,\mathbf{\Omega} \times \dot{\mathbf{u}}$, then the equation of motion in a rotating frame of reference is

$$\mu\,\nabla^2 u_i + (\lambda+\mu)\nabla e - \gamma\,\nabla T - \delta_n\,\nabla N = \rho\left[\ddot{u}_i + [\Omega\times\Omega\times\mathbf{u}]_i + 2(\mathbf{\Omega}\times\dot{\mathbf{u}})_i\right]. \tag{5}$$

5. Coupled plasma transport equation (parabolic equation [35]):

$$D_E\nabla^2 N - \frac{N}{\tau} + \kappa\,T = \frac{\partial N}{\partial t}\,, \tag{6}$$

where N is the carrier density, T is the thermodynamic temperature above the reference temperature T_0, σ_{ij} are the stress components, ε_{ij} are the strain components, λ, μ are Lame' constants, $\gamma = (3\lambda + 2\mu)\alpha_t$, α_t is the thermal expansion coefficient, δ_n is the difference of deformation potential of conduction and valence band such that $\delta_n = (3\lambda + 2\mu)d_n$, δ_{ij} is the Kronecker delta, K is the coefficient of thermal conductivity, θ is the conductive temperature, a^* is the two temperature parameter, ρ is the mass density, c_e is the specific heat at constant strain, E_g is the energy gap of semiconductor, D_E is the carrier diffusion coefficient, τ is the photo-generated carrier lifetime, τ_0 is the thermal relaxation time and $\kappa = \frac{\partial N_0}{\partial T}\frac{1}{\tau}$, N_0 is the carrier concentration at temperature T.

The governing equations can be put into a more convenient form by using the following non-dimensional variables:

$$\begin{gathered}(x', y', u', v') = \frac{1}{C_T t^*}(x, y, u, v), \qquad (t', \tau_0') = \frac{1}{t^*}(t, \tau_0),\\ \{T', \theta'\} = \frac{\gamma}{(\lambda+2\mu)}\{T, \theta\}, \qquad N' = \frac{\delta_n}{(\lambda+2\mu)}N,\\ \sigma_{ij}' = \frac{1}{\mu}\sigma_{ij}, \Omega' = t^*\,\Omega, \qquad C_T^2 = \frac{(\lambda+2\mu)}{\rho}, \qquad t^* = \frac{K}{\rho c_e C_T^2}\,.\end{gathered} \tag{7}$$

Introducing the displacement potentials $\Phi(x, y, t)$ and $\Psi(x, y, t)$, which related to displacement components by the relations

$$u = \Phi_{,x} + \Psi_{,y} \qquad v = \Phi_{,y} - \Psi_{,x}\,. \tag{8}$$

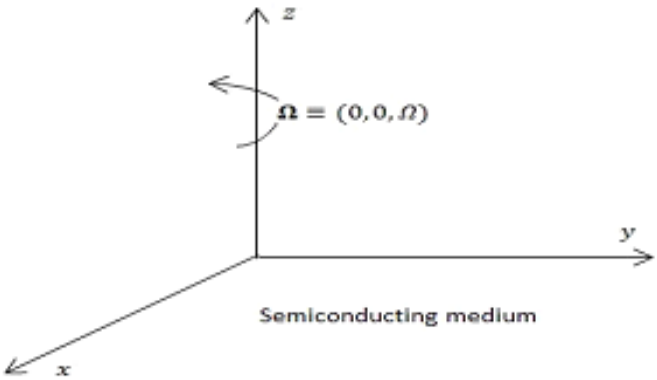

Figure 1: Schematic diagram of the problem.

Using Eqs. (2) and (8), in Eqs. (3)–(6), we obtain (the dashed above quantities have been removed for convenience):

$$\left[\nabla^2+\Omega^2-\frac{\partial^2}{\partial t^2}\right]\Phi-2\Omega\frac{\partial\Psi}{\partial t}-(1-a_0\nabla^2)\theta-N=0\,, \tag{9}$$

$$2\Omega\,\beta^2\frac{\partial\Phi}{\partial t}+\left[\nabla^2+\beta^2\,\Omega^2-\beta^2\frac{\partial^2}{\partial t^2}\right]\Psi=0\,, \tag{10}$$

$$\left\{\left[1+a_0\left(1+\tau_0\frac{\partial}{\partial t}\right)\frac{\partial}{\partial t}\right]\nabla^2-\left(1+\tau_0\frac{\partial}{\partial t}\right)\frac{\partial}{\partial t}\right\}\theta-\varepsilon_1\left(1+\tau_0\frac{\partial}{\partial t}\right)\nabla^2\dot{\Phi}+\varepsilon_2 N=0\,, \tag{11}$$

$$\left[\nabla^2-\frac{Kt^*}{\rho c_e\tau D_E}-\frac{K}{\rho c_e D_E}\frac{\partial}{\partial t}\right]\mathrm{N}+\varepsilon_3\,(1-a_0\nabla^2)\theta=0\,, \tag{12}$$

$$\mathrm{T}=(1-a_0\nabla^2)\theta\,. \tag{13}$$

For the stress-tensor components, we have the following expressions:

$$\sigma_{xx}=\beta^2u_{,x}+(\beta^2-2)v_{,y}-\beta^2T-\beta^2N\,, \tag{14}$$

$$\sigma_{yy}=(\beta^2-2)u_{,x}+\beta^2v_{,y}-\beta^2T-\beta^2N\,, \tag{15}$$

$$\sigma_{zz}=(\beta^2-2)\nabla^2\Phi-\beta^2T-\beta^2N\,, \tag{16}$$

$$\sigma_{xy}=u_{,y}+v_{,x},\qquad \sigma_{xz}=\sigma_{yz}=0\,, \tag{17}$$

where:
$\varepsilon_1=\frac{\gamma^2\,T_0\,t^*}{K\rho}$, $\varepsilon_2=\frac{\alpha_t E_g t^*}{\rho\,c_e\,\tau\,d_n}$, $\varepsilon_3=\frac{K\kappa\,d_n t^*}{\rho\,c_e\,\alpha_t D_E}$, $\beta^2=\frac{(\lambda+2\mu)}{\mu}$, and $a_0=\frac{a^*}{C_T^2\,t^{*2}}$.

3 Normal mode analysis

The solution of considered physical quantities can be decomposed in terms of normal mode as follows:

$$[\Phi,\ \Psi,\ T,\ \theta,\ \mathrm{N},\ \sigma_{ij}](x,y,t) = [\Phi^*,\ \Psi^*,\ T^*,\ \theta^*,\ N^*,\ \sigma_{ij}^*](y)\exp(\omega\, t + ia\, x)\ , \tag{18}$$

where a is the wave number in the x-direction, $i = \sqrt{-1}$, ω is a complex constant, Φ^*, Ψ^*, T^*, θ^*, N^*, and σ_{ij}^* are the amplitudes of the field quantities Φ, Ψ, T, θ, N, and σ_{ij}.

Using Eq. (18), Eqs.(9)–(12) become respectively:

$$(D^2 - b_1)\Phi^* - b_2\Psi^* + (a_0\, D^2 - b_3)\theta^* - N^* = 0\ , \tag{19}$$

$$b_4\, \Phi^* + (\mathrm{D}^2 - b_5)\, \Psi^* = 0\ , \tag{20}$$

$$-\, b_6\, (D^2 - a^2)\ \Phi^* + (b_7\, D^2 - b_8)\ \theta^* + \varepsilon_2\ N^* = 0\ , \tag{21}$$

$$(b_9\ D^2 - b_{10})\, \theta^* - (D^2 - b_{11})\, N^* = 0\ , \tag{22}$$

where:
$b_1 = a^2 + \omega^2 - \Omega^2$, $b_2 = 2\,\omega\,\Omega$, $b_3 = (1 + a_0\, a^2)$, $b_4 = b_2\,\beta^2$,
$b_5 = a^2 + \beta^2\,(\omega^2 - \Omega^2)$, $b_6 = \varepsilon_1\,\omega\,(1 + \tau_0\,\omega)$, $b_7 = 1 + a_0\,\omega\,(1 + \tau_0\,\omega)$,
$b_8 = a^2\, b_7 + \omega\,(1 + \tau_0\,\omega)$, $b_9 = a_0\,\varepsilon_3$, $b_{10} = \varepsilon_3\,(1 + a_0\, a^2)$, $b_{11} = a^2 + \alpha$,
$\alpha = \frac{K\, t^*}{\rho\, c_e \tau D_E} + \frac{K\omega}{\rho\, c_e D_E}$, $D = \frac{d}{d\, y}$.

Eliminating $\Phi^*(y)$, $\Psi^*(y)$, $\theta^*(y)$, and $N^*(y)$ between Eqs. (19)–(22), the following eighth order ordinary differential equation satisfied by $\Phi^*(y)$, $\Psi^*(y)$, $\theta^*(y)$, and $N^*(y)$ can be obtained:

$$(D^8 - A\, D^6 + B\, D^4 - C\, D^2 + E)\,[\Phi^*(y),\ \Psi^*(y),\ \theta^*(y),\ N^*(y)] = 0\ , \tag{23}$$

where:
$A = \frac{1}{(a_0\, b_6 + b_7)}[(b_1 + b_5 + b_{11})\, b_7 + b_8 - (\varepsilon_2 - b_6)\, b_9 + a_0\, b_6\, (a^2 + b_{11})$
$+ b_6\, (a_0\, b_5 + b_3)]$,

$B = \frac{1}{(a_0\, b_6 + b_7)}[b_3\, b_5\, b_6 + b_8\, b_{11} - \varepsilon_2\, b_{10} + (b_1 + b_5)\, (b_7\, b_{11} + b_8 - \varepsilon_2\, b_9) +$
$(b_1 b_5 + b_2 b_4)\, b_7 + a^2\, b_6 (a_0 b_{11} + b_9) + b_6 (a_0\, b_5 + b_3)(a^2 + b_{11}) + b_6\, (b_5\, b_9 + b_{10})]$,

$C = \frac{1}{(a_0 b_6 + b_7)}[(b_1 + b_5)(b_8 b_{11} - \varepsilon_2 b_{10}) + (b_1 b_5 + b_2 b_4)(b_7 b_{11} + b_8 - \varepsilon_2 b_9)$
$+ a^2\, b_6\, b_{11} (a_0\, b_5 + b_3) + b_3\, b_5\, b_6\, (a^2 + b_{11}) + b_5\, b_6\, b_{10} + a^2\, b_6 (b_5\, b_9 + b_{10})]$,

$E = \frac{1}{(a_0\, b_6 + b_7)}\left[(b_1\, b_5 + b_2\, b_4)\,(b_8\, b_{11} - \varepsilon_2\, b_{10}) + a^2\, b_5\, b_6 (b_3\, b_{11} + b_{10})\right].$

Equation (23) can be factored as

$$(\mathrm{D}^2 - k_1^2)(\mathrm{D}^2 - k_2^2)(\mathrm{D}^2 - k_3^2)(\mathrm{D}^2 - k_4^2)\{\Phi^*(y),\ \Psi^*(y),\ \theta^*(y),\ \mathrm{N}^*(y)\} = 0, \tag{24}$$

where k_j^2 $(j = 1, 2, 3, 4)$ are the roots of the characteristic equation given by Eq. (24). The limit of Eq. (24), solution as $y \to \infty$, reads:

$$\Phi^*(y) = \sum_{n=1}^{4} M_n\, e^{-k_n\, y}\ , \tag{25}$$

$$\Psi^*(y) = \sum_{n=1}^{4} H_{1n}\, M_n\, e^{-k_n\, y}\ , \tag{26}$$

$$\theta^*(y) = \sum_{n=1}^{4} H_{2n}\, M_n\, e^{-k_n\, y}\ , \tag{27}$$

$$N^*(y) = \sum_{n=1}^{4} H_{3n}\, M_n\, e^{-k_n\, y}\ , \tag{28}$$

here M_n $(n = 1, 2, 3, 4)$ are some coefficients and $H_{1\mathrm{n}} = \frac{b_4}{(b_5 - k_n^2)}$,

$H_{2\mathrm{n}} = \dfrac{b_6\,(k_n^2 - a^2)\,(k_n^2 - b_{11})}{[(k_n^2 - b_{11})(b_7\, k_n^2 - b_8) + \varepsilon_2\,(b_9\, k_n^2 - b_{10})]}$, $H_{3\mathrm{n}} = \dfrac{(b_9\, k_n^2 - b_{10})\, H_{2n}}{(k_n^2 - b_{11})}$.

Using Eqs. (8), (13), (18), and (25)–(28), the displacement components and the thermo-dynamic temperature can be obtained in the following form:

$$u^*(y) = \sum_{n=1}^{4} v_{1n}\, M_n\, e^{-k_n\, y}\ , \tag{29}$$

$$v^*(y) = -\sum_{n=1}^{4} v_{2n}\, M_n\, e^{-k_n\, y}\ , \tag{30}$$

$$T^*(y) = \sum_{n=1}^{4} v_{3n}\, M_n\, e^{-k_n\, y}\ . \tag{31}$$

Using Eqs. (14)–(18) and (25)–(31), we obtain

$$\sigma_{xx}^* = \sum_{n=1}^{4} H_{4n}\, M_n\, e^{-k_n y}\ , \tag{32}$$

$$\sigma^*_{yy} = \sum_{n=1}^{4} H_{5n}\, M_n\, e^{-k_n y}\ , \tag{33}$$

$$\sigma^*_{zz} = \sum_{n=1}^{4} H_{6n}\, M_n\, e^{-k_n y}\ , \tag{34}$$

$$\sigma^*_{xy} = -\sum_{n=1}^{4} H_{7n}\, M_n\, e^{-k_n y},\ \sigma^*_{xz} = \sigma^*_{yz} = 0\ , \tag{35}$$

where: $v_{1n} = i\,a - k_n\,H_{1n}$, $v_{2n} = k_n + i\,a\,H_{1n}$, $v_{3n} = [1 - a_0(k_n^2 - a^2)]H_{2n}$, $H_{4n} = (\beta^2 - 2)k_n\,v_{2n} + \beta^2(i\,a\,v_{1n} - v_{3n} - H_{3n})$, $H_{5n} = i\,a\,(\beta^2 - 2)\,v_{1n} + \beta^2(k_n\,v_{2n} - v_{3n} - H_{3n})$, $H_{6n} = (\beta^2 - 2)(k_n^2 - a^2) - \beta^2(v_{3n} + H_{3n})$, $H_{7n} = k_n\,v_{1n} + i\_a\,v_{2n}$.

4 Boundary conditions

The coefficients M_n $(n = 1, 2, 3, 4)$ have to be chosen such that the boundary conditions on the surface $y = 0$, take the form

$$\begin{gathered} \sigma_{xx} = -P_1^* \exp(\omega\,t + iax)\ , \quad \sigma_{xy} = 0\ , \\ T = P_2^* \exp(\omega\,t + i\,a\,x)\ , \\ D_E \frac{dN}{dy} = sN\ , \end{gathered} \tag{36}$$

where P_1^*, P_2^*, and s are constants.

Applying the boundary conditions (4) at the surface $y = 0$, we obtain a system of four equations. After applying the following inverse of matrix method

$$\begin{bmatrix} M_1 \\ M_2 \\ M_3 \\ M_4 \end{bmatrix} = \begin{bmatrix} H_{41} & H_{42} & H_{43} & H_{44} \\ H_{71} & H_{72} & H_{73} & H_{74} \\ v_{31} & v_{32} & v_{33} & v_{34} \\ (k_1+s_1)H_{31} & (k_2+s_1)H_{32} & (k_3+s_1)H_{33} & (k_4+s_1)H_{34} \end{bmatrix}^{-1} \begin{bmatrix} -p_1^* \\ 0 \\ p_2^* \\ 0 \end{bmatrix} \tag{37}$$

we obtain the values of coefficients M_n $(n = 1, 2, 3, 4)$, where

$$s_1 = \frac{s\,C_T\,t^*}{D_E}\ .$$

5 Particular cases

1. The expressions for the displacement components, force stresses, carrier density and temperature distribution in a rotating generalized semiconducting medium can be obtained from the above equations by taking $a^* = 0$ ($a^* = 0$ indicates one type temperature).
2. Neglecting the angular velocity (i.e., $\Omega = 0$) in the above equations, one can obtain the displacement components, carrier density, stress components, conductive temperature and thermodynamic temperature distribution in a non-rotating generalized semiconducting medium with two-temperature.

After substituting $\Omega = 0$ in Eq. (5), and use Eqs. (2), (8), and (18), it can be reached that

$$[D^2 - (a^2 + \omega^2)]\Phi^* + (a_0\, D^2 - b_3)\theta^* - N^* = 0\,, \tag{38}$$

$$(D^2 - m^2)\,\Psi^* = 0\,, \tag{39}$$

$$-\,b_6\,(D^2 - a^2)\;\Phi^* + (b_7\, D^2 - b_8)\;\theta^* + \varepsilon_2\; N^* = 0\,, \tag{40}$$

$$(b_9\; D^2 - b_{10})\,\theta^* - (D^2 - b_{11})\,N^* = 0\,. \tag{41}$$

Eliminating $\Phi^*(y)$, $\theta^*(y)$, and $\mathrm{N}^*(y)$ in Eqs. (38), (40), and (41), the following sixth order ordinary differential equations for $\Phi^*(y)$, $\theta^*(y)$, and $N^*(y)$ can be obtained

$$(D^6 - A_1\, D^4 + B_1\, D^2 - E_1)\,[\Phi^*(y),\, \theta^*(y),\, N^*(y)] = 0\,. \tag{42}$$

Equation (42) can be factored as

$$(D^2 - k_1^2)(D^2 - k_2^2)(D^2 - k_3^2)[\Phi^*(y),\, \theta^*(y), N^*(y)] = 0\,, \tag{43}$$

where $k_n^2 (n = 1, 2, 3)$ are the roots of the characteristic equation of Eq. (43),
$m^2 = a^2 + \beta^2\,\omega^2$,
$A_1 = \frac{1}{(a_0\, b_6 + b_7)}[(a_0\, a^2 + a_0\, b_{11} + b_3)\, b_6 + (a^2 + \omega^2 + b_{11})\, b_7 + b_8 + (b_6 - \varepsilon_2)\, b_9]$,
$B_1 = \frac{1}{(a_0\, b_6 + b_7)}[b_6\,(a^2\, a_0\, b_{11} + a^2\, b_3 + a^2\, b_9 + b_{10} + b_3\, b_{11}) + b_8\, b_{11} - \varepsilon_2\, b_{10}$
$+(a^2 + \omega^2)\,(b_8 + b_7\, b_{11} - \varepsilon_2\, b_9)]$,
$E_1 = \frac{1}{(a_0\, b_6 + b_7)}[(a^2 + \omega^2)\,(b_8\, b_{11} - \varepsilon_2\, b_{10}) + a^2\, b_6(b_3\, b_{11} + b_{10})]$.

The solution of Eqs. (43) and (39), take the form

$$\Phi^*(y) = \sum_{n=1}^{3} G_n \, e^{-k_n y} \, , \tag{44}$$

$$\theta^*(y) = \sum_{n=1}^{3} R_{1n} \, G_n \, e^{-k_n y} \, , \tag{45}$$

$$\mathrm{N}^*(y) = \sum_{n=1}^{3} R_{2n} \, G_n \, e^{-k_n y} \, , \tag{46}$$

$$\Psi^*(y) = G_4 \, e^{-m y} \, , \tag{47}$$

where G_n $(n = 1, 2, 3, 4)$ are some coefficients,

$$R_{1\mathrm{n}} = \frac{(k_n^2 - b_{11})\,[k_n^2 - (a^2 + \omega^2)]}{[(b_9\, k_n^2 - b_{10}) - (k_n^2 - b_{11})(a_0\, k_n^2 - b_3)]}, \text{and} \quad R_{2\mathrm{n}} = \frac{(b_9\, k_n^2 - b_{10})\, R_{1n}}{(k_n^2 - b_{11})}.$$

Using Eqs. (8), (13)–(18), and (44)–(47), the expressions for the displacement components, the thermodynamic temperature and the stress components distribution in a non-rotating generalized semiconducting medium with two temperature can be written as follows:

$$u^*(y) = \sum_{n=1}^{3} i\, a\, G_n \, e^{-k_n y} - m\, G_4 \, e^{-m y} \, , \tag{48}$$

$$v^*(y) = -\sum_{n=1}^{3} k_n \, G_n \, e^{-k_n y} - i\, a\, G_4 \, e^{-m y} \, , \tag{49}$$

$$T^*(y) = \sum_{n=1}^{3} R_{3n} \, G_n \, e^{-k_n y} \, , \tag{50}$$

$$\sigma_{xx}^* = \sum_{n=1}^{3} R_{4n} \, G_n \, e^{-k_n y} - 2\, i\, a\, m\, G_4 \, e^{-m y} \, , \tag{51}$$

$$\sigma_{yy}^* = \sum_{n=1}^{3} R_{5n} \, G_n \, e^{-k_n y} + 2\, i\, a\, m\, G_4 \, e^{-m y} \, , \tag{52}$$

$$\sigma_{zz}^* = \sum_{n=1}^{3} R_{6n} \, G_n \, e^{-k_n y} \, , \tag{53}$$

$$\sigma^*_{xy} = -\sum_{n=1}^{3} R_{7n}\, G_n\, e^{-k_n\, y} + (a^2 + m^2)\, G_4\, e^{-m\, y}, \quad \sigma^*_{xz} = \sigma^*_{yz} = 0\ , \quad (54)$$

where $R_{3n} = [1 - a_0(k_n^2 - a^2)]\, R_{1n}$, $R_{4n} = (\beta^2 - 2)k_n^2 - \beta^2(a^2 + R_{2n} + R_{3n})$, $R_{5n} = \beta^2(k_n^2 - R_{2n} - R_{3n}) - a^2(\beta^2 - 2)$, $R_{6n} = (\beta^2 - 2)(k_n^2 - a^2) - \beta^2(R_{2n} + R_{3n})$, $R_{7n} = 2\, i\, a\, k_n$.

Applying the boundary conditions (4) at the surface, $y = 0$, a system of four equations is obtained. After solving this system, the coefficients G_n $(n = 1, 2, 3, 4)$ can be defined as follows:

$$\begin{bmatrix} G_1 \\ G_2 \\ G_3 \\ G_4 \end{bmatrix} = \begin{bmatrix} R_{41} & R_{42} & R_{43} & -2iam \\ R_{71} & R_{72} & R_{73} & -(a^2 + m^2) \\ R_{31} & R_{32} & R_{33} & 0 \\ (k_1 + s_1)R_{21} & (k_2 + s_1)R_{22} & (k_3 + s_1)R_{23} & 0 \end{bmatrix}^{-1} \begin{bmatrix} -p_1^* \\ 0 \\ p_2^* \\ 0 \end{bmatrix}. \quad (55)$$

6 Numerical results

Silicon, Si, is chosen as the material for numerical simulations. The parameters for silicon are taken as (Song *et al.* [11,13]):
$\lambda = 3.64 \times 10^{10}\ \mathrm{N\,m^{-2}}$, $\mu = 5.46 \times 10^{10}\ \mathrm{kg\,m^{-1}s^{-2}}$, $K = 150\ \mathrm{W\,m^{-1}K^{-1}}$,
$\alpha_t = 3 \times 10^{-6}\ \mathrm{K^{-1}}$, $\rho = 2.33 \times 10^{3}\ \mathrm{kg\,m^{-3}}$, $C_E = 695\ \mathrm{J\,kg^{-1}\,K^{-1}}$,
$T_0 = 300\ \mathrm{K}$, $\Omega = 0.4\ \mathrm{s^{-1}}$, $a^* = 0.4$, $a = 0.5$, $p_1^* = p_2^* = 0.01$, $\tau_0 = 0.01$,
$t = 0.02$, $\varepsilon_3 = -\,450$, $x = 0.5$, $\omega = \omega_{Re.} + i\omega_{Im}$, $\omega = \omega_{Re} = 0.6$,
$\omega_{Im} = 0$, $d_n = -\,9 \times 10^{-31}\ \mathrm{m^3}$, $D_E = 2.5 \times 10^{-3}\ \mathrm{m^2 s^{-1}}$,
$E_g = 1.12ev$, $\tau = 5 \times 10^{-5}\ \mathrm{s}$, $s = 2\ \mathrm{m\,s^{-1}}$.

The thermophysical data, outlined above, were used for the determination of the distribution of the real part of displacement components u, v, thermodynamic temperature T, conductive temperature θ, carrier density N, stress components σ_{xx}, σ_{yy}, σ_{zz}, and σ_{xy} in the presence and absence of the rotation as well as the two temperature parameter. Here, all variables are taken in the non-dimensional form. The results are shown in Figs. 2–10.

In these figures, the solid lines represent the solution for $\Omega = 0.4$, $a^* = 0.4$, the dashed ones represent the solution derived for $\Omega = 0$, $a^* = 0.4$, and the dot-dashed lines represent the solution for $\Omega = 0.4$, $a^* = 0$. Due to the boundary conditions, the stress components σ_{xx} and σ_{xy} always start from negative values and zero, respectively, and terminate at a zero value.

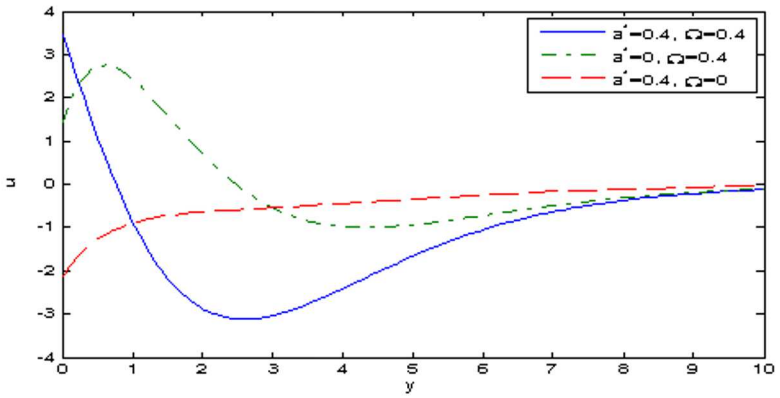

Figure 2: Distribution of horizontal displacement u.

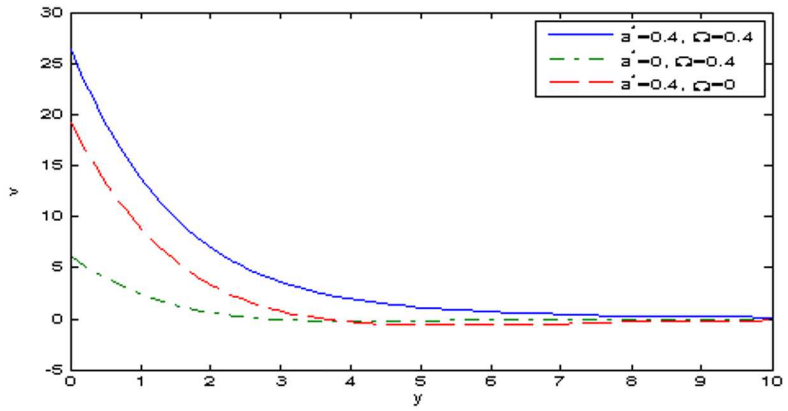

Figure 3: Distribution of vertical displacement v.

Figure 2 describes the variation of the horizontal displacement u against the distance y. It is clear from Fig. 2 that the values of u decrease in the range $0 \leq y \leq 2.5$, then increase and go to zero in the range $2.5 \leq$

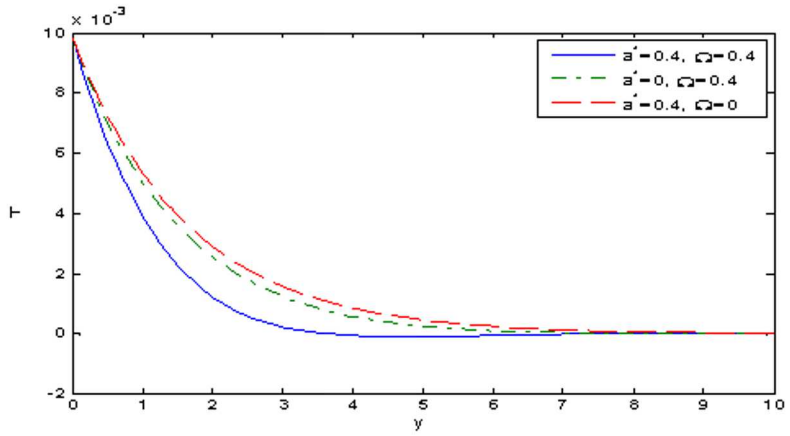

Figure 4: Distribution of the thermodynamic temperature T.

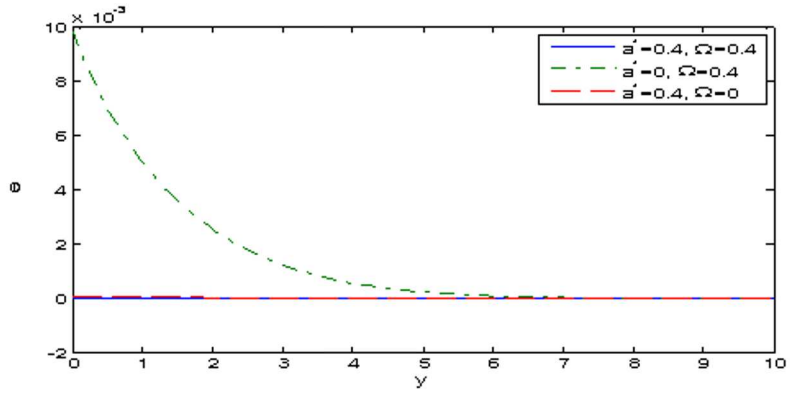

Figure 5: Distribution of the conductive temperature θ.

$y \leq 10$, for $\Omega = 0.4$, $a^* = 0.4$, while, it increases in the range $0 \leq y \leq 0.9$ then decrease in the range $0.9 \leq y \leq 5$ and finally increase and go to zero for $\Omega = 0.4$, $a^* = 0$, while u is an increasing function in the range $0 \leq y \leq 10$ for $\Omega = 0$, $a^* = 0.4$. Figure 3 shows the variation of the vertical displacement v. In this figure, a significant difference in the vertical displacement v is noticed for different values of the two temperature parameter a^* as well as rotation. It shows that the magnitude of v for $a^* = 0.4$ is higher than that of $a^* = 0$. It is also observed from this figure that the rotation acts to increase the magnitude of the real part of v.

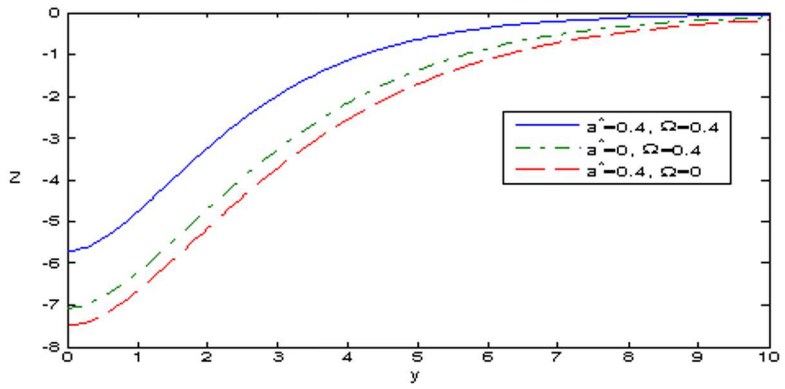

Figure 6: Distribution of the carrier density N.

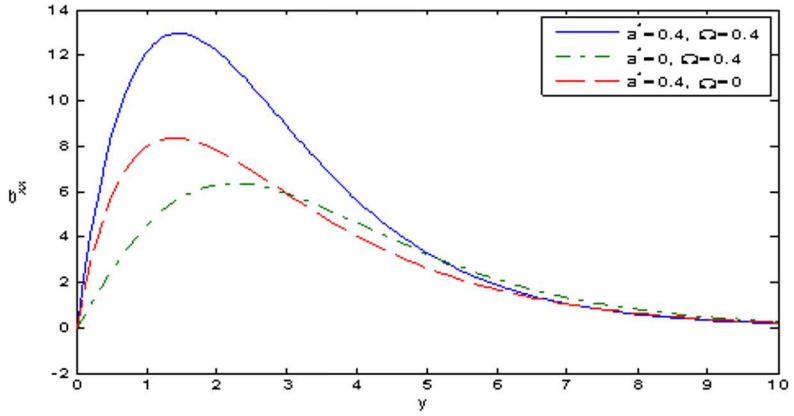

Figure 7: Distribution of stress component σ_{xx}.

Figure 4 is plotted to show the variation of the thermodynamic temperature T. It is observed that the thermodynamic temperature, T, decreases in the range $0 \leq y \leq 8$ and finally goes to zero for the different cases. It is also clear that the parameter a^* of two-temperature and the rotation, Ω, act to decrease the values of T. It is clear that the values of conductive temperature, θ, as shown in Fig. 5, in the two-type temperature cases are small compared to those for one-type temperature case. It is also noticed that the conductive temperature θ is inversely proportional to the rotation. Figure 6 clarifies that the values of the carrier density N always begin

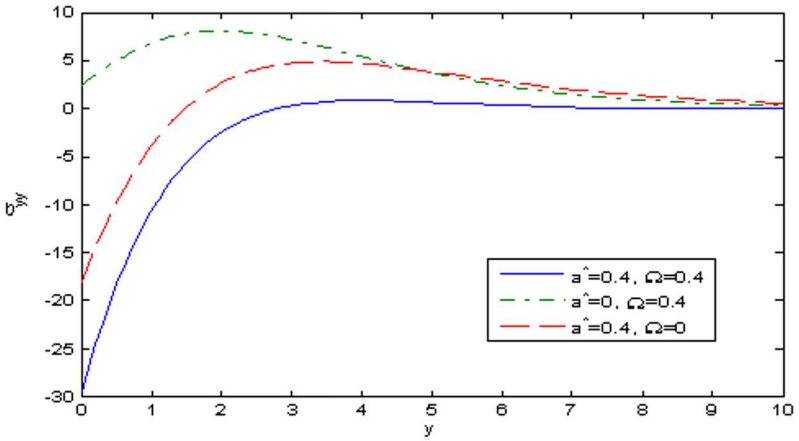

Figure 8: Distribution of stress component σ_{yy}.

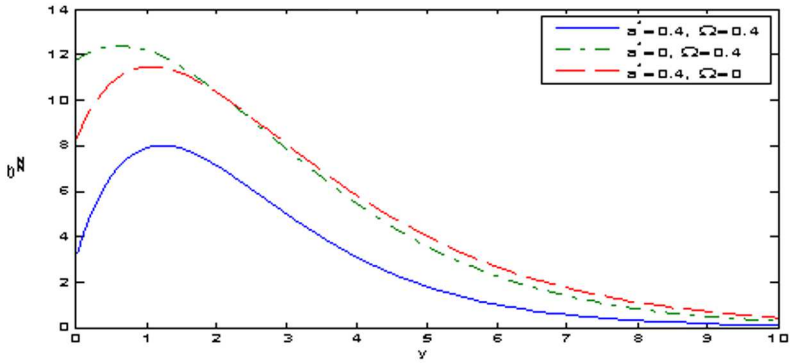

Figure 9: Distribution of stress component σ_{zz}.

from negative values and increase in the range $0 \leq y \leq 10$, then go to zero for the different cases. It is also seen that the carrier density N is directly proportional to the rotation and the two-temperature parameter. Figure 7 represents the change in the stress component σ_{xx} with distance y. The values of σ_{xx} always start with increasing to a maximum value then decrease and finally go to zero. It is noticed that σ_{xx} is strongly affected by the two temperature parameter as well as the rotation. It is directly proportional to both of them. It is clear that the two-temperature parameter a^* and the rotation act to decrease the values of σ_{yy} as shown

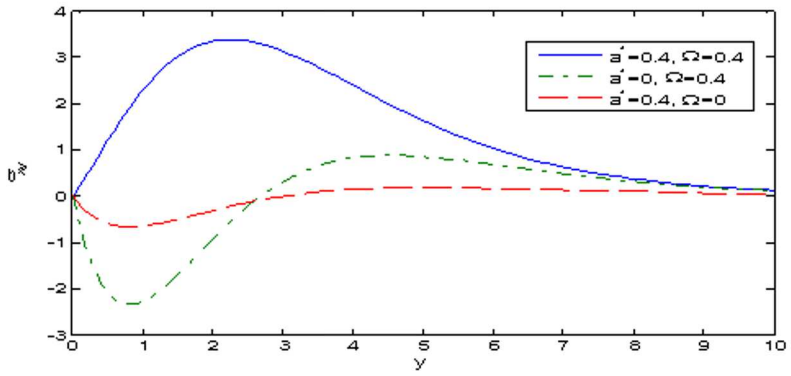

Figure 10: Distribution of stress component σ_{xy}.

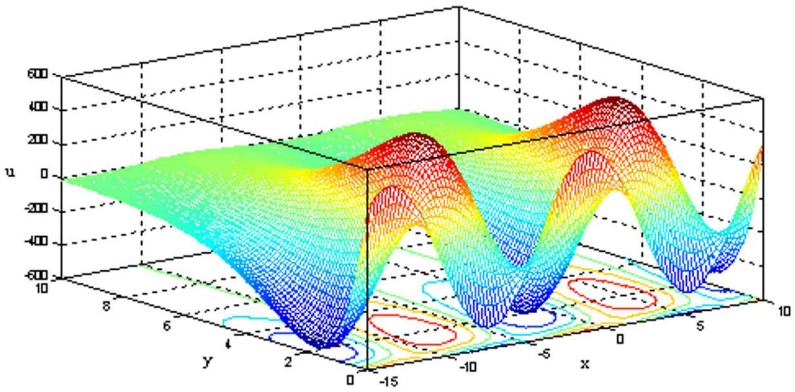

Figure 11: Distribution of the displacement component u versus components of distance at $\Omega = 0.4$ and $a^* = 0.4$.

in Fig. 8. Figure 9 depicts that the distribution of stress component σ_{zz} always begins from positive values. For different cases, the values of σ_{zz} start with increasing to a maximum value in the range $0 \leq y \leq 1.2$, then decrease in the range $1.2 \leq y \leq 10$ and finally tend to zero. It is clear that the two-temperature parameter a^* as well as, the rotation acts to decrease the values of σ_{zz}. Figure 9 explains that the distribution of the stress component σ_{xy} always starts with zero at the origin which agrees with the boundary conditions. It is clear that the two-temperature parameter a^* acts to increase the values of σ_{xy}. It can be also observed from this figure

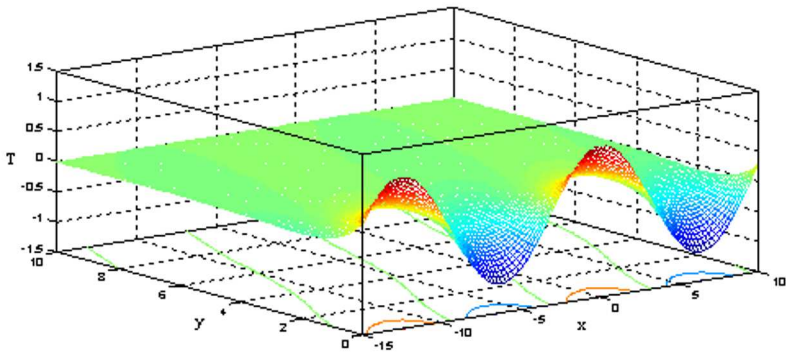

Figure 12: Distribution of the thermodynamic temperature T versus components of distance at $\Omega = 0.4$ and $a^* = 0.4$.

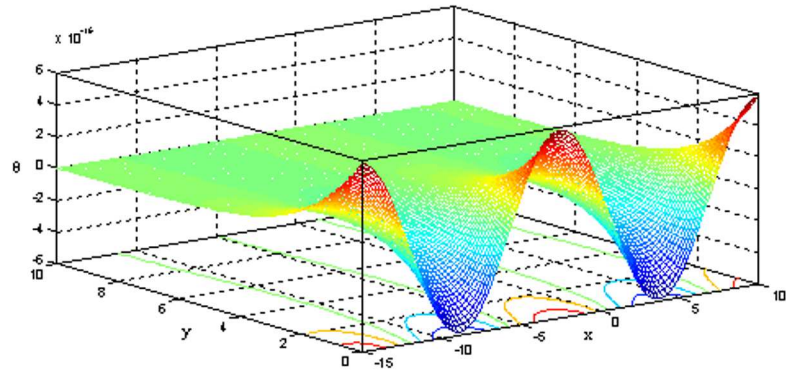

Figure 13: Distribution of the conductive temperature θ versus components of distance at $\Omega = 0.4$ and $a^* = 0.4$.

that the values of the stress component σ_{xy} in the presence of rotation are higher than those in the absence of rotation. Figures 10–15 depict the 3D curves which represent the relation between the physical quantities and both components of distance in the context of the (L-S) theory for $\Omega = 0.4$, and $a^* = 0.4$, these figures are very important to study the dependence of these physical quantities on the vertical component of distance. The curves obtained are highly depending on the vertical distance and all the physical quantities are moving in the wave propagation.

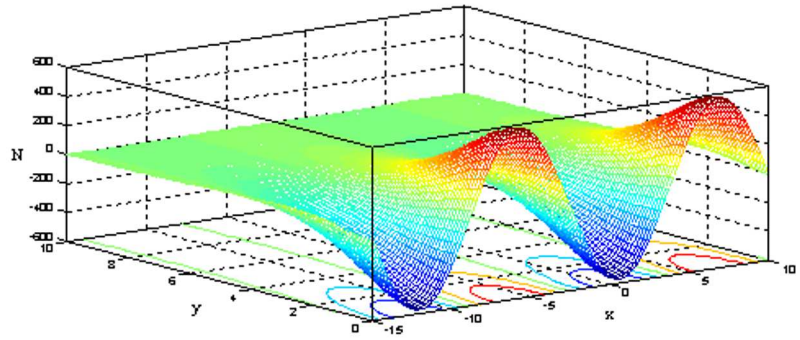

Figure 14: Distribution of carrier density N versus components of distance at $\Omega = 0.4$ and $a^* = 0.4$.

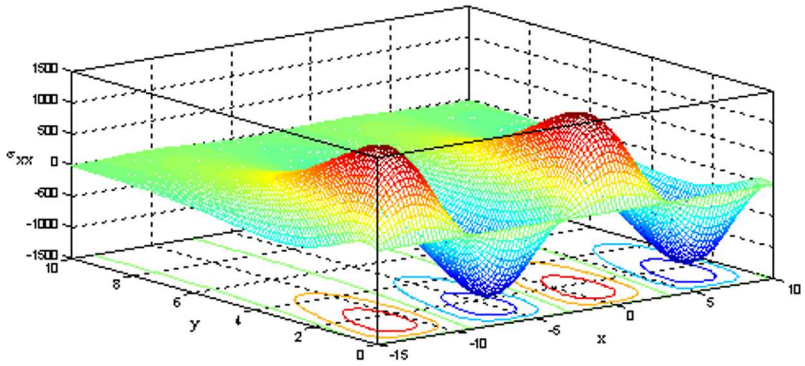

Figure 15: Distribution of stress component σ_{xx} versus components of distance at $\Omega = 0.4$ and $a^* = 0.4$.

7 Conclusion

According to the results of this work, one can see the effect of rotation as well as of the two temperature parameter on the wave propagation of all fields and how they play a vital role in increasing or decreasing the amplitude of different physical quantities. This work proves the importance of distinguishing between the conductive temperature and the thermodynamic temperature. Also, the figures show that the presence of either the two temperature parameter or the rotation has the same effect on the different physical quantities. This work can serve for the analysis and design

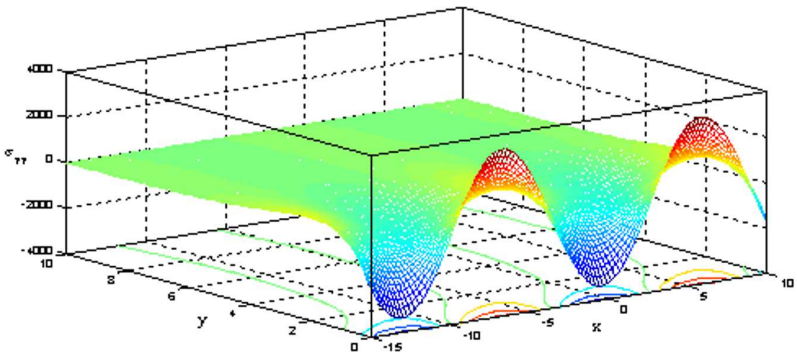

Figure 16: Distribution of stress component σ_{yy} versus components of distance at $\Omega = 0.4$ and $a^* = 0.4$.

of the thermal resistance coated materials. There are a lot of applications on diverse field as semiconducting and the reactions during a photothermal process and other fields in physical engineering, electronic devices, transistors, also in physical chemistry and medical physics.

Received 2 November 2016

References

[1] Biot M.A.: *Thermoelasticity and irreversible thermodynamics*. J. Appl. Phys. 27(1956), 3, 240–253.

[2] Lord H.W., Shulman Y.A.: *Generalized dynamical theory of thermo-elasticity*. J. Mech. Phys. Solids. **15**(1967), 5, 299–30.

[3] Maxwell J.C.: *On the dynamical theory of gases*. J. Philos. Trans. Roy. Soc. London. **157**(1867), 49–88.

[4] Cattaneo C.: *Sur une forme de l'equation de la chaleur elinant le paradoxe d'une propagation instantance*. CR Acad. Sci. **247**(1958), 431–432 (in France).

[5] Vernotte P.: *Les paradoxes de la theorie continue de l'equation de la chaleur*. CR Acad. Sci. **246**(1958), 3154–3155 (in Franch).

[6] Dhaliwal R., Sherief H.H.: *Generalized thermoelasticity for anisotropic media*. Quart. Appl. Math. **33**(1980), 1, 1–8.

[7] Othman M.I.A., Said S.M.: *The effect of rotation on two-dimensional problem of a fiber-reinforced thermoelastic with one relaxation time*. Int. J. Thermophysics. **33**(2012), 1, 160–171.

[8] Gordon J. P., Leite R.C.C., Moore R.S.: *Long-transient effects in lasers with inserted liquid samples*. J. Appl. Phys. **36**(1965), 1, 3–8.

[9] Kreuzer L.B.: *Ultralow gas concentration infrared absorption spectroscopy*. J. Appl. Phys. **42**(1971), 7, 2934–2943.

[10] Todorovic D.M., Nikolic P.M., Bojicic A.I.: *Photoacoustic frequency transmission technique: Electronic deformation mechanism in semiconductors*. J. Appl. Phys. **85**(1999), 7716–7726.

[11] Song Y.Q., Todorovic D.M., Cretin B.: *Study on the generalized thermoelastic vibration of the optically excited semiconducting micro-cantilevers*. Int. J. Solids Struct. **47**(2010), 14-15, 1871–1875.

[12] Todorovic D.M.: *Plasma, thermal, and elastic waves in semiconductors*. Rev. Sci. Instrum. **74**(2003), 1, 582–585.

[13] Song Y.Q., Bai J.T., REN Z.Y.: *Study on the reflection of photothermal waves in a semiconducting medium under generalized thermoelastic theory*. Acta Mech. **223**(2012), 7, 1545–1557.

[14] Schoenberg M., Censor D.: *Elastic waves in rotating media*. Q. J. Appl. Maths. **31**(1973), 1, 115–125.

[15] Chand D., Sharma J.N., Sud S.P.: *Transient generalized magneto-thermo-elastic waves in a rotating half space*. Int. J. Eng. Sci. **28**(1990), 547–556.

[16] Destrade M.: *Surface waves in rotating rhombic crystal*. Proc. Royal Soc. **A 460**(2004), 653–665.

[17] Othman M.I.A.: *Effect of rotation in the case of 2-D problems of the generalized thermoelasticity with thermal relaxation*. Mech. Mech. Eng. **9**(2005), 2, 115–130.

[18] Othman M.I.A., Singh B.: *The effect of rotation on generalized micropolar thermoelasticity for a half-space under five theories*. Int. J. Solids Struct. **44**(2007), 2748–2762.

[19] Othman M.I.A, Hasona W.M., Eraki E.E.M.: *Effect of magnetic field on generalized thermoelastic rotating medium with two temperature under five theories*. J. Comput, Theor. Nanos. **12**(2015), 8, 1677–1686.

[20] Hayat T., Mumtaz S., Ellahi R.: MHD unsteady flows due to non- coaxial rotations of a disk and a fluid at infinity. Acta Mech. Sinica. **19**(2003), 3, 235–240.

[21] Hayat T., Ellahi R., Asghar S., Siddiqui A.M.: *Flow induced by non-coaxial rotation of a porous disk executing non-torsional oscillating and second grade fluid rotating at infinity*. Appl. Math. Model. **28**(2004), 6, 591–605.

[22] Hayat T., Ellahi R., Asghar S.: *Unsteady periodic flows of a magneto-hydrodynamic fluid due to non- coaxial rotations of a porous disk and fluid at infinity*. Math. Comput. Model. **40**(2004), No. 1-2, 173–179.

[23] Hayat T., Ellahi R., Asghar S.: *Unsteady magnetohydrodynamic non-Newtonian flow due to non-coaxial rotations of a disk and a fluid at infinity*. Chem. Eng. Commun. **194**(2007), 1, 37–49.

[24] Ellahi R., Asgahr S.: *Couette flow of a Burgers' fluid with rotation*. Int. J. Fluid Mech. Res. **34**(2007), 548–561.

[25] Hayat T., Ellahi R., Asghar S.: *Hall effects on unsteady flow due to noncoaxially rotating disk and a fluid at infinity*. Chem. Eng. Commun. **195**(2008), 8, 958–976.

[26] Chen P.J., Gurtin M.E.: *On a theory of heat conduction involving two temperatures*. ZAMP **19**(1968), 4, 614–627.

[27] Chen P. J., Gurtin M.E., Williams W.O.: *A note on non-simple heat conduction*. ZAMP **19**(1968), 6, 969–970.

[28] Chen P.J., Gurtin M.E., Williams W.O.: *On the thermodynamics of non-simple elastic materials with two temperatures*. ZAMP **20**(1969), 1, 107–112.

[29] BOLEY B. A., SnplaceTOLINS SnI. S.: *Transient coupled thermoelastic boundary value problems in the half-space*. J. App. Mech. **29**(1962), 4, 637–646.

[30] Warren W.E., Chen P.J.: *Wave propagation in the two-temperature theory of thermoelasticity*. Acta Mech. **16**(1973), 1-2, 21–33.

[31] Youssef H.M.: *Theory of two-temperature generalized thermoelasticity*. IMAJ. Appl. Math. **71**(2006), 3, 383–390.

[32] Youssef H.M.: *Two-dimensional problem of two-temperature generalized thermoelastic half-space subjected to Ramp-type heating*. J. Comp. Math. Model. **19**(2008), 201–216.

[33] Abbas I.A., Youssef H.M.: *Two-temperature generalized thermoelasticity under ramp-type heating by finite element method*. Meccanica **48**(2013), 2, 331–339.

[34] Bijarnia R., Singh B.: *propagation of plane waves in a rotating transversely isotropic two temperature generalized thermoelastic solid half-space with voids*. Int. J. of Appl. Mech. Eng. **21**(2016), 1, 285–301.

[35] Kaviany M.: *Heat Transfer Physics*. Cambridge Univ. Press, Cambridge 2008.

Notes for Contributors

Archives of Thermodynamics publishes original papers which have not previously appeared in other journals. The journal does not have article processing charges (APCs) nor article submission charges. The language of the papers is English. The paper should not exceed the length of 25 pages. All pages should be numbered. The plan and form of the papers should be as follows:

1. The heading should specify the title (as short as possible), author, his/her complete affiliation, town, zip code, country and e-mail. Please indicate the corresponding author. The heading should be followed by *Abstract* of maximum 15 typewritten lines and *Keywords*.
2. More important symbols used in the paper can be listed in *Nomenclature*, placed below *Abstract* and arranged in a column, e.g.:
   u – velocity, m/s
   v – specific volume, m/kg
   etc.
   The list should begin with Latin symbols in alphabetical order followed by Greek symbols also in alphabetical order and with a separate heading. Subscripts and superscripts should follow Greek symbols and should be identified with separate headings. Physical quantities should be expressed in SI units (*Système International d'Unités*).
3. All abbreviations should be spelled out first time they are introduced in the text.
4. The equations should be each in a separate line. Standard mathematical notation should be used. All symbols used in equations must be clearly defined. The numbers of equations should run consecutively, irrespective of the division of the paper into sections. The numbers should be given in round brackets on the right-hand side of the page.
5. Particular attention should be paid to the differentiation between capital and small letters. If there is a risk of confusion, the symbols should be explained (for example *small c*) in the margins. Indices of more than one level (such as B_{f_a}) should be avoided wherever possible.
6. Computer-generated figures should be produced using **bold lines and characters**. No remarks should be written directly on the figures, except numerals or letter symbols only. Figures should be as small as possible while displaying clearly all the information requires, and with all lettering readable. The relevant explanations can be given in the caption.
7. The figures, including photographs, diagrams, etc., should be numbered with Arabic numerals in the same order in which they appear in the text. Each figure should have its own caption explaining the content without reference to the text.
8. Computer files on an enclosed disc or sent by e-mail to the Editorial Office are welcome. The manuscript should be written as a MS Word file – $*.doc$, $*.docx$ or LaTeX file – $*.tex$. For revised manuscripts after peer review process, figures should be submitted as separate graphic files in either vector formats (PostScript (PS),

Encapsulated PostScript (EPS), preferable, CorelDraw (CDR), etc.) or bitmap formats (Tagged Image File Format (TIFF), Joint Photographic Experts Group (JPEG), etc.), with the resolution not lower than 300 dpi, preferably 600 dpi. These resolutions refer to images sized at dimensions comparable to those of figures in the print journal. Therefore, electronic figures should be sized to fit on single printed page and can have maximum 120 mm x 170 mm. Figures created in MS World, Exel, or PowerPoint will not be accepted. The quality of images downloaded from websites and the Internet are also not acceptable, because of their low resolution (usually only 72 dpi), inadequate for print reproduction.

9. The references for the paper should be numbered in the order in which they are called in the text. Calling the references is by giving the appropriate numbers in square brackets. The references should be listed with the following information provided: the author's surname and the initials of his/her names, the complete title of the work (in English translation) and, in addition:

   (a) for books: the publishing house and the place and year of publication, for example:
   [1] Holman J.P.: *Heat Transfer*. McGraw-Hill, New York 1968.

   (b) for journals: the name of the journal, volume (Arabic numerals in bold), year of publication (in round brackets), number and, if appropriate, numbers of relevant pages, for example:
   [2] Rizzo F.I., Shippy D.I.: *A method of solution for certain problems of transient heat conduction*. AIAA J. **8**(1970), No. 11, 2004–2009.

   For works originally published in a language other than English, the language should be indicated in parentheses at the end of the reference.

   Authors are responsible for ensuring that the information in each reference is complete and accurate.

10. As the papers are published in English, the authors who are not native speakers of English are obliged to have the paper thoroughly reviewed language-wise before submitting for publication.

Manuscript submission Manuscripts to be considered for publication should be electronically submitted to the Editorial Office via the online submission and reviewing system, the Editorial System, at http://www.editorialsystem.com/aot. Submission to the journal proceeds totally on line and you will be guided stepwise throughout the process of the creation and uploading of your files. The body of the text, tables and figures, along with captions for figures and tables should be submitted separately. The system automatically converts source files to a single PDF file article, for subsequent approval by the corresponding Author, which is then used in the peer-review process. All correspondence, including notification confirming the submission of the manuscripts to the Editorial Office, notification of the Editorsñs decision and requests for revision, takes place by e-mails. Authors should designate the corresponding author, whose responsibility is to represent the Authors in contacts with the Editorial Office. Authors are requested not to submit the manuscripts by post or e-mail.

The illustrations may be submitted in color, however they will be printed in black and white in the journal, so the grayscale contributions are preferable. Therefore, the figure

caption and the entire text of the paper should not make any reference to color in the illustration. Moreover the illustration should effectively convey author's intended meaning when it is printed as a halftone. The illustrations will be reproduced in color in the online publication.

Further information All manuscripts will undergo some editorial modification. The paper proofs (as PDF file) will be sent by e-mail to the corresponding author for acceptance, and should be returned within two weeks of receipt. Within the proofs corrections of minor and typographical errors in: author names, affiliations, articles titles, abstracts and keywords, formulas, symbols, grammatical error, details in figures, etc., are only allowed, as well as necessary small additions. The changes within the text will be accepted in case of serious errors, for example with regard to scientific accuracy, or if authors reputation and that of the journal would be affected. Submitted material will not be returned to the author, unless specifically requested.
A PDF file of published paper will be supplied free of charge to the Corresponding Author.

Submission of the manuscript expresses at the same time the authors consent to its publishing in both printed and electronic versions.

Transfer of Copyright Agreement Submission of the manuscript means that the authors automatically agree to assign the copyright to the Publisher. Once a paper has been accepted for publication, as a condition of publication, the authors are asked to send by email a scanned copy of the signed original of the Transfer of Copyright Agreement, signed by the Corresponding Author on behalf of all authors to the Managing Editor of the Journal. The copyright form can be downloaded from the journal's website at http://www.imp.gda.pl/archives-of-thermodynamics/ under Notes for Contributors.

The Editorial Committee